

Development Techniques for Supersonic Turbines

Von der Fakultät Luft- und Raumfahrttechnik und Geodäsie
der Universität Stuttgart zur Erlangung der Würde eines
Doktors der Ingenieurwissenschaften (Dr.-Ing.) eingereichte
Dissertation

Vorgelegt von

Samuel Sudhof

aus Frankfurt am Main

Hauptberichter

Mitberichter

Mitberichter

Tag der mündlichen Prüfung

Institut für Raumfahrtssysteme der Universität Stuttgart

2020

Contents

Zusammenfassung	9
Abstract	11
1. Introduction	13
1.1. Definition of Transonic and Supersonic Turbines	14
2. Thermodynamics and Mean-Line Models of Turbines	17
2.1. Useful Work in Turbines	17
2.2. Efficiency in Turbine Stages	21
2.3. Degree of Reaction	24
2.3.1. Influence on Gas Velocities	26
2.4. Interaction of Losses and Power Generation	27
2.5. Blade and Channel Height	29
2.6. Limitations of Mean-Line Models	32
3. Development of Supersonic Turbine Blade Rows	35
3.1. Case Study in Supersonic Turbine Blading	36
3.1.1. Nozzle Design	37
3.1.2. Rotor Design	40
3.2. State of the Art for Two-Dimensional Profile Generation	42
3.3. Design Goals of Parametric Blade Generation Methods	45
3.4. Proposed Blade Profile Design Methods	47
3.4.1. Specific Geometry Features in Supersonic Nozzles	50
3.4.2. A General Nozzle Blading Scheme	53
3.4.3. Recent Studies on Rotor Profile Design	55
3.4.4. Draft of a Parameter System for Supersonic Rotors	61
3.5. Analytical Methods of Parameter Value Choice	65
3.5.1. Known and Novel Methods for Determining the Required Blade Stagger	65

3.5.2.	The Throat Area Problem	69
3.5.3.	Fair Curves	76
3.6.	3D Blade and Channel Shape Generation	78
3.6.1.	Documented 3D Blade Generation Techniques	78
3.6.2.	Segment-Wise Context-Aware Projection Technique	81
3.6.3.	Possible Applications of Three-Dimensional Blade Shape Generation	83
3.6.4.	Flow Path Shaping	86
3.7.	Optimization	88
3.7.1.	Nozzle Optimization by Uniformity	90
3.7.2.	Comparison to Dejc's Throat Area Guideline	92
3.8.	Possible Inferences for Shock Management in Nozzles	93
4.	Cascade Design for Supersonic Turbine Nozzles	95
4.1.	Shock Absorbing Structure	96
4.2.	Test Facility	98
4.3.	Test Procedure	98
4.4.	Pressure Tap Experiments	99
4.5.	Optical Experiments	102
4.5.1.	Analysis of Resulting BoS Images	103
4.5.2.	High Speed Camera Analysis	105
4.6.	Conclusions from the Cascade Experiment	106
5.	Conclusion	109
	Appendices	123
A.	Isentropic and Polytropic Work	125
B.	Segment Curves for Blade Shaping	129
B.1.	General Conic Segment	129
B.1.1.	Parameter Study	130
B.1.2.	Transfer Function	130
B.1.3.	Considerations for Blade Shaping	131
B.2.	Rational Cubic Curve (Paluszny Curve)	131
B.2.1.	Parameter Study	132
B.2.2.	Transfer Function	132
B.2.3.	Considerations for Blade Shaping	133

B.3. Non-Rational Quartic Curve	133
B.3.1. Parameter Study	136
B.3.2. Transfer Function	137
B.3.3. Considerations for Blade Shaping	138
B.4. Other Curves	138

List of Figures

1.1.	Nomenclature	16
2.1.	Mass Flow Density Plot	32
2.2.	Simulation of Convergent Nozzle Flow	33
2.3.	Outlet Flow Angle Simulation	33
2.4.	Total Pressure over Axial Distance Plot	33
3.1.	Axisymmetric and Slot Nozzles	39
3.2.	Vulcain 2 LOX Turbine Simulation	43
3.3.	Blade Shaping Paradigms	45
3.4.	Supersonic Trailing Edge Flow	51
3.5.	Kink Nozzle Profiles	52
3.6.	Supersonic Nozzle Parameter System	54
3.7.	Optimized Rotor Blade Comparison	57
3.8.	Rotor Inlet Sketch	59
3.9.	Supersonic Rotor	62
3.10.	Blade Stagger Correlations	66
3.11.	Rotor Profile Proposed by Boxer et Al.	70
3.12.	Effect of Length Measures on Blade Geometry	78
3.13.	Blade Mantle Surface Generation by Lofting	84
3.14.	M1 Turbine Tangential Velocity	85
3.15.	Flow Path Shape Comparison	87
3.16.	Nozzle Optimization	92
3.17.	Area Ratios in Optimization	93
4.1.	Cascade Overview	96
4.2.	Separator Hole Pattern	96
4.3.	Flow Periodicity Comparison	97
4.4.	Test Stand Flow Schematic	98
4.5.	Pressure Tap Locations	99

4.6.	Pressure Tap Measurements Series 2	101
4.7.	Pressure Tap Measurements Series 1	102
4.8.	Optical Setup for BoS	103
4.9.	Schlieren Images and Simulation	104
4.10.	Frequency-Amplitude Plots	107
A.1.	h - s Diagram for Nitrogen	126
B.1.	Conic Segment Parameter Study	130
B.2.	Paluszny Segment Parameter Study	132
B.3.	Quartic Segment Parameter Study	136

Zusammenfassung

Diese Doktorarbeit behandelt Überschallturbinen wie sie in den Turbopumpen von Raketenantrieben zum Einsatz kommen. Andere Anwendungsgebiete, wie zum Beispiel Turbinen in Organic Rankine Cycle-Anlagen werden nicht explizit diskutiert, einige Ergebnisse werden jedoch auch auf diese übertragbar sein.

Der wissenschaftliche Inhalt der Arbeit ist in drei Kapitel aufgeteilt. Das erste hiervon (Kapitel 2) beschäftigt sich mit den thermodynamischen Grundlagen von gasbeaufschlagten Turbinen im Allgemeinen. Dies dient der Unterstützung von Lehrbüchern des Fachgebiets, die vornehmlich hocheffiziente Unterschallturbinen thematisieren. Probleme der Voraussage von Überschallturbinen, die mit einem einfachen Thermodynamik-Modell, wie etwa dem Stromfadenmodell, zu erklären sind werden hier erörtert. Dazu ist eine grundsätzliche Diskussion der Methode der Leistungserzeugung in Turbinen und deren Zusammenhang mit der Effizienz notwendig.

Ein Abschnitt befasst sich allein mit Definitionen des Reaktionsgrads, da dieser in der Literatur diverse Definitionen hat, deren Unterschiede zwar bei hocheffizienten Turbinen gering sind, bei gängigen Überschallturbinen jedoch immens sein können.

Ein typisches Problem der Überschallturbinen in kleineren Raketenantrieben ist die geringe Durchflussmenge, die zu einer unzureichenden Schaufelhöhe führt. Hierzu werden verschiedene Lösungsansätze auf Basis einfacher Thermodynamik erörtert. Das Kapitel schließt ab mit einigen Simulationsergebnissen die die inhärenten Begrenzungen einfacher Thermodynamik illustrieren.

Im dritten und umfangreichsten Kapitel werden verschiedene Aspekte der Schaufelerzeugung für Stator- und Rotorschaukeln diskutiert, um einen Kontext für die zahlreichen Neuerungen zu schaffen, die auf diesem Gebiet im Rahmen der Forschungsarbeit erreicht wurden. Das Kapitel beginnt mit einer Retrospektive der Entwicklung der Vulcain-Turbinen, die für die Arbeit instruktiv war. Im Folgenden werden Methoden und Ziele der Profilgestaltung parallel diskutiert. Ein Abschnitt, der sich mit Gestaltungselementen von Statorprofilen befasst, schließt mit der Beschreibung einer parametrischen Profilgeometrie ab, deren Optimierung später im Kapitel auch diskutiert wird. Es findet auch eine Diskussion von Gestaltungselementen von Rotorschaukeln statt, und es wird auch hier

eine parametrische Darstellung vorgeschlagen.

Für zwei wichtige Gestaltungsparameter, dem Stafflungswinkel und dem Flächenverhältnis des Düsenhalses, werden neue Abschätzungsmethoden vorgestellt. Außerdem werden “Schönheits”-Parameter (“fairness”) als Möglichkeit der Schaufeloptimierung ohne großen Rechenaufwand eingeführt.

Ein weiterer Abschnitt betrifft Methoden der dreidimensionalen Gestaltung von Schaufelmantelflächen. Hierzu wird, basierend auf den Ergebnissen der zweidimensionalen Profilgestaltung, eine Methode der Übertragung eines Profils in die Dreidimensionalität dargestellt, die einige Probleme der ebenfalls diskutierten konventionellen Verfahren umgeht. Insbesondere können gleichzeitig sowohl die Länge des Profils als auch die wichtigen Schaufelwinkel, (zum Beispiel am Eintritt, im Hals und am Austritt) unverzerrt erhalten bleiben.

Daraufhin wird eine erste Optimierungsstudie zusammengefasst, in der die zuvor erwähnte parametrische Darstellung des Statorprofils optimiert wurde. Eine Nachrechnung der transienten Strömung zeigt für das optimierte Profil, gegenüber einer zuvor eingesetzten Turbine, eine geringere Lastamplitude auf die Rotorschaufeln und eine erhöhte Gesamteffizienz der Turbine auf. Das Kapitel schließt mit einer Diskussion über die möglichen Implikationen, die die Optimierungsergebnisse für die Entwicklung von neuen Statorschaufeln hat.

Das vierte Kapitel stellt einen neuen Aufbau für eine Linearkaskade dar, mit der unter geringem Aufwand die Strömung durch Statorschaufelkanäle bei Überschall visualisiert werden kann. Hierzu wurde eine permeable Abtrennung so angeordnet, dass die Strömung selbst eine Absaugung durch die Abtrennung induziert. Somit wird die Reflektion von Stößen im Austritt stark reduziert.

Abstract

This thesis concerns supersonic turbines as they are used in turbopumps of rocket engines. Other applications of supersonic turbines, such as in Organic Rankine cycle facilities, are not explicitly discussed, but some results will be transferable to those.

The substance of this thesis is laid out in three chapters. The first of these (chapter 2) concerns the basic thermodynamics of gas-driven turbines in general. This supplements textbook explanations of the same topic, which commonly focus on highly efficient low specific work turbines. Problems of the predesign of supersonic turbines which are explainable in terms of a simple mean-line model are discussed here. To this end, the chapter also contains a discussion of the fundamental method of power generation in a turbine and its connection to common measures of efficiency.

A section discusses different definitions of the degree of reaction. Various definitions of this term are used interchangeably in textbooks, as they are numerically similar in highly efficient turbine stages. With lower efficiency the definitions tend to diverge, which necessitates a more precise study of the quantities in question.

A typical problem of supersonic turbines in smaller rocket engines is low volume flow, which leads to insufficient blade height. Several solution strategies for this issue are discussed on the basis of thermodynamics. The chapter closes with some computational simulations illustrating the inherent limitations of mean-line thermodynamics in describing supersonic turbines.

The third and most extensive chapter discusses various aspects of blade generation for nozzle and rotor blades, as context for the various innovations achieved in these matters in the course of the research for this thesis. The chapter opens with a retrospective of the well-documented development of the turbines for the Vulcain and Vulcain 2 engines, which was instructive for the efforts in this work. In the following, means and ends of profile design are discussed in parallel. A section concerning the shape of nozzle blades closes with the description of a proposed blade geometry. The previously published optimization of this geometry is likewise discussed in this chapter. There is also a discussion of the design of rotor profiles. Here as well, a parametric representation is proposed.

Another section concerns methods to generate three-dimensional blade geometries for

blade mantle surfaces. Based on the previous results in two-dimensional profile design, a method is proposed to transfer these profiles into a three-dimensional space. This avoids issues of conventional methods, that are also discussed in the section. Specifically, both the relevant length parameters as well as the relevant blade angles (for example in inlet, throat and outlet) are preserved without distortion.

New estimation methods are described for two key parameters, the stagger angle and the throat area ratio. Further, the possibility of using “fairness”-variables as a computationally inexpensive means to reduce the number of open parameters is discussed.

Finally, an optimization study is summarized in which the parameters of the previously mentioned representation of nozzle blades are optimized using computational simulations. In a transient follow-up simulation, increased efficiency and decreased rotor load amplitude was predicted when compared to a flight-proven turbine. The chapter closes with a discussion of the possible implications these optimization results have for the development of future nozzle blades.

In the fourth chapter, a new configuration for a linear cascade experiment is presented, that allows the visualization of supersonic internal flow in the blade channels at reduced effort. To this end a permeable separator is arranged in such a manner that the flow itself induces a suction flow through the separator. Thereby, the reflection of shocks in the outlet flow is greatly reduced.

1. Introduction

Turbines in general are components that draw energy from a flow by redirecting it in a rotor. Given a set of flow angles of this redirection, the faster the flow, the more energy will be extracted. For turbines in commercial airplanes or power plants, efficiency is of overriding importance. This requirement is at odds with the desire for higher power when flow velocities reach supersonic speed, as gas dynamic effects cause an increase in losses.

In rocket engine turbopumps, turbine efficiency is often not a relevant factor in the overall vehicle performance, and thus supersonic gas velocities in the turbine are a practical option. The central matter of this thesis is the description of the consequences this choice has on the design of the turbine.

The second chapter will discuss what implications result from the desire for high specific work for the predesign of turbines, and also critically discusses the validity of predesign models when used to describe gasses at supersonic velocities. The third chapter describes the specific challenges that occur in blade shaping and how to address them. The fourth chapter discusses how blades in supersonic flow can be tested in a cost-effective manner.

The specific subject of supersonic turbines is far less studied than that of subsonic turbines and many of the present studies are conducted for a very specific purpose, giving only a narrow window into the complexities of these turbines. Thus, a lack of context is a large obstacle to understanding their significance in the overall design process.

The most extensive known systematic description of supersonic turbine design methodology comes from the Soviet Union, where authors such as Dejc and Trojanovskij^[13,14] summarized developments of different design bureaus and universities in order to create a canonized method for designing turbines. These sources do not provide a complete picture either because they are largely based on a specific set of profiles developed at the time.

Therefore, a central element of this thesis will be to provide as much context for the understanding of supersonic turbines as possible. Gaining an understanding from three main kinds of sources, those on subsonic turbines, those on specific supersonic turbines and those on Soviet design methodology, was an exercise in assembling and aligning information. To resolve any conflicts between them and help advance the scientific understanding of the topic, implicit limitations and assumptions of common design methods are made explicit

here by cross-referencing material from multiple sources.

This general framework is also necessary to motivate the specific advancements made in the course of this dissertation. The largest of those are the technique of designing new profile parameter systems described in section 3.4, the new method of 3D blade generation described in section 3.6 and the newly refined cascade testing methodology described in chapter 4. There are likewise descriptions of several other contributions, such as the new or refined methods to estimate key parameters analytically as documented in section 3.5.

1.1. Definition of Transonic and Supersonic Turbines

The designation “supersonic turbine”, as used in the title of this thesis, is somewhat ambiguous. This semantic question is relevant here insofar as it defines the scope of this thesis. The following properties of a turbine could be used to distinguish between supersonic and subsonic turbines.

1. Supersonic outlet flow in the first stage nozzle exit
2. Supersonic flow in the rotor relative frame
3. Meridional flow velocity component higher than the speed of sound
4. First stage nozzle with convergent-divergent shape

Sometimes turbines fulfilling some, but not all of these criteria have been called “transonic” turbines.

As an example, the “supersonic” M1 Turbine has a nozzle outlet Mach number of 1.3^[42], but a strong shock exists in the rotor inlet. The resulting rotor inlet Mach number after the shock is not homogeneous, but mostly subsonic in the rotor relative frame, so only conditions 1 and 4 are met.

Giles describes a turbine of similar Mach number, but a strictly convergent nozzle, as transonic^[25]. On the other end, Mee describes a generally subsonic turbine with only small supersonic flow regions on the nozzle suction side (buffeting) as “transonic”^[63].

Griffin et al. optimized a turbine blade geometry and starting with a convergent-divergent nozzle shape, they arrived at a strictly convergent shape^[38], although average Mach numbers remained unchanged. By definition 4 this would indicate that the result is not a supersonic turbine.

Simulations of the Vulcain 2 Turbine Oxygen Turbopump turbine indicate that there are substantial regions of subsonic flow even in a turbine with a relative rotor inlet Mach number of about 1.5^[44].

In conclusion, the labels “subsonic”, “transonic” and “supersonic” turbine have no known agreed-upon borders, and the terms have a large amount of overlap in their meaning. To simplify the issue, any turbine fulfilling criteria 1 will be called supersonic, because it is at this point that supersonic phenomena, which are discussed in some detail in chapter 3 become central to the blade shaping. There will therefore be no further distinction of transonic turbines.

A Selection of Variables

A, B	placeholder for an arbitrary station from 1 to 4, or total stations 01 to 04
c_p	heat capacity at constant pressure
d_{As}	shroud diameters
d_{Ah}	hub diameters
d_m	stage middle diameter $d_m \stackrel{!}{=} \frac{d_{h1} + d_{s1}}{2}$
h_A	static enthalpy at station A
h_{0A}	total enthalpy at station A
\dot{m}	mass flow per second
p	pressure
P	power output
P_n	profile junction point n
R	degree of reaction $R = \frac{h_4 - h_3}{\Delta h_{01 \rightarrow 04}}$
R_s	substance-specific ideal gas constant
$\Delta h_{A \rightarrow B}$	specific work between the stations A and B
$\Delta h_{A \rightarrow B, is}$	isentropic work between the thermodynamic stations A and B
α	flow angle in the absolute frame
α'	flow angle in the relative frame
β	blade angle
ζ	degree of admission
η	efficiency
κ	isentropic exponent
ρ	specific density
ϕ	blade stagger angle
ω	rotational speed

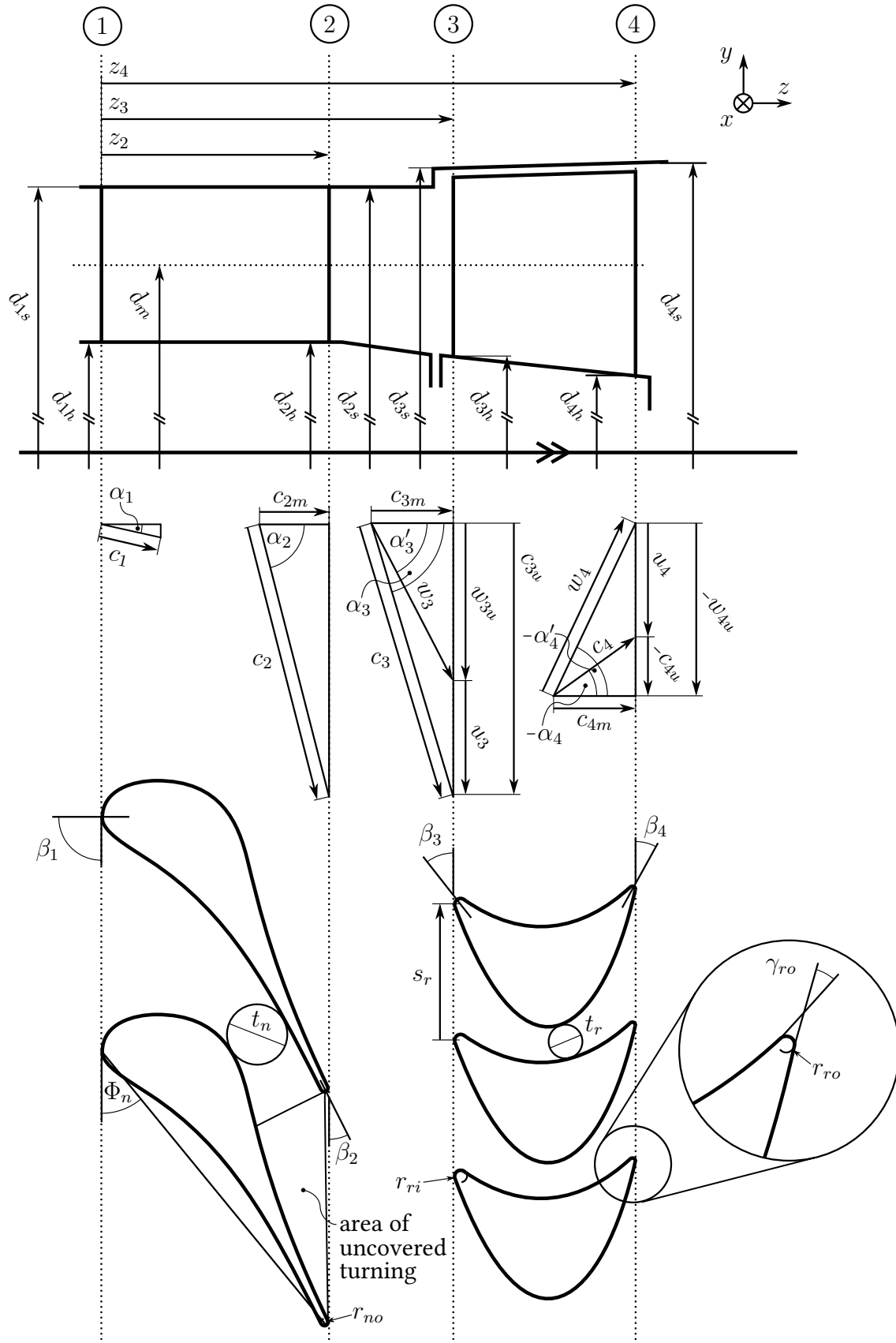


Figure 1.1.: Nomenclature

2. Thermodynamics and Mean-Line Models of Turbines

The thermodynamic model of turbines assumes the existence of locations along the turbine where the flow has well-defined thermodynamic states (“stations”) as a vehicle for their understanding. For the purposes of this thesis, figure 1.1 shows the assumed locations of all stations used here. These are:

1. Immediately upstream of nozzle inlet
2. Immediately downstream of nozzle outlet
3. Immediately upstream of rotor inlet
4. Immediately downstream of rotor outlet

It should stand out that the enumeration above describes locations as “immediately upstream” or “immediately downstream”, without a precise definition of the word “immediately”. The reasons for this is that this “mean-line model” represents an idealized turbine in which some aspects of a turbine are represented, while others are not. Especially in a supersonic turbine it is important to understand the stations as locations in a model, not locations in any physical reality. The model is applicable in system development and turbine pre-design without being an entirely accurate representation of the actual flow phenomena. This chapter will close with a discussion of these limitations and their influence on the model’s usefulness, section 2.6.

2.1. Useful Work in Turbines

As mentioned in the introduction, turbines draw power from a fluid by redirecting it in a rotor. Gas-driven turbines usually operate by converting some thermal energy of the fluid to movement energy by expansion in a nozzle and simultaneously, in a rotor, transferring part of this movement energy onto a shaft. More specifically, the nozzle releases a flow of

gas onto the rotor with mainly two velocity components: the meridional component c_m and the tangential component c_u . The useful work per massflow (“specific work”) Δh_{use} in a turbine stage with the circumferential velocity u is given by Euler’s turbomachine formula^[98]:

$$\Delta h_{use} = c_{3u}u_3 - c_{4u}u_4 \quad (2.1)$$

With

Δh_{use} specific work drawn from the fluid
(velocities defined in figure 1.1)

The absence of any term relating to the meridional velocity c_m reveals that only the tangential velocity component c_u directly contributes to the turbine stage’s useful work, and a larger difference between the terms c_{3u} and c_{4u} means that more work is extracted in the rotor. In other words, if the redirection in the rotor is larger, the specific work of a turbine stage is larger as well.

A simple estimation for a turbine that operates efficiently at high specific work is made by using the following assumptions:

1. The meridional speed c_m is constant
2. The diameter d_m is constant between the stations - i.e. u is constant
3. The relative tangential velocities w_{3u} and w_{4u} , are equal and opposite, i.e. $w_{4u} = -w_{3u}$

Relationships between relative velocities w and absolute velocities c are read off figure 1.1.

$$\begin{aligned} c_{3u} &= w_{3u} + u \\ -w_{4u} &= u + (-c_{4u}) \\ \Leftrightarrow c_{4u} &= w_{4u} + u \end{aligned}$$

With the assumption number 3 ($w_{4u} = -w_{3u}$), c_{4u} in terms of c_{3u} is

$$\begin{aligned} c_{3u} &= -w_{4u} + u \\ &= (u - c_{4u}) + u \end{aligned}$$

$$c_{3u} = -c_{4u} + 2u$$

Inserted into Euler's equation, this yields:

$$\begin{aligned}\Delta h_{\text{use}} &= u(c_{3u} - c_{4u}) \\ &= u((-c_{4u} + 2u) - c_{4u}) \\ \Delta h_{\text{use}} &= 2u^2 - 2c_{4u}u\end{aligned}\tag{2.2}$$

$$\Delta h_{\text{use}} = 2c_{3u}u - 2u^2\tag{2.3}$$

$$u = d_m\pi\omega\tag{2.4}$$

With

d_m mean diameter

ω rotational speed

Equation 2.2 is significant in the very earliest steps of turbine design, because it relates the power requirement to the rotational speed. If the rotational speed is dictated by cavitation in the pump inducer, and the mean radius is estimated from structural or space consideration, the circumferential velocity u is predetermined (see equation 2.4). With u known, equations 2.2 and 2.3 allow making two independent observations.

Equation 2.3 makes a statement about the maximum expected velocities in the turbine stage, and thus determines whether a supersonic Mach number will be necessary. As established above, a turbine stage optimized for maximum specific work, rather than maximum efficiency, will have as much flow redirection as possible. This means that α_3 will be as close to a right angle as possible, which in turn means that the blade angle β_2 will be as small as possible. Lower angles carry higher risk of flow detachment, so a small range from 17° ^[102] to 14.5° ^[42] is commonly used, with extreme designs going down to 8° ^[37]. Assuming a value of 15° , c_3 is calculated as $c_3 = c_{3u} \cdot 1/\cos(15^\circ) = c_{3u} \cdot 1.04$. Knowing the inlet conditions and the heat capacity of the fluid, the temperature in station 3 is determined by subtracting the movement energy $1/2c_3^2$ from the inlet total enthalpy. This allows calculation of the speed of sound and with it, the required Mach number.

An Example

A single stage hydrogen/oxygen gas generator turbine operating with the following characteristics:

The required specific power is

	value	unit
T_{01}	875	K
d_m	0.323	m
ω	221.5	1/s
P	3076	kW
\dot{m}	2.70	kg/s
κ	1.37	-
c_p	8.1	kJ/kgK
M	3.83	kg/kmol

Table 2.3.: Example requirements of a turbine, similar to the Vulcain LOX turbine^[102]

$$\begin{aligned}
\Delta h_{\text{use}} &= \frac{P}{\dot{m}} \\
&= \frac{3076 \text{ kW}}{2.7 \frac{\text{kg}}{\text{s}}} \\
&= 1139 \frac{\text{kJ}}{\text{kg}}
\end{aligned}$$

From equation 2.3

$$\begin{aligned}
\Delta h_{\text{use}} &= 2c_{3u}u - 2u^2 \\
c_{3u} &= \frac{\Delta h_{\text{use}}}{2u} + u \\
c_{3u} &= \frac{1139 \frac{\text{kJ}}{\text{kg}}}{2 \cdot 224.8 \frac{\text{m}}{\text{s}}} + 224.8 \frac{\text{m}}{\text{s}} \\
&= 2758 \frac{\text{m}}{\text{s}} \tag{2.5}
\end{aligned}$$

Assuming $\beta_2 = 15^\circ$ nozzle outlet angle, no flow deviation and no change in flow direction between stations 2 and 3

$$\begin{aligned}
c_3 &= \frac{c_{3u}}{\cos(15^\circ)} = \frac{2758 \frac{\text{m}}{\text{s}}}{\cos(15^\circ)} \\
&= 2856 \frac{\text{m}}{\text{s}}
\end{aligned}$$

$$T_3 = T_{01} - \frac{\frac{1}{2}c_3^2}{c_p}$$

$$\begin{aligned}
&= 875\text{K} - \frac{\frac{1}{2} \left(2856 \frac{\text{m}}{\text{s}} \right)^2}{8.1 \frac{\text{kJ}}{\text{kgK}}} \\
&= 623.3\text{K} \\
a_3 &= \sqrt{\kappa \frac{R}{M} T} = 1360 \frac{\text{m}}{\text{s}} \\
M_3 &= \frac{c_3}{a_3} \\
M_3 &= \underline{\underline{2.1}} \tag{2.6}
\end{aligned}$$

Equation 2.6 shows that in order to extract the required specific work from the flow in one turbine stage, with the given assumptions, the lowest possible nozzle outlet Mach number is 2.1. The input data shown in table 2.3 was based on the design of the Vulcain engine oxygen turbopump turbine, as documented by Wåhlén^[102], who presented a design with a slightly higher nozzle outlet Mach number of 2.4, due to the fact that the initial assumption number 3 was not the design that was ultimately chosen. The implications of this are further discussed in section 2.3.

Since this calculation, based a perfect gas model, does not include any pressure, it is thus independent of efficiency. To someone unfamiliar with efficiencies in turbomachines, it may come as a surprise that efficiency is not directly dependent on velocities, although the energy is extracted by means of a velocity change. Instead, efficiency is based on the preventable loss of pressure in the stage, as will be elaborated on in the following.

2.2. Efficiency in Turbine Stages

Efficiency, in the most general terms, is defined by a division with some form of gain as the numerator and a cost as the denominator (gain/cost).

Defining the efficiency of a turbine is not as straightforward as it may be for other machines. For example, a car engine receives a certain amount of chemical energy in the form of fuel per second and releases a lower amount of mechanical power. By the same logic, the turbine receives thermal energy and releases mechanical power. However, turbines do not lose significant amounts of heat between inlet and outlet. Therefore, the only way for heat to leave the gas flow is in the form of mechanical energy through the rotor. An efficiency simply defined as useful work/(heat out – heat in) will therefore always be 1, making no determination of the turbine's actual performance.

In whole turbine stages or rotor rows, the numerator may be calculated from the torque

on the shaft as follows:

$$\text{useful work} = \Delta h_{01 \rightarrow 04} = \Delta h_{03 \rightarrow 04} \quad (2.7)$$

$$P = \tau \cdot \omega \quad (2.8)$$

$$\Delta h_{01 \rightarrow 04} = \frac{P}{\dot{m}} \quad (2.9)$$

$$\Delta h_{01 \rightarrow 04} = \frac{\tau \cdot \omega}{\dot{m}} \quad (2.10)$$

With

P useful power

τ torque on the Shaft

It can also be determined from the difference in total temperature of inlet and outlet flow, but in this case, more care must be taken when calculating an average value (time-average and mass-flow-average), in order to avoid possible problems with the respective equation of state (see section 2.6).

For nozzle rows, the useful specific work does not have a generally accepted definition. However, the movement energy contained in the tangential component of the outlet gas flow appears to be a good choice because it allows comparisons between turbines of different outlet flow angle. If the entire movement energy was used, profiles with a smaller outlet flow angle α_2 could get an unintended advantage.

$$h_{\text{use, nozzle row}} = \frac{1}{2} c_{2u}^2 \quad (2.11)$$

With

c_{2u} tangential velocity component in the nozzle row outlet

In discussions of the denominator, the principle difference between *isentropic work* and *polytropic work* must be considered. It is a topic about which there is a considerable amount of confusion, possibly because some discussions of it insufficiently differentiate between exact and approximate solutions or equations that are general and those that are specific to ideal gasses^[8]. Appendix A addresses these questions in detail. For reasons given in that appendix, polytropic work is usually the preferable option.

Both of these ideal processes, as all thermodynamic processes, have a starting point (A) and an end point (B), and in turbines there are two commonly options for the states A and B . In *total-to-total efficiency* calculations, A is the total state at station 1, here called state 01, and the B is the total state at station 4, i.e. 04. In *total-to-static efficiency* calculations,

the state B is the static state in station 4.

While the practical difference between the isentropic and polytropic efficiency is in exchanging simplicity (isentropic) for generality (polytropic), the decision of whether to use total-to-total or total-to-static efficiencies must be made based on the specific use case of the turbine in question. Usage of total-to-static efficiency implies that the dynamic pressure in the outlet of the stage is considered completely lost, while total-to-total efficiency indicates that it is completely recoverable.

When considering a stage in a multi-stage turbine, for example, it is reasonable to work with total-to-total efficiency, as the flow velocity in the outlet of one stage can immediately be used in the next stage. However, in a different situation, a turbine exhaust may be connected by piping to some other component using the gas further, such as an auxiliary nozzle or a different turbine. In such a case, one should assume a worst-case, which is that all dynamic pressure is lost, and only the remaining static pressure is usable further downstream. Hence, a total-to-static efficiency should be chosen, unless the pressure recovery can be estimated.

Specifically for some rocket engine turbines, another way to define efficiency may be introduced, the *total-to-ambient isentropic efficiency*. The rationale for this definition of efficiency is as follows:

Certain types of rocket engines have turbine inlet pressures that are dictated by components other than the turbine. For example, in LUMEN (Liquid Upper-Stage Demonstrator Engine) the gas from the thrust chamber cooling channels is partly used for driving the turbines and partly injected into the combustion chamber^[41]. Therefore, the turbine inlet gas pressure needs to be much higher than the combustion chamber pressure. Further, the turbine outlet gas flow is not used in the cycle, so it only needs to keep a stability margin to the ambient pressure. Therefore, there is a largest specific work that a turbine could possibly extract. This work is the isentropic work between the inlet state and the lowest acceptable outlet pressure. This is an absolute measure of efficiency for such a turbine.

$$\begin{aligned}
 \frac{T_{\text{amb,is}}}{T_{01}} &= \left(\frac{p_{\text{amb}}}{p_{01}} \right)^{\frac{\gamma-1}{\gamma}} \\
 T_{\text{amb,is}} &= T_{01} \left(\frac{p_{\text{amb}}}{p_{01}} \right)^{\frac{\gamma-1}{\gamma}} \\
 \Delta h_{01 \rightarrow \text{amb,is}} &= c_p (T_{\text{amb,is}} - T_{01}) \\
 \eta_{\text{is,ta}} &= \frac{\Delta h_{\text{use}}}{\Delta h_{01 \rightarrow \text{amb,is}}}
 \end{aligned} \tag{2.12}$$

With

- Δh_{use} useful enthalpy change
- $\Delta h_{01 \rightarrow \text{amb}, \text{is}}$ isentropic heat change between the turbine inlet state and the minimum required outlet pressure
- $\eta_{\text{is}, \text{ta}}$ isentropic total-to-ambient efficiency

The main advantage of this definition is that different designs of turbine can be compared by efficiency. Using the measures described earlier, a turbine that uses only a small part of the available pressure ratio may be much more efficient than one that uses a larger part of the pressure ratio. However, since the pressure ratio used in the turbine is not relevant to the overall function of the engine (so long as the minimum outlet pressure is maintained) all that really matters to the engine cycle is the amount of work extracted. The absolute maximum of work that can possibly be extracted is the isentropic total-to-ambient work $\Delta h_{01 \rightarrow \text{amb}, \text{is}}$. A turbine could therefore be considered efficient solely based on the useful fraction of this work.

2.3. Degree of Reaction

The degree of reaction is colloquially understood as a ratio of how much of the thermodynamic change of a stage is accomplished in the rotor compared to the stage as a whole. However, there are different schools of thought regarding which quantity should be used to measure the amount of thermodynamic change. The definition used by Carmichael^[10] and Aungier^[5] is:

$$R = \frac{\Delta h_{3 \rightarrow 4}}{\Delta h_{01 \rightarrow 04}} \quad (2.13)$$

That is, the static enthalpy change in the rotor is compared to the total enthalpy change in the stage, which is equal to $\Delta h_{03 \rightarrow 04}$, since no work is extracted in the nozzle. Dixon^[15] and Yoon^[105] use a variant of this, with the static enthalpy drop in the denominator instead:

$$R_D = \frac{\Delta h_{3 \rightarrow 4}}{\Delta h_{1 \rightarrow 4}} \quad (2.14)$$

Traupel^[98] defines the degree of reaction with the ratio of isentropic work.

$$R_T = \frac{\Delta h_{3 \rightarrow 4, \text{is}}}{\Delta h_{1 \rightarrow 3, \text{is}} + \Delta h_{3 \rightarrow 4, \text{is}}}$$

Cordes^[11] uses a similar definition:

$$R_C = \frac{\Delta h_{3 \rightarrow 4, \text{is}}}{\Delta h_{1 \rightarrow 4, \text{is}}}$$

Dixon further notes the existence of this definition:

$$R_p = \frac{p_3 - p_4}{p_1 - p_4}$$

There is a conceptual difference in the first set of two (R, R_D) compared to the following definitions (R_T, R_C, R_p), in that the first two are directly related to velocities (as described below and by Dixon^[15]) and with that, blade shapes, whereas blade shapes can only be determined from the latter definitions if the efficiency is known. As a matter of nomenclature R and R_D are called *enthalpy-based* definitions here, while R_T, R_C, R_p and others like them are called *pressure-based* definitions of the degree of reaction, taking into account that the isentropic work is a function of the pressure ratio.

For a 100% efficient repeating stage (i.e. stages with the equal inlet and outlet velocities) with perfect gas flow, all these definitions, except R_p , become equal. Since turbine stages for many applications come close to this^[11], the definitions could be used interchangeably for a rough pre-design. However, this is not the case for the high specific work supersonic turbines which are discussed here.

In stages with substantial outlet swirl, the definitions R and R_D are still equal in the case of zero reaction ($\Delta h_{3 \rightarrow 4} = 0$), as the numerator is equal, but differ in all other cases, because the denominator is different by the change in dynamic enthalpy. In rocket turbopumps, stages with very large outlet swirl are not uncommon^[42,102].

The distinction becomes especially important when discussing the limits within which the degree of reaction may be chosen. Conventional wisdom holds that the degree of reaction should not be lower than 0 nor higher than 0.5^[11]. As Dixon^[15] points out, at least the lower limit should only be applied to pressure-based definitions.

An impulse stage is a stage with no pressure change over the rotor^[98]. It is also described as a stage with a low positive or zero degree of reaction^[7]. The two definitions are only equal if a pressure-based definition for the degree of reaction is chosen. If $R = 0$ in a stage affected by losses, there is a decrease of pressure from inefficiency over the rotor. To achieve zero reaction in a pressure-based definition, the flow has to be slowed down in the rotor to compensate the losses.

This would in turn mean that $R < 0$, which is exactly what one finds when applying this definition to real-world examples, such as the Vulcain oxygen-side turbine presented

by Wåhlén^[102]. While precise data is not available for the complete stage design, the value of R is roughly -1, based on the available Mach numbers, while in text, Wåhlén describes the degree of reaction, without specifying the definition, as slightly positive.

In conclusion, enthalpy-based definitions are useful for pre-design, since they allow relating a specific work to a required blade shape, while pressure-based definitions can be used to verify that the resulting design is within empirically established limits of competent turbine design. When the turbine efficiency is predicted to be low, or the outlet flow has significant velocity, it is crucial not to conflate the definitions.

2.3.1. Influence on Gas Velocities

The following derivation serves to illustrate the influence the degree of reaction R has on the speeds in a turbine stage, and by extension, the specific work.

Steps from 2.15 onward assume a constant meridional speed; steps from 2.16 onward assume a constant mean diameter d_m .¹

$$\begin{aligned}
 h_{0A} &= h_A + \frac{1}{2}c_A^2 \\
 h_3 - h_4 &= (h_{03} - \frac{1}{2}c_3^2) - (h_{04} - \frac{1}{2}c_4^2) \\
 &= (h_{03} - h_{04}) - \frac{1}{2}(c_3^2 - c_4^2) \\
 &= (h_{03} - h_{04}) - \frac{1}{2}(c_m^2 + c_{3u}^2 - (c_m^2 + c_{4u}^2)) \quad | c_m = \text{const} \quad (2.15)
 \end{aligned}$$

$$\begin{aligned}
 h_3 - h_4 &= (h_{03} - h_{04}) - \frac{1}{2}(c_{3u}^2 - c_{4u}^2) \\
 R &= \frac{h_{03} - h_{04} - \frac{1}{2}(c_{3u}^2 - c_{4u}^2)}{\Delta h_{01 \rightarrow 04}} \quad | \Delta h_{01 \rightarrow 04} = h_{03} - h_{04} \\
 &= 1 - \frac{c_{3u}^2 - c_{4u}^2}{2(h_{03} - h_{04})} \\
 &= 1 - \frac{(c_{3u} + c_{4u})(c_{3u} - c_{4u})}{2u(c_{3u} - c_{4u})} \quad (2.16)
 \end{aligned}$$

$$\begin{aligned}
 R &= 1 - \frac{c_{3u} + c_{4u}}{2u} \quad (2.17) \\
 &= 1 - \frac{w_{3u} + u + w_{4u} + u}{2u}
 \end{aligned}$$

$$R = -\frac{w_{3u} + w_{4u}}{2u} \quad (2.18)$$

Equation 2.18 is an intuitively understandable formulation for the way that the degree of reaction influences the speeds in the rotor. w_{4u} , the rotor outlet relative tangential speed,

1. Aungier^[5] makes a similar derivation on page 137, but it seems to contain an error in the denominator of his equation (6-4) missing a factor of 2; Dixon^[15] makes similar derivations, but his definition of the degree of reaction differs.

is always negative in high specific work turbines. For $R = 0$, it follows that $|w_{4u}| = |w_{3u}|$, which indicates that the rotor blade profiles have a symmetrical shape, which is another formulation of assumption number 3 from the discussion of useful work in turbines above.

Another conclusion from equation 2.18 is that the degree of reaction R is very sensitive to small design changes in stages with high ratios of tangential velocity w_u to circumferential velocity u . For example, in the Vulcain oxygen turbine^[102], the relative tangential Mach number at the inlet is 2.1 and the outlet tangential Mach number is 1.6. The Mach number of the circumferential velocity u is only about 0.2. If the conventionally accepted range of 0 to 0.5 were applied to R (and changes in temperature are disregarded), the rotor outlet velocity w_4 would have to be chosen in the narrow range between 1 and 1.1 times the inlet velocity w_3 .

2.4. Interaction of Losses and Power Generation

All discussions on velocities up to this point are independent of efficiency so long as losses do not influence the meridional speed. As was discussed in section 2.2, losses in turbine stages lead to a reduced outlet pressure when compared to the outlet pressure of an ideal turbine. The higher the losses, the lower the outlet pressure. To understand the effect this has on the velocities, the continuity equation is required:

$$c_{Am} = \frac{\dot{m}}{\rho_A A_A} \quad (2.19)$$

A loss of pressure causes a decrease in density. For an ideal gas the relation is

$$p_A = \rho_A R_S T_A$$

With

R_S ideal gas constant of the medium

A an arbitrary station 1...4

Together, these two equations indicate that with no changes in flow area, the meridional speed would increase, given a lower pressure. In a turbine, there is the option to enlarge the flow area by increasing the shroud radius or reducing the hub radius in the blade row outlet, and thereby holding the meridional speed constant^[5]. Using the computational methods laid out by Aungier^[5], it is possible to quickly simulate a large number of such configurations. In turbines with large losses, such an analysis would indicate that large flare angles

ϵ are necessary. In reality, large flare angles may cause additional losses of their own, due to the additionally needed radial redirection, which is counter to the design intent. Known supersonic turbines have small flare angles^[42] or none at all^[102].

As losses manifest as a decrease in pressure, they influence primarily the meridional velocity component, and other velocity components only indirectly. Whether and how power generation, involving tangential velocities, is affected depends on the design of the turbine.

While this means that, at least at the pre-design stage, pressure loss and power generation may be addressed separately, the dynamic pressure of the outlet swirl (i.e. the tangential velocity at the turbine outlet, c_{4u}) may also have to be considered a loss, and it is linked to the required specific work. Turbine stages in conventional applications, such as aircraft and power plants, are primarily designed to achieve high efficiency, and thus have little outlet swirl^[5]. However, high efficiency is not always possible in high specific work turbines.

In the example given on page 19, the required mass-flow-specific work is 1 139 kJ/kg. Assuming no outlet swirl ($c_{4u} = 0$), zero degree of reaction ($R = 0$), and constant meridional velocity, equation 2.17 yields the following:

$$\begin{aligned} R &= 1 - \frac{c_{3u} + c_{4u}}{2u} \\ 0 &= 1 - \frac{c_{3u}}{2u} \\ c_{3u} &= 2u \\ \Delta h_{01 \rightarrow 04} &= c_{3u}u = 2u^2 = 2 \cdot (224.8 \frac{m}{s})^2 = 101 \frac{kJ}{kg} \end{aligned} \quad (2.20)$$

Equation 2.20 indicates that with the given assumptions, a turbine stage with no exit swirl can only produce $2u^2$ in specific power, which in this example is not even one tenth of the required power. To mitigate this, some of the initial assumptions must be lifted. As mentioned before, the degree of reaction R may be negative, so long as R_p stays positive^[15]. Even at $R \approx -1$, this will not make up for the majority of the discrepancy. The outlet swirl condition must also be lifted, so that the outlet flow is a fast swirling fluid.

In the final design of the Vulcain oxygen turbine, the outlet tangential Mach number is 1.4^[102]. While there are two rows of guide vanes and a diffuser downstream of the turbine to recuperate some of the associated dynamic pressure, a large part of it will be lost^[102].

One way to achieve higher efficiencies is to add an additional stage, which means that much more specific energy is extracted without introducing exit swirl. This is the solution that was implemented in the Vulcain 2 Oxygen turbine^[100].

If a turbine is designed to have a low degree of admission, the additional windage losses

may largely negate the gains of an additional stage^[13,98]. In this case, adding a second stage is not an option.

The last option is to increase the circumferential velocity u , which may be done by increasing the rotational speed ω or the mean diameter d_m . Increasing the rotational speed increases the required net positive suction head of the pump^[20], which would increase the tank pressure, requiring stronger tank walls. This in turn would likely increase the tank weight, which is a major contributor to the overall vehicle mass. Therefore, increasing the rotational speed is unlikely to be an option for mitigating a turbine component problem.

This leaves a larger mean diameter d_m as a possible way to create a greater circumferential velocity. Several considerations need to be taken into account to determine if this is possible. A larger mean blade diameter would lead to a larger disk, which would increase the rotor's weight as well as its moment of inertia. Both of these reduce the rotor's critical frequencies^[101]. An analysis of rotordynamics is required to check if any problems arise from this.

A larger disk will also create greater axial thrust given equal pressure difference $p_3 - p_4$, which must either be born by the bearings, or an adequately designed thrust compensation. Furthermore, a larger disk may not fit in the specified physical envelope of the engine power pack, especially if it is much larger than the pump and volute on the other side of the machine. Lastly, a larger disk causes a lower blade height, or lower degree of admission, as will be discussed in the next section.

2.5. Blade and Channel Height

Turbines for smaller rocket engines sometimes run into problems of insufficient blade height due to a low design mass flow. Short blades mean that the channel is very narrow, leading to proportionally large boundary layers at the shroud and hub. The reason this occurs is the following:

In so-called "open cycle rocket engines", the gas used to drive the turbine is not injected into the main combustion chamber after passing through the turbines, but ejected from the engine at a lower velocity than the main chamber combustion gasses. The higher the mass flow through the turbine is, the lower the average velocity of all gasses leaving the rocket. Since the required fuel mass for an orbital maneuver depends on the average velocity of the ejected gas, decreasing the turbine mass flow and thereby increasing the average velocity is beneficial for overall vehicle performance^[82].

Blade height is especially important for the rotor, because tip leakage plays a larger role in short blades, since gaps do not scale proportionally with the blade height. Unshrouded

radially milled rotors offer lower manufacturing cost than shrouded rotors^[48], but have even more tip leakage^[5], which may induce rotordynamic oscillations as well^[89].

The blade height is easily calculated from the continuity equation (2.19)

$$\begin{aligned}
c_{Am} &= \frac{\dot{m}}{\rho_A A_A} \\
A_A &= \zeta \pi \frac{d_{As}^2 - d_{Ah}^2}{4} \\
A_A &= \zeta \pi \frac{(d_{Am} + H_A)^2 - (d_{Am} - H_A)^2}{4} \\
A_A &= \zeta \pi d_{Am} H_A \\
H_A &= \frac{\dot{m}}{\zeta \rho_A c_{Am} d_{Am}}
\end{aligned} \tag{2.21}$$

With

ζ degree of admission

A annulus area

H blade height

A an arbitrary station 1...4

While the lowest acceptable blade height depends on a number of factors, such as the achievable clearance, the desired efficiency, and the blade tip design, NASA Monograph SP-8107 recommends not building blades smaller than 3.8 mm^[82]. Equation 2.21 gives a number of ways that blade height may be increased, given a certain mass flow and specific work requirement.

1. Reducing the Mean Diameter d_{Am}

Reducing the mean blade diameter increases the blade height, but leads to more outlet swirl in high specific work turbines, as discussed above.

2. Reducing the Meridional Velocity c_{Am}

The meridional velocity changes with the blade angles, if the blade is adequately designed to expand and redirect the flow without separation. Choosing a low nozzle outlet angle β_2 , gives a low ratio of meridional to tangential velocity $\frac{c_{2m}}{c_{2u}}$. This means that the blade height is increased. Achievable outlet angles depend on the blading methods chosen. Circular cross-section nozzles are not viable for small outlet angles^[87]. Conventional nozzle profiles have outlet angles β_2 around 15°^[42], but single-digit outlet angles can be achieved with specially developed blading^[87], as was done for STME TPO^[76]. These issues will be further discussed in chapter 3.

3. Reducing the Degree of Admission ζ

A reduced arc of admission is a well documented technique for increasing the blade height^[98]. While efficiency decreases with lowering degree of admission^[56], the exact penalty is hard to predict. Dejc and Trojanovskij^[13] present a variety of correlations, but caution that there was still a great deal of uncertainty, which seems to be the case even now.

4. Reducing the Density ρ_A

Since the tip leakage makes blade height especially critical for the rotor, increasing the rotor blade height is more important than increasing the nozzle height. To that end, one can reduce the degree of reaction R_p . If less of the stage pressure drop is expanded in the rotor, then more must be expanded in the nozzle, i.e. before the rotor. This decreases the pressure in the rotor inlet, which decreases the density.

A separate way to decrease the density exists in the Mach-Number-Area-Relation. In point 2 it was stated that the meridional speed may be reduced to increase the blade height, by choosing a steeper nozzle outlet angle β_2 . This is true, so long as the meridional velocity component is subsonic. With every increase in outlet angle, the Mach number increases, which means that the gas becomes less dense. If the expansion is beyond the point where the meridional velocity component becomes supersonic, the overall expression $\rho_2 c_{2m}$ (i.e. the mass flow density) starts to decrease, because with increasing Mach number, the density ρ_2 decreases so fast that it overcomes the increase in c_{2m} .

Figure 2.1 gives an overview of this situation. While the numerical values are just an example, the principle works independent of the choice of perfect gas parameters. To take just one value, the overall design of a turbine stage could call for a nozzle outlet tangential velocity c_{2u} of 565 m/s and the minimum blade height and mass flow could dictate that the massflow density cannot be higher than 200 kg/m²s. A 10° outlet angle profile could be used to meet the criteria, but this is technologically challenging. The same criteria could also be met with a 45° profile.

The key difference in the solution involving the 45° profile is that a large meridional Mach number is generated along with the tangential velocity. This additional velocity component cannot be used to generate useful work, as the work in a turbine is not directly influenced by the meridional component. In the example, the meridional Mach number for the 10° case is 0.27, while it is 1.96 if the 45° profile is chosen.

While the additional required expansion is a considerable cost for the engine cycle, it may be reasonable in some special cases, such as a multi-staged supersonic turbine, where the velocity is used for more than one stage, or in cases where the no axial subsonic turbine

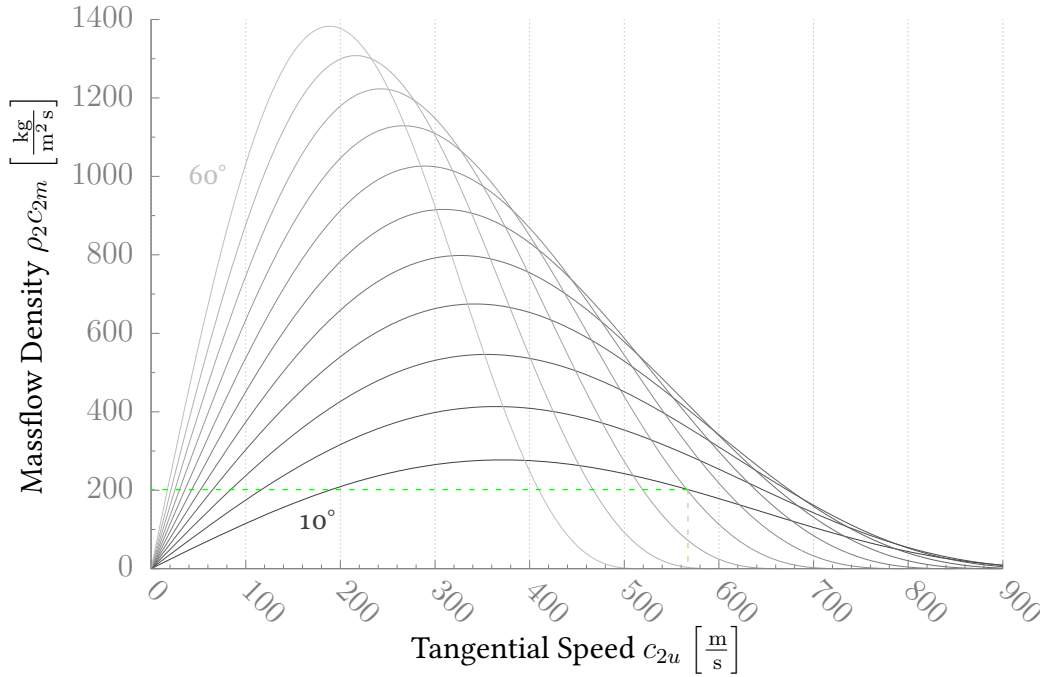


Figure 2.1.: Mass flow density plotted over tangential velocity for 11 different nozzle angles from 10° to 60° , in 5° increments (perfect gas nitrogen expanded from $T_0 = 500\text{K}$, $p_0 = 1\text{MPa}$, $\eta_p = 0.85$)

can be made to meet the required blade height. In such a case, the diffuser behind the turbine should be given focus in development, so that as much of the dynamic pressure as possible is recuperated^[100].

2.6. Limitations of Mean-Line Models

The often used model described in this chapter so far has a key assumption, which Dixon names explicitly: Blade-To-Blade differences within one station must be small^[15]. In supersonic turbines this is not necessarily the case. Especially if there are shocks crossing one of the stations, thermodynamic variables are often very different within one plane.

The first problem with this kind of non-uniformity is that equations of state are no longer exact, when applied to averages. While per definition, in an ideal gas $p = \rho RT$ ^[5] is always true, this equation does not hold if p, ρ and T are averages taken over disparate values. If a mass-flow weighted average is taken, the difference between the left and right side of the ideal gas equation of state in the plane pictured in figure 2.2 is about 1.5%. This equals the stated uncertainty in the efficiency prediction of the mean-line loss model by Kacker-Okapuu^[50], which is widely used^[5,15].

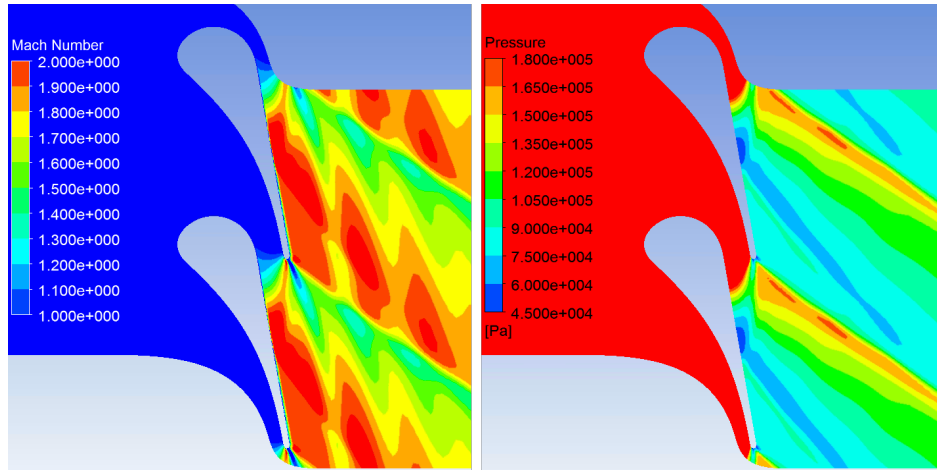


Figure 2.2.: Ideal gas simulation of a periodic linear cascade with convergent nozzle profiles ($\beta_2 = 10^\circ$) at supersonic exit velocity

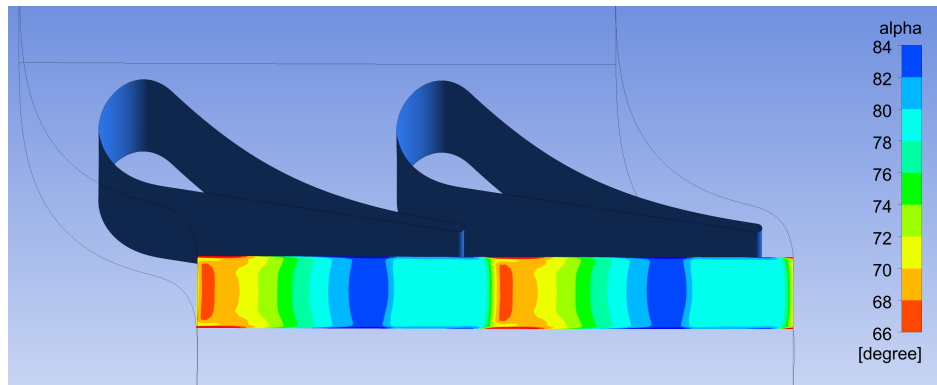


Figure 2.3.: Distribution of outlet flow angle in the same cascade as is pictured in figure 2.2

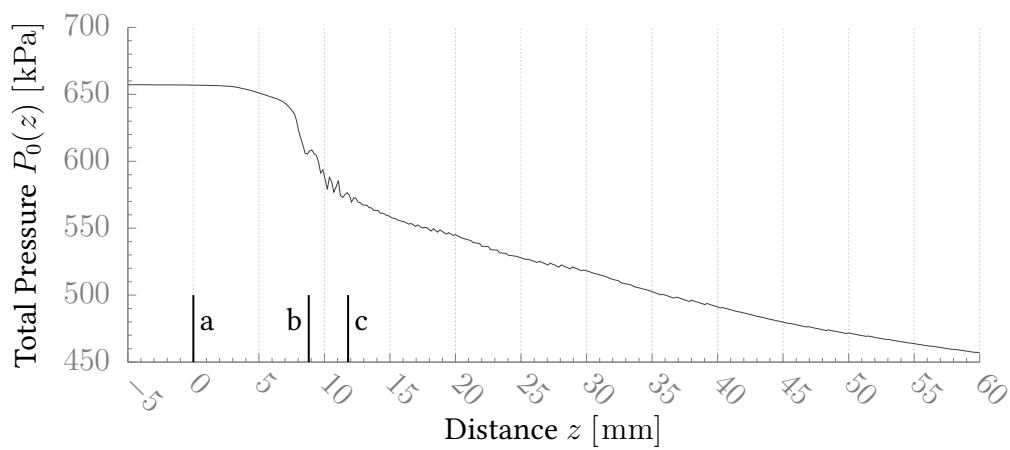


Figure 2.4.: Massflow-weighted average of total pressure over z -location

Another issue is the selection of a fitting rotor inlet angle, which depends on the nozzle outlet angle. Figure 2.3 shows the distribution of flow angle α in the nozzle outlet. The massflow-weighted average would be 74.85° , but this value only exists in a narrow band of grass-green color. The half of the mass flow that has a steeper outlet angle is largely parallel to the $\beta_2 = 10^\circ$ suction side (ergo $\alpha = 80^\circ$), and the other half of the mass flow is concentrated in the expansion fan near the trailing edge. No mean-line model is known to include a variable that accounts for this divergence in the outlet angle, when calculating the incidence losses for the rotor.

Lastly, mostly due to the outlet angle of the nozzle, there is a steep gradient of total pressure in the outlet. Figure 2.4 shows this. The locations a and b mark the beginning and end of the nozzle blades. The location b is 3 mm distant from the trailing edge and marks the location of a possible rotor leading edge. This is the location of the plane in figure 2.3.

Stations are a valuable tool for estimating the possible performance of turbines, but their limitations need to be considered when they are being used. Aungier proposed a method to improve upon the accuracy of mean-line models by considering the radial distributions of velocity at each station using a radial equilibrium model^[5]. In this section, several observations were put forth indicating that for a supersonic turbine factors entirely outside of the scope of the station model, such as circumferential velocity differences and averaging issues, generate considerable uncertainty. This puts the value of additional refinements within the scope of a station model into question. During the work for this thesis, Aungier's method was implemented in a computer program, but upon reflection, a simpler mean line approach is much less complex in implementation, and may serve just as well, because inherent limitations mandate that results are checked using CFD simulations and experiments either way.

3. Development of Supersonic Turbine Blade Rows

Chapter 2 contains a discussion of velocities and flow directions that must be generated in order to fulfill the work requirements put to a turbine. In this chapter there will be a discussion of the process of making profiles that cause fluid to flow in the desired fashion.

This chapter contains considerations of means, and considerations of ends. Within the discussions of ends, there are those that are direct goals, such as aerodynamic performance, and there are indirect goals, that is goals that facilitate reaching the direct goals. Indirect goals are often specific to a chosen method.

This circumstance makes the writing of this chapter challenging, because the means are geometric and computational methods, while the ends are performance characteristics of turbines, or variables that indicate favorable performance characteristics (so-called proxy variables).

These two topics are very dissimilar and the reader may be overly taxed by a chapter that meanders wildly back and forth between issues of aerodynamics, the mathematics of NURBS curves and notable algorithms.

One solution would be to first describe the kind of flow that one wants to achieve (ends), and then describe how to achieve it (means). This works well for a historical perspective, because in the past this represented the development logic of turbines. In so-called inverse methods, the desired distribution of pressure on the blade is first determined, and then a blade is made to match it.

More advanced computers opened the possibility for a less restrictive approach. In general computational fluid dynamics (CFD) it is no longer necessary to specify a blade surface pressure distribution, and so it becomes possible to define the performance characteristics or their proxy variables as the ends, and use optimization software to obtain suitable bladings. A resulting blade profile may well be counter to conventional wisdom of how the blades 'ought to' look. In such a case it may be more feasible to learn from observing the optimization results, instead of dictating them by restricting the optimization parameters tightly.

Some compromise had to be made in the structure of this chapter, and it is as follows: The first section discusses a historical perspective, specifically the development program of the Vulcain engine turbines. The amount of available material on this topic allowed writing a section just on those aspects that are most relevant for the later sections. The purpose is to provide a basis of understanding for the choice of topics for the original research that was conducted.

The following section covers the existing research on the topic of current blading techniques, and a discussion on how they compare to and contrast with the blading technique developed for the purposes of this thesis.

All programs written during the research for this thesis, including pre-design, blade design, and post-processing of test results span roughly 16 000 lines of source code and 5 000 lines of comments. Most of the numerous minor technical aspects solved therein will not be of great interest to the majority of readers. However, some few aspects of the implementation were deemed sufficiently important or innovative to be included. Those are found in section 3.6 and in appendix B.

Finally, this chapter ends with the continuation of a previously published work on blade optimization^[94] and a discussion of its implications for future projects.

3.1. Case Study in Supersonic Turbine Blading

The geometry of the blades is the key binding component to link theoretical considerations, such as the ones in chapter 2, to practical considerations of durability, performance and efficiency. These theoretical considerations can only be valid if the blading is adequate for the application. For example, if the blading fails to produce an attached flow, the predictive power of a mean-line model will be very limited^[91], and analytical models are inherently imprecise with larger circumferential variance in flow properties (see section 2.6). But specifically for supersonic turbines, questions arise on how geometry can be used to reduce, redirect or utilize shocks and expansion fans in order to ultimately obtain the aforementioned practical goals.

Lessons may be drawn from programs which are well documented in public literature. One of the more recent developments led to the turbines for the Vulcain and Vulcain 2 engines. The program started the early 1980s, with the airplane engine manufacturer Volvo realizing that for the requirements of the then-planned Vulcain Engine, a set of supersonic turbines (one for each turbopump) was necessary^[20]. The entire development process from early tests^[20] to lessons learned and applied to later projects^[3,99] is laid out with such candor that the general process can be reconstructed, as will be shown in the following. At various

points during the design, and for various reasons, changes had to be made, leading to a final set of turbines which are much different from what was originally conceptualized. Some of these changes are especially relevant to supersonic blade development in general and will be examined here.

Rather than just recounting the events, Vulcain will be discussed in the context of other development projects, most notably, the following:

- The reusable launch vehicle (RLV) turbine modified by Griffin et al.^[39]
- FASTRAC Turbine simulated by Griffin et al.^[36]
- Japanese development programs based on the turbines of the M1 Engine^[6,42,77]

3.1.1. Nozzle Design

Designers initially relied on the previous works of Goldman et al.^[29,30]. Using a computer program based on this work, they designed a stator as an arrangement of nozzles, which were unclearly described as “wrapped around”¹. The first stage of the oxygen turbopump turbine and the hydrogen side turbine were designed using the same method in order to reduce development cost^[20]. The oxygen side was initially designed as a partial admission turbine.

It is specifically mentioned^[20] that the radial distribution of pressure produced by the nozzle original arrangement led to high losses, and had to be abandoned in favor of a design of straight slot nozzles very early on. Marke^[62] shows a perspective view of this stator, showing the nozzles as they are arranged. This is a similar arrangement of nozzles that was the baseline for Griffin’s optimization of an RLV turbine^[39], which she called a “traditional” arrangement.

There are two other common types of nozzles used in supersonic turbines. The first arrangement used in any rocket turbopump employed conic de Laval nozzles^[19]. They have circular cross-sections and are angled at the rotor blades. Lastly, the design generally considered most efficient^[39] is the vaned channel. Here, the flow channels are formed by blades, just like in a regular turbine, but often form a convergent-divergent channel through specifically designed profiles.

In summary, the available nozzle shapes (see figure 3.1) are

- Circular cross-section de Laval nozzles

1. The middle lines in figure 3 of that publication^[20], may indicate that the channels were axisymmetric, but this is not explicit in the text.

- Straight slot nozzles
- Vaned nozzles

All three types appear in the recent studies listed above. FASTRAC uses circular cross section nozzles^[36], M1 uses vaned nozzles^[42], and Vulcain uses straight slot nozzles. RLV used straight slots as a baseline, but found that performance was much improved by using vaned nozzles^[39].

The first two types have in common that the flow channel is straight in space, as opposed to the curved flow channel of a typical vaned nozzle. Hub and Shroud walls are said to be straight if the flow path in the meridional cut is straight, but the medium needs to flow around the turbine hub diameter d_{Ah} . This causes a centrifugal force on the flow^[104].

Smirnov et al.^[87] investigate the loss sources associated with curved flow channels, such as those of vaned nozzles. In conclusion, they recommend a quite distinct shape of nozzle where the flow path is straight in the subsonic part, but curved in the supersonic part. According to their investigation this shape effectively suppresses the formation of a secondary flow structure called “vortex pair”^[83]. Their findings may be related to the initial problems observed by Eriksson et al. in the development of the Vulcain turbines^[20]. Eriksson et al. found that low nozzle efficiency of their first designs was caused by extreme radial pressure gradients. The approach of Smirnov to prevent such problems is still novel and there seems to be no experimental validation that this is a feasible way to build a stator yet, however when taken together with the results of Eriksson, it clearly indicates that radial pressure gradients can be a key challenge to modern supersonic turbine nozzle design.

Straight flow paths (slot-shaped or axisymmetric) have other challenges due to their geometry. Neither kind can fill their respective rotor interface completely with flow, as shown in figure 3.1. The unfilled interface surface is colored blue. It seems likely that the unsteadiness of the fluid flow to the rotor caused by these gaps is the reason for the reduced efficiency that Griffin et al.^[39] observed. Overlapping nozzles are known^[13,97], but introduce additional geometric and aerodynamic complexity.

Furthermore, these types of nozzles are larger in the outer radius than the rotor tips. If this space cannot be provided due to package size limitations, then the rotor would have to be made smaller. For the example they studied, Kawatsu et al.^[53] found that rotor diameter is strongly positively correlated with efficiency.

There is one potentially important difference between the slot type nozzles studied by Volvo^[62] and those studied by Griffin et al.^[39], however. Griffin’s slots are extruded vertically, while Volvo’s slots seem to be extruded radially. As pictured in figure 3.1 2a) and 2b), this conceptual difference causes the trailing edge in the Griffin’s nozzle (2a) to be thinner

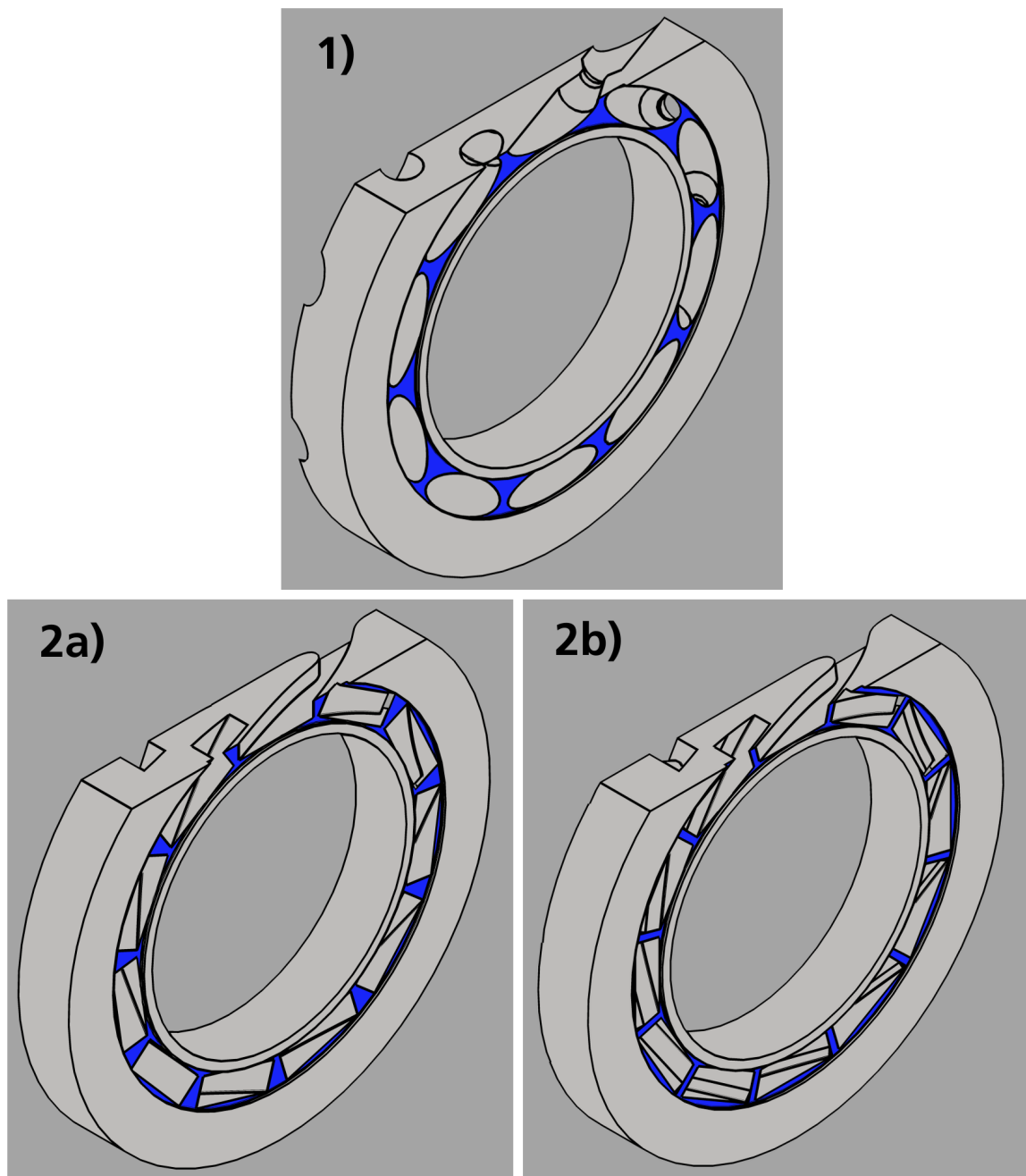


Figure 3.1.: Cut-away view of axisymmetric and slot types of nozzle rows

at the hub and thicker at the shroud. Going from published pictures, Volvo's nozzle (2b) does not appear to have this property. In this arbitrary illustration, one additional nozzle of the same mean geometry fits into the turbine arc without the nozzles intersecting. As a result, the area not producing outlet flow is much reduced in 2b). While Griffin et al. found a strong performance advantage of vaned nozzles over slot nozzles, it should be studied if the type of slot is responsible for a large part of the difference, before this type of nozzle is dismissed because of insufficient efficiency.

Due to the sharp edges in the nozzles made with EDM (Electrical Discharge Machining), Volvo Aero encountered cracks in the trailing edges which were caused by high cycle fatigue after hot gas tests^[62]. Although hydrogen was the flow medium, chemical effects, such as hydrogen embrittlement, were deemed not to be the reason for the damage^[100]. Because of the slow growth of these cracks, the issue was not seen as pressing for this particular turbine at the time, but it presents a cautionary example that structural issues are not limited to the rotor.

After arriving on the slotted design of nozzle, Volvo iterated on the shape, and eventually created a parametric system for representing and optimizing them^[2]. For the development of Vulcain 2, structural issues were addressed by strengthening the trailing edges of the hydrogen turbine nozzles^[102].

3.1.2. Rotor Design

As with the nozzle design, the rotors were originally based on Goldman's approach^[20,31], and even when the specific blading methods were superseded by newer techniques, Goldman's observations of supersonic turbine aerodynamics were taken into consideration^[4].

Perhaps most pertinent to rotor blade design of any kind is the question of whether the blade will be unstarted supersonic (sometimes referred to as transonic) or started supersonic. Started supersonic rotors are designed to maintain a relative supersonic flow from inlet to outlet, whereas in unstarted rotors, there is a strong shock at some position between the nozzle outlet and the location in the rotor with the smallest area (t_r). While total pressure loss from a strong shock is trivial for low supersonic turbines, it rises sharply with the Mach number, so while a rotor can operate in an unstarted domain if the inlet Mach number is 1.2, a strong shock before the rotor or in the convergent area at the rotor inlet at Mach 2.2 likely indicates a failed design. In a perfect gas flow with isentropic exponent $\kappa = 1.4$, the a normal shock in the former flow will reduce the total pressure to 99.3% of the initial value, while in the latter case, the total pressure will be reduced to 62.8%^[84].

Because of the large required Mach number, Volvo decided to design a started super-

sonic rotor for both oxygen and hydrogen turbopump turbines. A pressure-compounded unstarted two-stage turbine was considered for the hydrogen side, but instead a velocity-compounded turbine was chosen with a started supersonic first stage and a mostly subsonic second stage^[20].

Goldman's blading methods assume infinitely thin trailing and leading edges, and cover boundary layer behavior only in a simplified manner. The developers at Volvo therefore ran into issues when applying this practically^[20]. A radius was added to the leading and trailing edges to provide mechanical strength. Perhaps due to the influence of the resulting inlet shocks, the boundary layer grew much faster than anticipated, detached and caused the turbine to become unstarted. Volvo recognized this early in cascade and turbine component tests, and was able to redesign the rotor blading.

At this early stage, Eriksson^[20] put three goals of good supersonic profile design into writing. Methods to achieve these goals are further discussed in section 3.4.

- The leading edge geometry should generate shocks in such a way that the losses and nozzle interaction is limited
- The boundary layer on the suction side must be stabilized
- Growth of the boundary layer and pressure losses must be compensated by adequately large channel heights

Writing nine years later, after the completion of the development program, Volvo released two papers^[62,102] that show the final versions of the blades used in the Vulcain engines. The oxygen turbopump turbine having an inlet Mach number of 2.2 is shaped with a small pitch to chord ratio and a convergent-divergent channel. Conventional wisdom may indicate that reducing and then accelerating the flow would grow the boundary layers because of the resulting adverse pressure gradient, but as other authors have found^[13], the lower speeds present in the curved section of the flow channel cause an overall reduction in the losses and prevent flow detachment. The trailing and leading edges are sharp, which reduces the shock losses^[102] and helps prevent the profile from becoming unstarted^[62], since an unstart at such high Mach numbers would likely prevent the turbine from performing adequately, as discussed above.

The leading and trailing edges on the hydrogen side are rounded. No reason for this is specifically given, but since the rotational speed of the hydrogen turbopump is larger, it seems reasonable to assume that fatigue life considerations played a role, especially since Wåhlén references mechanical strength as a limiting factor for the radii^[102]. With the lower relative inlet Mach number, the pressure loss from a stronger inlet shock is also less severe.

The pitch to chord ratio is large for these blades and the channel is of mostly constant width, with a slightly concave segment in the area of uncovered turning.

As mentioned above, the trailing edges of the nozzle are very thick. This carries a risk of the rotor blades becoming unstated with every nozzle wake passing. The relatively large blade pitch may in part be of the effort reduce this risk. It is specifically mentioned that a three-dimensional shaping technique was employed to prevent unstarts^[102]. Sadly, this technique is not specifically described and the resulting nozzles are not pictured.

A large part of the development of the turbines was to find a forging method that provided an adequate grain size to meet the fatigue life needs of the rotor discs^[62]. The blades are manufactured separately by EDM, and fixed using a fir tree attachment. Additionally, each all rotor blades contain a tip shroud and an internal damper, in order to limit vibration amplitudes^[62].

For the Vulcain 2 engine, Volvo decided to depart from the single-staged approach of the Vulcain 1 LOX turbine, in order increase the power output and efficiency^[100]. This led to a blading very similar to the one in the Vulcain 1 hydrogen turbine, and also containing the concave section in the area of uncovered turning of the first stage rotor^[44].

The Vulcain 2 LOX turbine appears to be the only one of these turbines of which a picture from an unsteady CFD simulation was published. It is reproduced unmodified in figure 3.2 for the purpose of discussion. It is not explicitly stated which variable is plotted, but judging from the magnitudes and the sharp boundaries between rotating and stationary domains, it appears to be a relative Mach number plot. From this plot it appears that the designer's goal of supersonic started operation, as stated by Wåhlén^[102] was mostly achieved. The first stage operates at a moderate inlet Mach number of 1.33-1.66, which means that it has a relatively high risk of not becoming started due to insufficient inlet Mach number^[27]. A normal shock can be seen in the first row only in places where the thick nozzle trailing edges block off part of the flow.

The second stage stator operates with a permanent normal shock before the inlet, and the second stage rotor flow is for the most part subsonic.

3.2. State of the Art for Two-Dimensional Profile Generation

The previous section presented a recent historical perspective of challenges and solutions in supersonic turbine design. One of the objectives of this thesis is to build on these lessons and to provide a path to generating better profiles in the future. To this end, it becomes

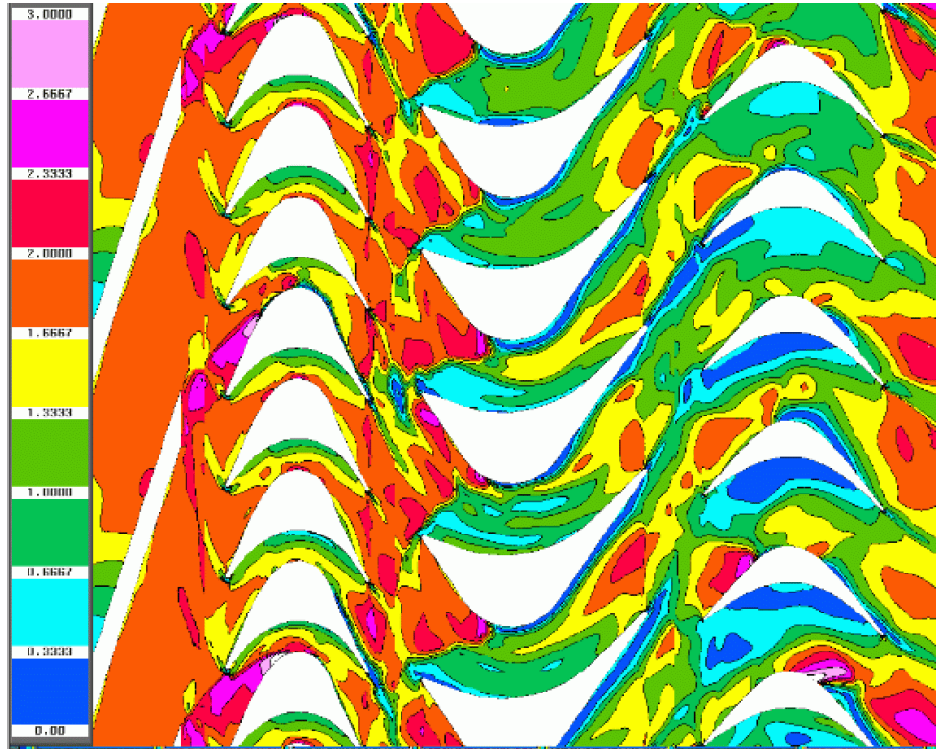


Figure 3.2.: Numerical simulation result of the unsteady flow in the Vulcain 2 LOX turbine, apparently showing relative Mach number. Reprinted from Holmedahl^[44].

necessary to discuss methods of profile generation in a more technical context, which is the content of this section.

One category of generation methods that is not further explored here are so-called inverse methods, whereby a profile is derived from a desired distribution of a flow variable, such as blade surface pressure^[1], using a fast calculation method, (e.g. potential flow^[11] or Euler solvers^[102]). Unfortunately, no such approach is known to be able to accurately predict shock boundary interactions or unsteady rotor-stator interactions. Furthermore, these methods require that the designer knows in advance which specific flow pattern would be optimal. That is not always the case. As design of blades may hinge on finding the optimal flow pattern, a more flexible approach is needed to make the most possible use of available computational capabilities. A review of the literature on current blading methods was therefore conducted.

Recent examples of blading methods include the work of Anders et al.^[1], Gräsel et al.^[33] and Koini et al.^[57]. All of these discuss primarily subsonic profiles, but offer applicable insights nonetheless.

For the methods described in the following, blade design is broken into two major stages. The first stage is specifying one or more blade “sections”, i.e. two-dimensional blade profiles

that are shaped to meet the demands of the predesign, as described in chapter 2. The second step is to generate a three-dimensional shape from these profiles.

In the section design, a profile, such as the nozzle and rotor profiles in figure 1.1, is sketched as a curve in a 2D space. External inputs, such as the desired blade angles at the blade row inlet and outlet (β) are used as parameters to define the shape of the 2D profile. In the papers discussed below, there are three general approaches to go from parameters to blade sections.

The first is profile selection, where the profiles are selected from a predefined set, such as NACA blades^[65] or Soviet profiles^[13]. Anders et al. describes this method as historic^[1], since it relies on adequate profiles being available for the precise configuration in question, and makes no use of current computational capabilities to optimize blading for a specific purpose. Even if the profiles were tested to work with a certain inlet condition in one turbine, myriad effects can cause a profile to fail to provide the desired flow field (e.g. surface roughness^[27], radial pressure distribution^[20], lack of inlet flow uniformity) or adequate mechanical strength (e.g. through inlet tip thickness scaling effects). This method offers no recourse in such a situation, other than modifying the profiles, which defeats the purpose of having validated profiles.

The second approach is camberline-thickness shaping and the last is surface shaping. In camberline-thickness shaping, a profile-defining skeleton-line (the camberline) is first defined. The actual blade shape is then generated by giving the distance between the camberline and the blade surface at any point on the profile surface^[33,57].

The last method is to define the blade outline directly, usually as some type of Non-Uniform Rational B-Spline (NURBS) curve, without first defining a central camberline^[1,33]. In the context of this thesis, they will be called direct profile shaping techniques.

Camberline-thickness shaping and direct profile shaping techniques are illustrated in figure 3.3. For the former case, the profile is defined by a number of discrete points, whereas for the latter case, it is defined by a control polygon.

A hybrid of these two approaches is also known. Herein, the NURBS control points of the profile surface are defined by their distance from a camberline^[57,90]. While camberline-thickness methods seem to be very prevalent in subsonic blade design, direct profile shaping methods appear to be the most suited to supersonic turbine blading, as more control over the exact shape of the surface is needed, as will be discussed in the following.

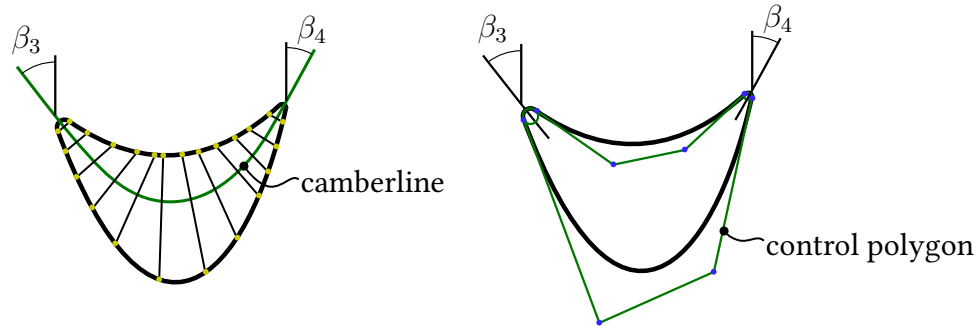


Figure 3.3.: Camberline-thickness shaping and direct profile shaping

3.3. Design Goals of Parametric Blade Generation Methods

Anders et al.^[1] describe many challenges that a parametric design program has to overcome. For example, they go into detail about how the emerging computational technologies of the 1990s led to design software that offered a large number of parameters and give two key reasons why parameters of a turbine profiling can be considered extraneous.

1. Duplication of Results

Functionally identical profiles can be expressed in more than one way in the parameter system. This can cause separate design optimizations to come up with very different parameter choices, although the resulting profiles are geometrically almost identical.

2. Unneeded Flexibility

The parametric system allows the creation of blades that can be excluded as candidates on purely geometric grounds, without even considering flow. For example, a profile where the suction and pressure side curves intersect cannot generate a sound geometry. In many situations, it is known from experience that geometric features such as inflection points^[74] or jumps in curvature^[11,57] cannot occur in certain places on well-designed profiles. Griffin et al. encountered such problems in their optimization procedure^[38,39], and noted how they complicated their chosen method of optimization.

A profile system that allows these features to exist on a profile offers the user or connected optimization method more flexibility than is needed, which complicates the usage

and makes an optimization more computationally expensive than required. For these reasons, avoidance of extraneous parameters is a prime example of a vital indirect goal for a blade design system.

Gräsel et al.^[33] additionally recognized the growing importance of Computer-Aided Design (CAD) software at all stages of the design process. Therefore, they proposed a system where the blade generation by a parameter system is well connected to a CAD system, but do not go so far as to propose integrating the blade generation into a general CAD system, as other authors have^[65].

Commonly used current CAD systems are based either on NURBS or subsets of NURBS, such as Bézier curves. The reason why NURBS curves are in such widespread use is that they have certain known mathematical properties^[73]. In direct surface shaping^[1] and hybrid approaches^[57] these known properties can be used to design a rule system that translates between human-readable parameters and NURBS-parameters.

For example, it is a property that the tangential direction at the start of the curve is the same as the direction of the straight line between the first two control points; likewise at the end with the last two control points. This can be used to form connections between two curve segments, where the pointing direction stays the same from both ends of the connection and the resulting geometry is therefore smooth at the connection point, in the sense that there is no kink. The resulting connection would be called a G₁ joint, because the geometric direction of the **first** derivative is constant between the joined segments. A G₂ joint is commonly understood to mean that the curvature is equal at the contact point^[69].

While the methods described above use only one curve for both pressure and suction side between the tips, there is another group of methods that use multiple. Koini^[57] mentions these “segmented approaches”, such as the blade shaping method by Pritchard^[74]. In Pritchard’s method, the suction side is subdivided at the point where the throat line meets the suction side, so that one curve represents the suction side from the end of the leading edge to the throat, and a separate curve represents the suction side from the throat to the trailing edge. Pritchard uses the graph of a third degree polynomial for the former curve and a circle segment for the latter curve. He likewise uses a third degree polynomial graph for the pressure side. Koini summarizes works in which these curves are replaced with Bézier curves, and notes that while these segmented curves do not have kinks at the joints, there would be a discontinuity in the curvature. Using G₂ joints, this defect can be avoided.

3.4. Proposed Blade Profile Design Methods

As described above, Koini argues for the use of methods to shape turbine blades so that they are infinitely differentiable from leading edge to trailing edge. This is done in order to avoid unwanted curvature discontinuities, which negatively influence the flow^[11,57]. There are two objections to be made in this regard. The first is, that Koini et al. do not discuss the possibility of curvature continuous segmented curves although several different methods to generate them are described in this section. The second is that forced curvature continuity, or even just first derivative continuity, is not necessarily desirable for supersonic turbine blades.

Many known supersonic turbine blade designs are not possible to make using such rigid methods. For example, Deje^[13] gives a large number of bladings for trans- and supersonic speeds that make use of kinks in the nozzle and rotor blades. Even the simpler designs of Goldman and Scullin^[29,30] (which were the basis for the development of the profiles used in Vulcain^[20]), cannot be represented in a system like those presented by Koini^[57], because they contain both straight and curved segments on the suction side. The rotor blades later presented by Andersson^[3] contain an inflection point in the outlet, which, while possible, would require a high number of control points, not just in this region, but in the whole blade.

The limitation of these approaches when making supersonic turbine bladings were also noted by Joly et al.^[49]. Having previously researched mainly subsonic bladings these authors seem to have reached their conclusions independently of earlier publications by Andersson et al.^[4] or Griffin et al.^[38].

In order to replicate and build upon the efforts of these previous researchers, a way to parametrically represent a wide array of blade shapes is needed. The solution employed here was to generalize and extend Pritchard's method^[74].

Some key aspects of Pritchard's method^[74] are listed here for later reference, but Pritchard's own illustrations are probably the best way to understand the method. In the interest of brevity they cannot all be reproduced.

Pritchard defines five locations, which the profile must pass through are defined, and at each of them a tangential direction is specified. The locations are:

1. Junction point of trailing edge and uncovered turning
2. Junction point of uncovered turning and covered suction side
3. Junction point of suction side and leading edge
4. Junction point of leading edge and pressure side
5. Junction point of pressure side and trailing edge

Pritchard gives a way to determine these locations from eleven parameters, which were already in common use as blade parameters at the time of publication^[17,22]. For many of these parameters, Pritchard gives illustrations on how they influence blade shape. The parameters are:

1. Pitchline radius
2. Axial chord
3. Tangential chord
4. Unguided turning angle
5. Inlet blade angle
6. Inlet wedge angle
7. Leading edge radius
8. Outlet blade angle
9. Trailing edge radius
10. Throat size
11. Number of blades

The second step in Pritchard's method is the creation of the connecting curves. Pritchard uses three types of curves:

1. Circle segments defined by center point, starting point, starting direction and angle span
2. Circle segments defined by starting point, end point, angle span and tangential relation to a circle (which defines the throat size) at the end point
3. Third order polynomial graphs defined by starting point, end point and tangential directions at both points

The leading and trailing edges use curve type 1, the uncovered turning uses curve type 2, and the suction and pressure sides are of the last type.

This method can now be compared to Anders'^[1] two standards of a successful parameter system, which is described above. Since the number of parameters is quite low, it is unlikely that there would be two very different parameter sets generating identical geometries, and indeed no such example could be found. By Pritchard's own admission^[74] however, the method allows the existence of two unwanted geometric features, which are inflection points on the suction side near the tip, and curvature discontinuity on the suction side in points 2 and 3. Both these issues can be addressed using NURBS curves.

Eliminating the possible inflection point alone is a trivial matter. All that is needed here is a curve that has the same geometric constraints (end points and end tangents), but cannot have an inflection point. Curves that do not have an internal inflection point are called

c-shaped curves. A simple curve type that is c-shaped, and fully defined by the given constraints is the parabola segment, which has also been used in profile design before^[17]. This specific replacement was also done by other researchers in the past^[64].

The second expansion of Pritchard's concept is the introduction of curvature continuity at specific junction points, by giving curvature either as an input variable or calculating it from geometric constraints. This allows the generation of blades which are less likely to have flow detachment on the suction side^[11,91]. Expansion of this concept to higher derivatives can also be considered in the future, if it can be shown that it is advantageous.

To achieve curvature continuity, a curve with more degrees of freedom than a parabola was required. This was first found in the work of Paluszny et al.^[69], who described a method by which all known c-shaped cubic (third degree) rational Bézier curves are described. The free parameters are the starting and end points as well as their tangents and local curvatures, and two additional free parameters. No aerodynamic research could be found that has cited Paluszny et al. previously.

A further expansion of Pritchard's method was making it possible to have elliptic leading edges. Weisstein^[18] assembled all relevant equations for determining points and tangents on an ellipse. Just by adding an eccentricity parameter e , and interpreting the inlet radius parameter as the semi-minor axis b of the ellipse, the two points (Points 3 and 4) can be calculated as points on an inlet ellipse.

In Sudhof et al.^[95], a version of Pritchard's method with the following modification was demonstrated in a cascade experiment. In this, the pressure side was a conic segment with constant middle control point weight of 1.2². The leading edge is an ellipse with an eccentricity of 0.85. The covered part of the suction side is a Paluszny curve, with interactively chosen curve parameters.

The area of uncovered turning is straight, which mirrors classical transonic profile designs^[22,32]. This would also have been possible in Pritchard's method by setting the uncovered turning parameter to 0.

In a different demonstration, the extended segment set was used to create a number of subsonic impulse rotor profiles^[91]. Such blades are largely symmetrical. Therefore, the suction side from the leading edge to the beginning of the covered channel is nearly as large as the uncovered turning segment, and should be given an extra segment in order to improve control over the blade shape. It was demonstrated that this extra segment allows the creation of efficient bladings with little manual input^[91].

2. This number relates to the Bézier representation of conics, which is described in detail by Piegel and Tiller^[73].

3.4.1. Specific Geometry Features in Supersonic Nozzles

A distinctive feature of supersonic nozzle profiles for axial turbines is the retraction of the throat into the flow channel. While there are examples of blades that do not have this feature^[13,39], a parameter system for supersonic nozzles should allow this feature to exist, and one parameter should control distance to which the throat is retracted. This parameter should produce viable results for no retraction at all, since Griffin et al.^[39] found an optimum in such a profile.

Furthermore, in supersonic nozzles, there is often, but not always^[13] an inflection point on the suction side. Since it was difficult to evaluate the relative merits of both with and without the inflection point geometries, a curve should be chosen here to allow both kinds of blade geometries. The non-rational quartic curve was specifically developed to fit this role while also allowing for the control of the end curvatures.

Influence of Trailing Edge Shape

The main concern for trailing edges in subsonic nozzles is the desire to have the flow detachment point as far back in the flow as possible and as symmetrical as possible^[13]. This allows the recovery of dynamic pressure behind the blade and reduces the unsteady forces on the rotor. The same consideration is also important in supersonic nozzles.

However, there is a critical difference in the influence of the detachment in that it is a local phenomenon in the subsonic case. In the supersonic case, it influences the entire downstream flow field because an oblique shock originates from the detachment point on both the pressure and the suction side of the profile: as pictured in figure 3.4, the flow expands around the trailing edge and the shock equalizes the flow direction to a common flow direction behind both sides of the trailing edge. The larger the Mach number, the more dominant the influence of the shock waves becomes over other considerations, due to the rapid increase in total pressure loss.

The later the detachment, the larger the expansion before the shocks, the stronger the shocks will be. For one thing, the shocks themselves lead to an increase in entropy, although the extent of this is strongly dependent on the Mach number of the velocity component relative to the shock^[84]. Even at low Mach numbers, the influence of the shocks on the thickness and stability of boundary layers are important.

The shock from the pressure side typically hits the suction side of the next nozzle profile and interacts with its boundary layer^[34], which may result in the detachment of the boundary layer at that point^[22]. The strength of interaction depends on the boundary layer thickness and the amount of turning through the shock^[35]. These factors can vary based on

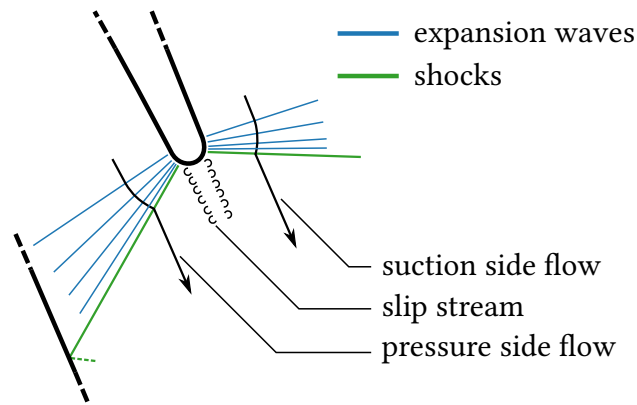


Figure 3.4.: Simplified illustration of the common expansion and shock pattern around a trailing edge at supersonic velocity (compare: figure 4.9)

blade shape^[32].

The shock from the suction side is potentially even more harmful, as it can interact with and exacerbate a shock that transiently forms in the room between nozzle and rotor suction side at each rotor blade passing. The transient formation of this shock can cause a rapid oscillation of the rotor's total lift, and therefore oscillation in the blade force^[25,70]. More research is necessary to determine if this lift oscillation is a main cause for mechanical failure^[24,62] of rotor blades in supersonic turbine development programs.

Although more research is needed, it seems that for high supersonic turbines, such as the Vulcain Oxygen Turbine^[102], sharp edged leading and trailing edges provide improved control of the shock pattern over rounded ones, as they produce an attached shock at the inlet and a shock emanating from a constant position at the outlet. For lower Mach number designs, such as the Vulcain Hydrogen Turbine^[102], the same considerations as for subsonic turbines dominate, so circular or elliptical edges may provide the best results.

There is a compromise between these two shapes that is not known to have been studied by other authors: a quarter-circle shape. This shape is pictured in figure 3.6 and was used in an optimization study^[94]. The rationale for this design is that the suction side shock directly interacts with the rotor, so it should be reduced as much as possible. A sharp cutoff should be optimal here, as the flow is not able to follow this contour and will separate without overexpansion if the pressure in the wake equals the pressure on the suction side.

The pressure side sees a circular shape, with twice the radius as in an equivalently sized circular trailing edge. This feature may allow the flow to follow the contour for a longer expansion, which may lead to a reduction in wake size. It also causes a pronounced shock emanating from the detachment point. However, since this shock interacts with the suction side of the next nozzle profile, the shape in the region where the shock impinges on the

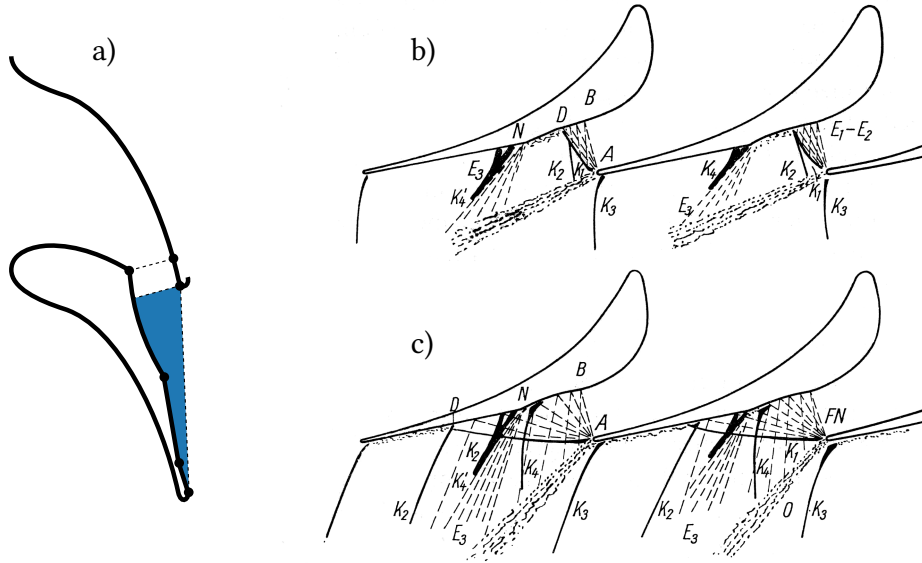


Figure 3.5.: a) Kink nozzle design with retracted throat. b)&c) Shock system around a different type of kink nozzle, at pressure ratios below (b) and above (c) the nominal design point. b)&c) reproduced for the purpose of commentary from Dejc and Trojanovskij^[13]

suction side could be modified to cancel or abate it.

Blade Shaping in the Area of Uncovered Turning

The area of uncovered turning of the nozzle is defined here as the triangle formed between the trailing edges of two adjacent blades and the point reached by starting from the center point of the higher of the two trailing edges and drawing a straight line to the suction side of the lower blade in the direction perpendicular to the blade outlet angle β_2 . The area is marked in figure 1.1, and colored blue in figure 3.5.

One way to stabilize the boundary layer on the suction side is to introduce a bend or even a kink. According to Dejc and Trojanovskij, who have studied this possibility extensively^[13], the Prandtl-Mayer expansion at the kink causes turbulent boundary layers to relaminarize, thus reducing losses. Further, they argue that the induction of additional shocks lowers the overall total pressure loss induced by the shocks.

Dejc^[13] gives a wealth of data from cascade experiments. Partly these are measurements of total pressure loss coefficient indicating that a kink of 3° turning causes a reduction in total pressure loss compared to a profile without a kink. Several questions are left open, however.

Given the large amount of shocks in the flow, how is the total pressure measured? As

discussed in section 2.6, the way the pressure is measured and the measurement is averaged can greatly influence the results. Given the very slight reduction in drag coefficient claimed by Dejc, it is unclear if the positive effect could have been due to the positioning of the pressure probe in the shock system.

Further, while it appears that such profiles have been used in stationary turbines^[13], it is unclear how the additional shocks interact with a passing rotor. Transient boundary separation events may increase in number, thereby decreasing the overall efficiency of the turbine. They may in addition induce vibration at a frequency greater than the blade passing frequency, thereby reducing the rotor's fatigue life.

Using a parametric blade profile generation method, it is easily possible to induce kinks, and it would be interesting to study this again using computer simulations. Dejc claims that especially the partial load performance is improved when compared to more conventional designs^[13] due to supposedly positive effects of shock-expansion interaction on the overall outlet flow (see figure 3.5).

On a separate but related note, concerning the area of uncovered turning, it has traditionally been held that nozzle profiles with low supersonic outlet flow should have a straight suction side in the area of uncovered turning^[11,22], and that higher Mach number flows require a concave nozzle-shape on the suction side. But not only Dejc deviates from this idea. In the optimization of a 2-staged turbine carried out by Griffin et al.^[39] the final optimum featured a nozzle row with no retraction of the throat, and a strongly curved area of uncovered turning, which they surmise positively influences the interaction between nozzle and rotor.

3.4.2. A General Nozzle Blading Scheme

Sudhof and Shimagaki^[94] demonstrated that disturbance in the outlet of a supersonic turbine nozzle can be greatly reduced using fast-converging optimization schemes, as described in section 3.7. In later results, using the resulting optimized profile, the dynamic rotor blade force amplitude was reduced to 86.2% of the value in the reference turbine (NASA-developed M1 Hydrogen turbine with minor modifications by JAXA).

The parametrization scheme used in this optimization is a version of the method described above, and was formulated to allow the optimization to arrive at whatever profile best minimizes the target function. It implements some of the aspects discussed above, but does not include kinks.

- Curvature continuity on the suction side
- Variable retraction^[94] of the throat

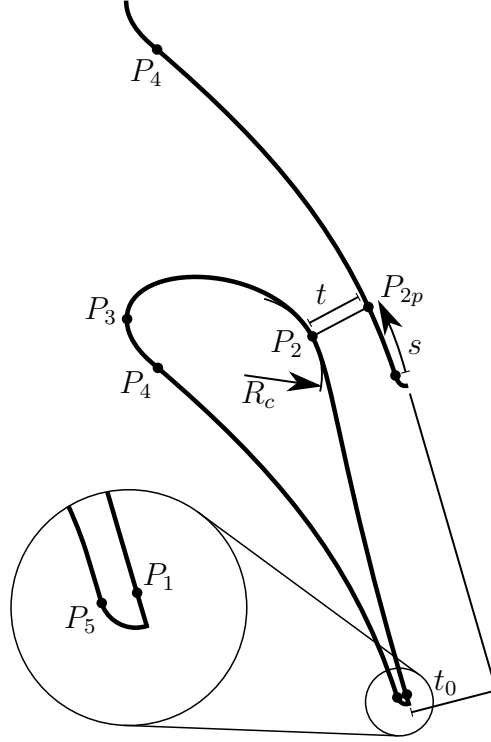


Figure 3.6.: Part of the parameter system for supersonic nozzles illustrated

- One-sided rounded trailing edge

The profile is formed in the following steps: First, junction points are created much like in Pritchard's method, but with some differences. The unconverged turning angle is replaced with a wedge angle of the trailing edge γ_{no} . Pritchard's throat size parameter is replaced with the contraction ratio t/t_0 , as seen in figure 3.6. The contraction ratio was chosen because it is a more common parameter in compressible flow problems. t_0 is calculated from the suction side outlet angle β_{2su} and the blade pitch.

$$t_0 = p \cdot \sin \beta_{2su} \quad (3.1)$$

$$\beta_{2su} = \beta_2 - \frac{1}{2}\gamma_{no} \quad (3.2)$$

Points P_1, P_4 and P_5 , are defined this way. To determine the location of point P_2 , the retraction parameter s is needed. The parameter is the fraction of the distance between P_5 and P_4 at which the geometric throat is on the pressure side (P_{2p}). The point P_2 is created by shifting the point P_{2p} in a direction perpendicular to the pressure side curve at that point, by the distance t . The point P_3 is located at the apsis of the inlet ellipse segment. The ellipse

now only exists on the pressure side, and is not continued on the suction side. The reason for this change is that, with the retraction of the throat, there were too many parameters controlling just a short segment between P_2 and the start of the inlet ellipse. That meant that parameters would only create reasonable profiles if they fell within a small and hard to predict range.

Between the points P_1 and P_2 , there is a non-rational quartic curve, with control of the end curvatures. The curvature at point P_1 is 0. The curvature at point P_2 is an open parameter. The lower limit for this parameter is determined by imagining the points P_{2p} and P_2 as being on concentric circles, with the location of the mid point determined by the local curvature of the pressure side curve at the point P_{2p} . The curvature radius R_c must now be as large as the concentric circle through P_2 or smaller (smaller radius meaning higher curvature). If the curvature radius at P_2 was any larger, there would not be a geometric throat at that position.

The section between P_2 and P_3 is a Paluszny curve, as described above. This avoids possible inflection points. Since the fluid flows with relatively low velocity in this section, it may be possible to reduce the parameter number by setting one or both of the open parameters of this curve to fixed values, in order to accelerate optimization.

The curve between points P_3 and P_4 is an ellipse, as described above. The section between P_4 and P_5 is a concic segment, with variable mid point weight.

3.4.3. Recent Studies on Rotor Profile Design

Within the body of work done for this thesis, there is no systematic study of supersonic rotors, so the descriptions in this subsection will rely on the most sophisticated available examples of rotor optimizations from the literature. Specifically, the ones conducted by Griffin et al.^[38,39], Papila et al.^[71] and Kawatsu et al.^[53].

Kato and Funazaki also conducted an optimization study that would be relevant^[51], however the study has the following procedural error: Although the simulation is optimizing an impulse turbine (M1 Fuel Turbine^[77]) as a baseline, it does not control for the degree of reaction in the results. Therefore, the optimization method seems to have created a reaction turbine. The resulting rotor has a restricted rotor inlet. This increases the pressure in the region between nozzle and rotor, causing the nozzles to become effectively overexpanded. The “optimized” rotor blades form a divergent channel to generate a transonic outlet flow.

The optimization did not modify nozzle geometry or allow for change in the outlet angle or camber of the rotor profiles. Properly designed reaction rotor blades have a much higher camber angle than impulse rotors^[98]. This is likely part of the reason for the flow

detachment on the suction side of the “optimized” rotor. Three main disadvantages of a reaction turbine over an impulse turbine are the increased axial load from the blade disk, increased tip leakage (both due to the axial pressure gradient), and some reduction of specific work at a given outlet flow angle (see chapter 2). If the simulation done by Kato and Funazaki included tip leakage or controlled for specific work, this is not stated in the paper^[51]. There seems to be no consideration of additional axial loading either. It should also be noted that the actual M1 fuel turbine is a partial admission turbine, but the simulation did not account for this. Operating a reaction turbine with partial admission would cause prohibitive amounts of sector end losses^[98].

In summary, the study is flawed because it seems to have resulted in a reaction turbine, but did not include the parameters necessary for creating a properly designed reaction turbine, or take the disadvantages of such a turbine into account.

Kato et al.^[52] also optimized a rotor based on the M1 fuel turbine, but only simulated a frozen rotor condition. Experience from simulating the same turbine as part of the nozzle optimization (see section 3.7) indicated that frozen rotor simulations represent the actual pressure loss in the turbine very poorly, even for the specific phase angle at which the rotor is frozen. This research is therefore also not evaluated further.

Griffin^[38,39] and Papila^[71] describe different aspects of an optimization of a turbine for a reusable engine. Several earlier papers on optimizations for this specific application exist, but it seems that the results are largely superseded by the three cited papers. Kawatsu^[53] describes a completely separate optimization, so the total number of independent optimization studies for this section is two. Several other works containing information about computer-aided supersonic rotor profile development exist, such as the work done for the Vulcain engines^[2-4,44,99,100,102]. However, Kawatsu on the one hand and Griffin and Papila on the other represent the only known optimizations employing unsteady RANS (Reynolds-averaged Navier-Stokes) calculations, which are currently considered state of the art.

Papila^[71] studies only the first stage of this two-stage turbine, and of this only one profile, while Griffin^[38] studies both stages (4 blade rows) and three profiles (hub, mean and shroud) for both rotor blades. Three-dimensional aspects will be briefly discussed in section 3.6. The relative inlet Mach number of the rotor is about 1.4^[71] (reading from their figure 7).

Kawatsu optimized a turbine with a similar inlet Mach number of about 1.4 or 1.5 (reading from their figure 14). In their conclusion, they select two separate profiles from a population, one for smallest possible diameter at constant efficiency, and one for highest possible efficiency at constant diameter. The diameter optimization is disregarded here because it is only relevant for turbines where this target variable is of major concern.

Papila et al.^[71] and Griffin et al.^[38,39] use the same parametric representation for the rotor,

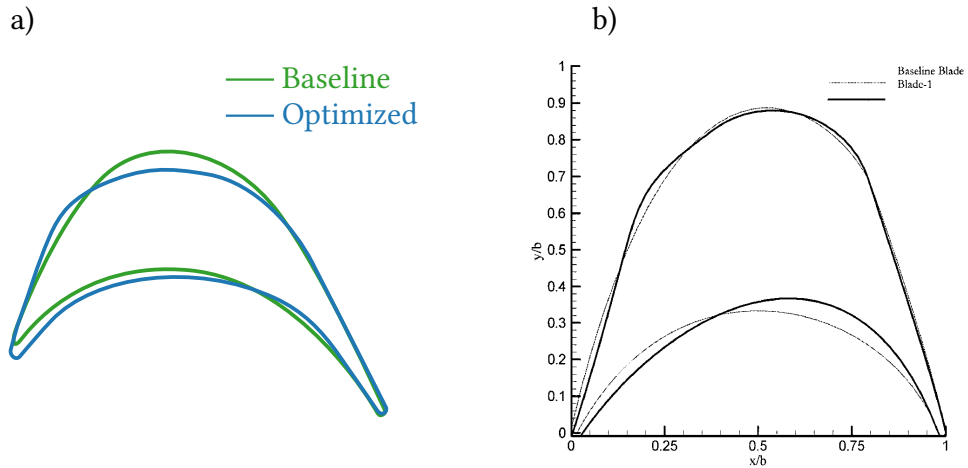


Figure 3.7.: a) Recreation of baseline and optimized profiles from separate figures in Kawatsu et al.^[53]. b) Reprinted figure from Papila et al. showing both baseline (dashed) and optimized (solid) rotor profiles superimposed. Reprinted for commentary.

which includes a circular segment in the covered part of the suction side. In this regard, the profile is like the ones proposed by Boxer et al.^[9]. Otherwise, most of the input variables are control point positions of 3rd degree non-rational Bézier curves, with no direct control over end curvature. Before profiles are evaluated in CFD, they are checked for a number of geometric defects, such as places where the blade is thinner than the trailing edge thickness, or suction side and pressure side intersecting. The authors of those papers also considered kinks defects, and therefore excluded profiles with large local curvature^[71].

Kawatsu et al. did not parameterize the blade directly in order to optimize it^[53]. Instead, the computational mesh was deformed, which changed the geometry of the blade within. This method makes it impossible for kinks to come about, but also limits the possible profiles in other ways. It is also conceivable that such an optimization could improve the target variable by stretching the mesh in such a way that the simulation accuracy is negatively affected, although there is no indication that this occurred.

Having established that Kawatsu et al.^[53] on the one hand, and Papila et al.^[71] and Griffin et al.^[38,39] on the other hand, carried out their optimizations using very different methods, it is now instructive to consider if there are convergent results between the disparate optimizations, even if the sample size of two is less than ideal.

As it happens, both groups arrived at profiles that do share prominent similarities in the rotor inlet geometry in the area of the suction side between the leading edge and the be-

ginning of the covered channel. In both cases, the baseline featured a geometry of steadily increasing curvature, and the optimization arrived at a straight edge followed by a pronounced sharp turn.

In the following, a model is proposed to explain this difference between the baselines and the respective optimization outcomes. Earlier design methods (such as Goldman's^[27] or the one used by Wåhlén^[102]), do not consider the unsteady nature of the rotor inlet flow, which is caused by the previously described system of shocks in the space between nozzle and rotor (see subsection 3.4.1). As seen in the entropy plots printed by Kawatsu^[53] (which match experience), the entropy gain over the shocks is minimal as the Mach numbers involved are moderate, and the shocks are so oblique that the shock normal Mach number is very close to unity. Entropy is almost exclusively generated in boundary layers and detached flow regions on which shocks have a major influence. It is therefore not entropy created by the shocks that is responsible for most loss, but the negative influence that impinging shocks have on boundary layers.

It follows that in the area of the most severe system of shocks, the aim of optimization is not the best possible redirection of a perfectly uniform potential flow, but a mitigation strategy for the adverse effects of shock-boundary interactions. It is put forth here that the specific mitigation strategy chosen by the optimization is as sketched in figure 3.8.

In that figure, shocks impinge on the rotor suction side in two locations. In any supersonic rotor profile, there is a bow shock^[93]. This is generated by the blade row itself, so it is also present in the case of uniform inflow. The second location where shocks impinge is at the uncovered area near the leading edge. In an ordinary profile, there are three sources for shocks that interact with the rotor boundary layer in this segment. The trailing edge shock from the pressure side of a nozzle, reflected on the area of unconverged turning of the nozzle; the trailing edge shock from the suction side interacting directly; and a shock that is generated by overexpansion in the space between rotor and nozzle^[25].

The fact that the frozen rotor optimization conducted by Kato et al.^[52] did not result in a similar geometry indicates at least tenuously that perhaps the unique effects of unsteady interactions provide the impetus for the optimization to reach this result. The mechanics could be explained thusly:

Typically, the second and the last of the three sources described above form a single combined shock, as described by Giles^[25] and Saxer^[81]. This shock sweeps across the rotor in the area indicated in figure 3.8. By interacting with the boundary layer this shock limits the blades' ability to turn the flow in a consistent manner. The amount of turning possible in this area is therefore dependent on the instantaneous position of the sweeping shock. In order to achieve a more time-steady blade behavior, it is therefore reasonable to forego any

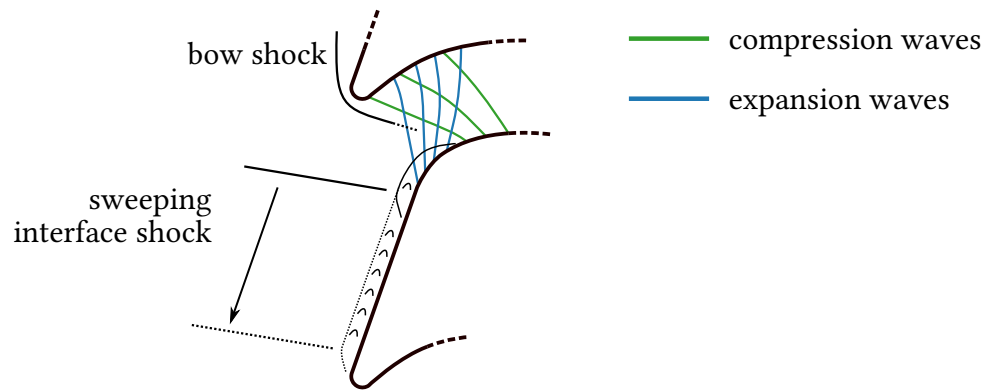


Figure 3.8.: Sketch of important compressible flow phenomena in the rotor inlet. Oscillating shock causes variable detachment point. Compare sketched expansion and compression waves (colored) to Goldman^[29].

turning here, and instead choose a largely straight section.

Directly following this straight section is the aforementioned area of strong turning, which, according to this explanation should start above the point where the sweeping shock first impinges on the blade. Expansion waves are created by this turning. Compression waves emanate from the pressure side but only interact with the suction side flow further into the channel.

A concentrated zone of expansion is well documented to cause re-attachment of disturbed boundary layers in supersonic turbine blades^[13]. Using this effect, which is also the basis for the aforementioned kink-nozzles^[13], the blades that Griffin^[38] and Kawatsu^[53] have developed, should be able to create a flow in the covered rotor flow channel that is much less dependent on the position of the sweeping shock, and therefore avoid transient thickening of the boundary layer on the suction side. While a specific reason for a more time-steady behavior being necessarily more efficient is not identified, this seems to be the case (see also section 3.7). The accompanying reduction in blade force amplitude is also valuable for improving the fatigue life of the blades.

Griffin et al. demonstrated in an experiment that an increase in efficiency of 9% over a traditionally designed 2-stage turbine is possible^[38]. Further public research into these methods should be conducted, and if these results can be repeated, earlier design methods should be superseded in comparable situations.

As mentioned above, however, the Mach number of the blade inlet flow was below two. In this scenario, oblique shocks are relatively weak^[84] and unlikely to produce total pres-

sure loss on the same order of magnitude as the boundary layers. The optimizations, accordingly, found a way to reduce pressure losses from boundary layers. At higher Mach numbers, these considerations may reverse, and management of the supersonic expansion and compression may be the most important consideration. Since this was the premise of Goldman's considerations^[27,29,30], it seems reasonable that his method may have a longer life in higher supersonic turbine blades, like the Vulcain oxygen turbine^[102].

Further, the lessons learned in the development of the Vulcain hydrogen turbine^[102] should not be discounted either. The considerations for which Volvo optimized their blades (in published works) are still relevant, and it seems reasonable that in finding a synthesis between both methods, even better results are achievable.

For example, the Vulcain 2 first stage rotor blades feature an inflection point in the rotor outlet^[3]. This allows for some additional expansion at the cost of a suction side geometry that has to accomplish additional turning, since some of it is reversed after the inflection point. The blade deformation done by Kawatsu et al.^[53] would likely have been unable to generate such a feature. The parametric representation used by Griffin et al.^[38] may have theoretically been able to generate this but only in a limited way. Specifically, the constraint that point L3 has a fixed tangential direction and cannot be retracted into the channel may prevent the optimization from finding a suitable geometry.

Without having investigated the matter closely, it is difficult to see which blade parametrization can represent all relevant blades for this problem without superfluous degrees of freedom. Tentatively, one could suggest the following arrangement, pending a pilot study.

Taking the junction points from Pritchard's^[74] method as a starting point, this basic structure lacks flexibility in the outlet and inlet regions of the suction side to generate the features described above. For the outlet, it may be sufficient to add one additional parameter, the inclination angle at the position that is the throat in Pritchard's model, the end of the covered channel. Depending on this angle, the true throat may become retracted into the channel as a geometric consequence.

On the inlet side, it seems that there is an advantage to having a mostly straight section before the covered channel begins. Changing any one part of a Bézier curve changes the entire curve^[73], so partitions in the curve are necessary to avoid the need to find "compromise" curves that are very good in one region at the cost of performance in another region. For example, it is conceivable that the inflection point on the suction side of the profiles generated by Papila^[71] is not actually a useful feature of the blade, but rather a flaw that the optimization accepts in order to make the uncovered part straighter than it could otherwise be. To avoid this, it may be advantageous to have a junction point at a point of maximum curvature, in order to have a curve of monotonically varying curvature (by definition, this

is called a “spiral curve”) at either side.

Unfortunately, there is no known a priori method to determine the ideal location for the point of highest curvature at the rotor inlet. To keep the number of open variables low, one could place a junction point directly opposite the next blade’s leading edge, as was done in a previous study with a different context^[91] with good results. In this previous study, the blade channel is of constant area, so there was no need for an additional throat width. This assumption may not serve here, however, since the channel may need to widen a bit in order to accommodate growing boundary layers. An additional parameter, the ratio of inlet width and outlet width defines this geometry feature.

3.4.4. Draft of a Parameter System for Supersonic Rotors

It is now possible to describe one parametrization of a rotor blade that may be better at accommodating the geometries that appear to be optimal for current and near-future optimizations.

In this proposed geometry, the following parameters are needed to generate the junction points:

- Pitchline diameter d_m
- Axial chord $z_4 - z_3$
- Tangential chord s_r
- Unguided turning angle at the inlet Γ_{ri}
- Inlet blade angle β_3
- Inlet wedge angle parameter
- Leading edge minor half-axis $\approx r_{ri}$
- Leading edge eccentricity
- Unguided turning angle at the outlet Γ_{ro}
- Outlet wedge angle γ_{ro}
- Outlet blade angle β_4
- Trailing edge radius r_{ro}
- Inlet opening size t_{ri}
- Overall channel expansion ratio t_{ri}/t_{ro}
- Number of blades N

The coordinate origin would be defined as in Pritchard’s method by the trailing edge circle, which leads to the trailing edge points P_1 and P_6 , using the trailing edge radius, angle and wedge angle.

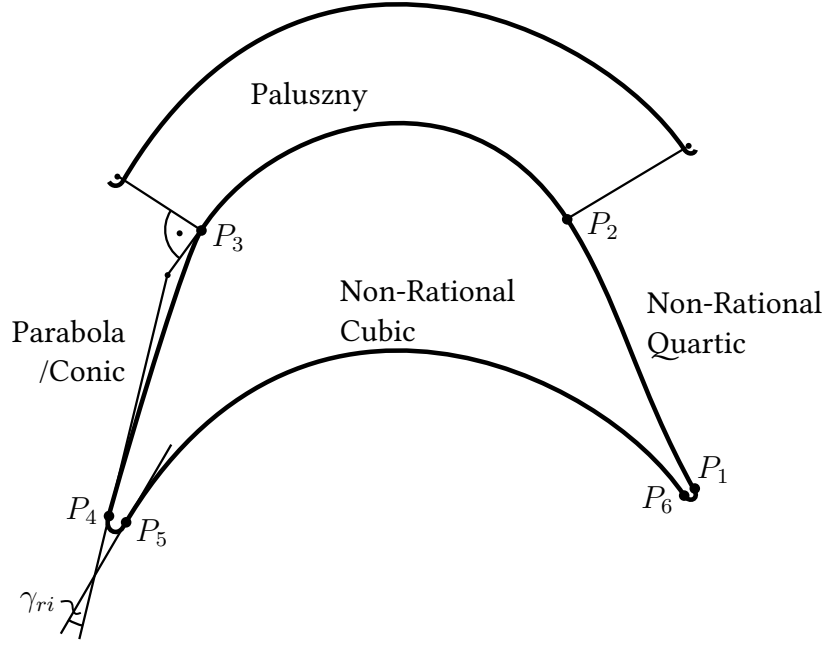


Figure 3.9.: Proposed rotor parametrization

Using the axial and tangential cord, as well as the ellipse parameters (eccentricity, minor half-axis), one can then define the position of the leading edge ellipse, although the positions of the leading edge points P_4 and P_5 are still dependent on the wedge angle, which must be determined from the wedge angle parameter as follows.

The point P_3 is determined from the focal point of the inlet ellipse (the one nearer to the edge) by counting the inlet opening as the distance between those two points and adding the local thickness of the ellipse. The direction of the opening is determined by adding the uncovered inlet turning angle Γ_{ri} to the inlet angle β_3 .

The inlet wedge angle can now be chosen using the inlet wedge angle parameter, which is always in the domain $]0,1[$. 0 could be defined as generating the degenerate case of a straight segment between P_4 and P_3 with a kink at P_3 , and 1 could be defined as the largest wedge angle which still gives a plausible profile. This could mean a vertical tangent at P_4 , i.e. $\gamma_{ri} = 2\beta_3$. Evidence from the two aforementioned optimizations suggests that lower values of this parameter will be the result. If it occurs that an optimization is hindered by the upper limit, the selection of this upper limit can be re-evaluated. Rotor profiles with very large leading edge wedge angles have been documented^[46,76]. The important function of this intermediate parameter is to prevent a failure of profile generation because the wedge angle is too small to generate a c-shaped curve in this space.

At this point all junction points and the tangents at these points are known. The remain-

ing effort is to find curves that provide adequate flexibility to accomplish their task, while adding as few free parameters as possible.

Between the points P_1 and P_2 , there could be a non-rational quartic curve segment³. This type of curve has specified end curvature while also retaining the ability to be either s or c-shaped, depending on end tangents. This allows generating profiles such as the ones developed by Volvo^[3], as well as those developed by Griffin et al.^[38], depending on parameter choice. A curvature of zero at the junction from uncovered turning to trailing edge (P_1) was used for section 3.7, and could be taken as a starting point. There are two internal parameters for this type of curve, termed here “pointedness” and “bias”. In order to reduce complexity the bias could be set to 0.5, and the pointedness could be determined by finding the fairest curve (see subsection 3.5.3). This would leave the curvature at P_2 and one internal parameter as additional variables.

Between P_2 and P_3 is the segment that is prone to cause flow detachment^[1], which should make it a focus of blade development. To give the optimization the best possible chance at solving such problems, a curve type should be chosen that offers very fine control over the curvature in every point. In experience, the best segment type for this requirement is a cubic rational curve, as described by Paluszny et al.^[69]. This type is always c-shaped, which would rule out some of the shapes described by Papila et al.^[71] because of the previously stated assumption that those shapes were generated as a by-product of the parametrization, and not because they offer a physical benefit. The end curvatures are determined by continuity to the adjacent curves. Two parameters remain open, and it may be best to leave both of these to be determined by an optimization.

Between P_3 and P_4 , there could be a general conic segment or a parabola. If a general conic is chosen, the mid point weight could be determined as the lowest weight that still guarantees a monotone change in curvature across the curve, as suggested by Frey^[23].

The leading edge between P_4 and P_5 will see substantial cyclic loading due to nozzle-interaction, which may lead to high cycle fatigue^[44]. In order to reduce notch-stress, an ellipse with low eccentricity or circle could be chosen here. The parameters for this are already included in the listing above. If a very high Mach number ($M_3 > 2$) is expected, an angular design may be better for controlling the inlet shock waves^[102].

Between P_5 and P_6 is the pressure side of the blade, which is half of the channel shape in the covered part. For this segment, a non-rational cubic Bézier curve was chosen, which would add two additional variables. If instead a Paluszny curve or non-rational quartic Bézier curve was chosen, two additional parameters would be needed in the end curvatures, but for a first design, two parameters may suffice.

3. See table 3.1 for a summary of the available segment types.

Curve Type	Additional Conditions	Method of Generation
Conic Segment	weight of middle control point	middle control point is at intersection of end tangents; weight as specified
	one internal point to interpolate	middle control point weight determined by interpolation point
	one end curvature	middle control point weight is determined by end curvature
Ellipse Segment	eccentricity, inclination angle	
Circle Segment	tangent circle	as described by Pritchard ^[74]
Non-Rational Cubic Curve	arbitrary number of points along the curve	least squares fit to points, maintaining end tangents
Rational Cubic Curve	end curvatures, two additional shape parameters	as in Paluszny et al. ^[69]
	end curvatures	as above, but with minimal bending energy or derivative bending energy
	end curvatures	as above, but with interactive selection of the free parameters
Non-Rational Quartic Curve	end curvatures, two additional shape parameters	as described in Appendix B

Table 3.1.: Major segment types implemented for profile development (see also: Appendix B)

The last segment is the trailing edge, and a circular segment is suggested here for simplicity, adding no further parameters. The total number of internal curve parameters would then be five.

3.5. Analytical Methods of Parameter Value Choice

Every additional parameter incurs a significant cost in optimization time^[26], so optimizing an entire stage using all of these parameters of both nozzle and stator in transient three-dimensional simulations is probably not feasible. It is therefore welcome when there are well-reasoned methods for selecting some of these parameters without them being part of the simulation.

For some parameters, this task is accomplished using additional input from other fields of research, such as the edge thicknesses, which may be determined by considerations of mechanical strength. Pitchline radii and axial cord length may be dictated by package size limitations.

For other parameters, it may be possible to separate optimizations with a smaller total computational cost. For example, one can separate the optimization of the nozzle from that of the rotor by a uniformity measure^[49,94]. Given the segmented nature of the blade, it may also be possible to separate an optimization of parameters in the outlet without influencing the nozzle-rotor interaction negatively.

For yet more parameters, there are guidelines, such as blade loading numbers by Ainley-Mathisson or Zweifel^[5], for estimating the required number of blades. Subsection 3.5.2 contains a detailed discussion on how this method can be supplemented by information from a specific supersonic method^[29] to predict the implications of rotor blade spacing for this case.

In all aspects where fluid properties are relevant, discussion in this section will rely on the assumption that the working fluid is a perfect gas. As these analytical models are approximate in nature, errors made in necessary assumptions for these models are likely to be larger than the deviations from ideal gas law.

3.5.1. Known and Novel Methods for Determining the Required Blade Stagger

The stagger angle is an important parameter for the efficiency of a turbine blade. If it is chosen too high, there is not enough length for the suction side to turn in a gentle enough manner to prevent flow detachment. If it is chosen too low, the additional camber length will

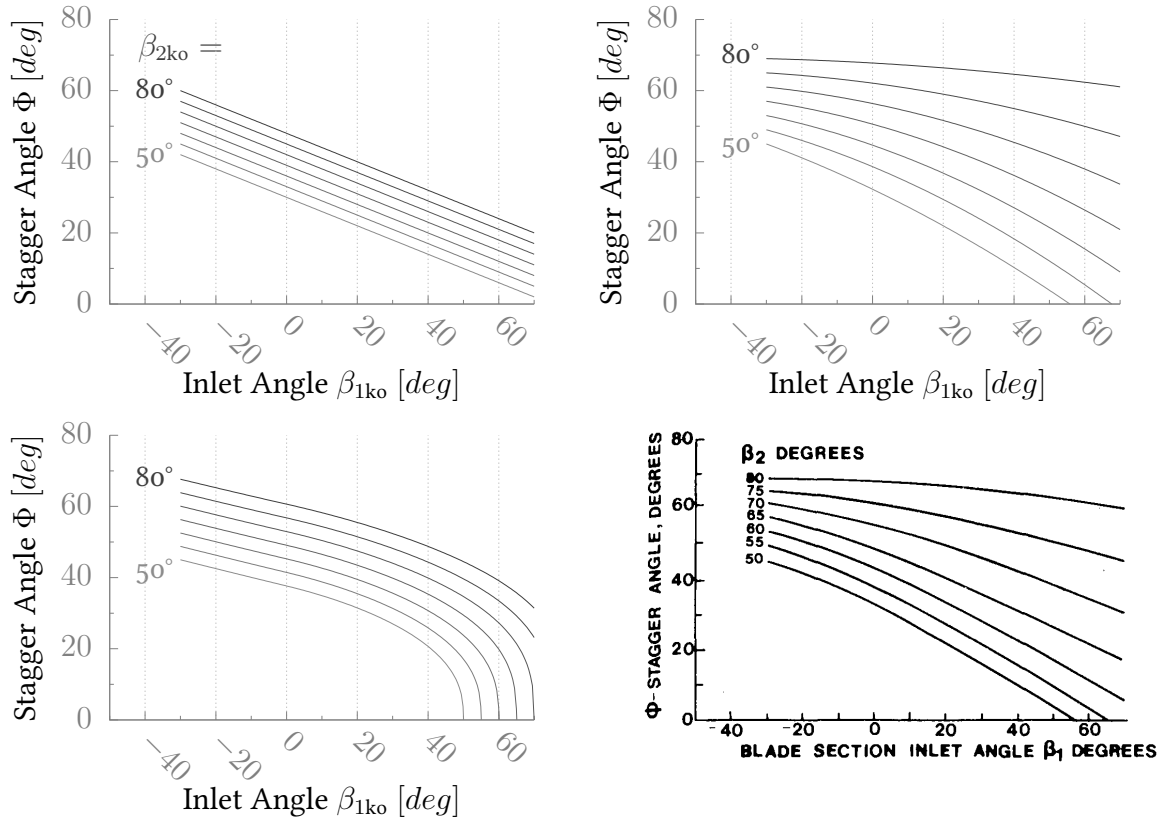


Figure 3.10.: Three estimations for blade stagger compared to the graphical representation by Kacker and Okapuu. Top left: Estimation suggested by Aungier^[5]; Top right: New Laplace-Approximation; Bottom left: New estimation based on Euler spirals; Bottom right: Reprinted from Kacker and Okapuu^[50]

cause unnecessary boundary layer growth. As in the rest of this thesis, all angle values are in degrees.

Aunger proposes the following equation to estimate the blade stagger angle^[5]

$$\Phi = \frac{180 - \beta_i + 1.5\beta_o}{2.5} \quad (3.3)$$

With

Φ blade stagger angle (see figure 1.1)

β_i blade row inlet angle

β_o blade row outlet angle

In several early attempts at blade row design, this estimation did not prove workable, usually giving far too low values for blade stagger. To find a better method, some additional literature research was conducted.

Kacker and Okapuu have written a very frequently cited work on loss in turbine blades^[50]. In this, they have a diagram for estimating the blade stagger. The contents of this diagram were approximated using the following Lagrange polynomial:

$$\begin{aligned}
x_0 &= -30 \quad x_1 = 20 \quad x_2 = 70 \\
y_0 &= 45 + 0.8 \cdot (40 - \beta_o) \\
y_1 &= 22 + 1.48 \cdot (40 - \beta_o) \\
y_2 &= -10 + 1.2 \cdot (40 - \beta_o)^{1.2} \\
y(x) &= y_0 \cdot \frac{(x - x_1) \cdot (x - x_2)}{((x_0 - x_1) \cdot (x_0 - x_2))} \\
&\quad + y_1 \cdot \frac{(x - x_0) \cdot (x - x_2)}{((x_1 - x_0) \cdot (x_1 - x_2))} \\
&\quad + y_2 \cdot \frac{(x - x_0) \cdot (x - x_1)}{((x_2 - x_0) \cdot (x_2 - x_1))} \\
\Phi &= 90 - y(90 - \beta_i)
\end{aligned} \tag{3.4}$$

Unfortunately, this also did not always result in estimates for blade stagger that were workable at the blade design stage either. A third method was devised to make better estimates. This method makes an explicit assumption about the shape of the camberline. Anders et al. suggested that a good blade shape would be one with curvature decreasing linearly with the curve length^[1] towards the trailing edge. In mathematical terms, this would be an Euler spiral, also known as a Cornu spiral. Assuming this curve as the shape of the camberline, the vanishing curvature at the trailing edge frequently led to stagger angles that were too high; perhaps this assumption is more suited to subsonic blades with a large angle of uncovered turning.

Instead, a camberline curve was assumed in which the curvature is proportional to the square of the curve length. Lee has published a description of such a curve on his website^[60], which was tested and confirmed to have the desired distribution of curvature.

$$\vec{x}(t) = \int_0^t \begin{bmatrix} \frac{\sin(a^{n+1})}{n+1} \\ \frac{\cos(a^{n+1})}{n+1} \end{bmatrix} da \tag{3.5}$$

With

n exponent of curvature change

t curve parameter

From the equivalent expression for normal Euler spirals ($n = 1$), the following expression was derived for the relationship between the inclination angle of the curve and the curve parameter t :

$$t(\alpha) = \left(\frac{\alpha \cdot \pi}{180} \cdot (n + 1) \pi^{\left(\frac{-n}{2} - 0.5\right)} \right)^{\frac{1}{n+1}} \quad (3.6)$$

For nozzle profiles with $\beta_i \geq 90^\circ$ the following steps were used:

$$\Delta\beta_{le} = (90 - \beta_o) + (90 - \beta_1) \quad (3.7)$$

$$\vec{x}_{le} = \vec{x}(t(\Delta\beta_{le})) \quad (3.8)$$

$$\Phi = \tan^{-1} \left(\frac{x_{le2}}{x_{le1}} \right) + \beta_o \quad (3.9)$$

With

$\Delta\beta_{le}$ the turning angle of the blade

\vec{x}_{le} the point on the spiral where the turning angle is reached

$x_{le1,2}$ the individual coordinates of this point

For rotor or stator blades, where the inlet angle β_i is less than 90° , the camberline curve is first calculated to 90° , and then mirrored at that position. The mirrored arc is clipped at the position where the desired inlet angle is reached. This position is the assumed leading edge from which the stagger angle can be calculated.

If an exponent of $n = 1$ is chosen, the results from the new method much more closely resemble the estimation that Aungier proposed^[5], although impulse bladings, where $\beta_i = \beta_o$, are predicted to have vanishing stagger angle. This gives weight to the hypothesis that the assumption $n = 1$ may be better for subsonic bladings, which is the topic of Aungier's work. If a large body of known good profile blades was available, perhaps a correlation between the exponent n and the design Mach number could be found.

All of these methods discussed in this subsection are compared to the figure presented by Kacker and Okapuu^[50] in figure 3.10, the stagger angle of seven different outlet angles is plotted over the inlet angle. Inlet and outlet angles in this diagram are in the notation used by Kacker, which is $\beta_{ko} = 90 - \beta$.

3.5.2. The Throat Area Problem

The area ratio of convergent-divergent profiles, whether for rotor or nozzle blades, has previously been studied by several authors^[9,13,20,29].

The first apparent solution to choosing the area ratio is the Mach number area relation, which describes the required area ratio for an isentropic nozzle with uniform flow (equation 3.10). This approach quickly falls short in blade channels, because the redirection of flow causes different speeds on the pressure and suction sides^[27]. Further, boundary layers block a significant portion of the available area^[20,30]. Or in other words, the flow in the throat of a turbine profile is neither uniform nor isentropic.

$$\frac{A_{o,id}}{A^*} = \frac{1}{M_o} \left[\left(\frac{2}{\kappa + 1} \right) \left(1 + \frac{\kappa - 1}{2} M_o^2 \right) \right]^{\frac{\kappa + 1}{2(\kappa - 1)}} \quad (3.10)$$

With

$A_{o,id}$ Outlet area of a Laval nozzle with the Mach number M_o

A^* throat area

M Mach number

κ isentropic exponent

Dejc^[13] gives the following empirical relation for the throat area of Soviet nozzle profiles with an outlet Mach number smaller than 2.4:

$$\frac{A_o}{A^*} = 1 + (0.3 \dots 0.6) \left(\frac{A_{o,id}}{A^*} - 1 \right) \quad (3.11)$$

Within equation 3.11 there is a free parameter. Dejc argues that smaller throat areas will lead to better performance at the design point, but a sharper drop off in off-design conditions.

It is unclear how much of these and other results are verified in full turbine stages, and how much is just verified in cascade tests. While Dejc^[13] gives at least three examples of full stages designed like this, it is not transparent how the parameters for these experiments were chosen. A rigorous study of the Russian language papers, on which the book is largely based, may shed some light on the issue.

Assuming that the recommendations are largely based on cascade data, it stands to reason

4. Dejc gives equation 3.10 as a function of the critical Mach number ($q(M^*)$), but the expressions are equivalent.

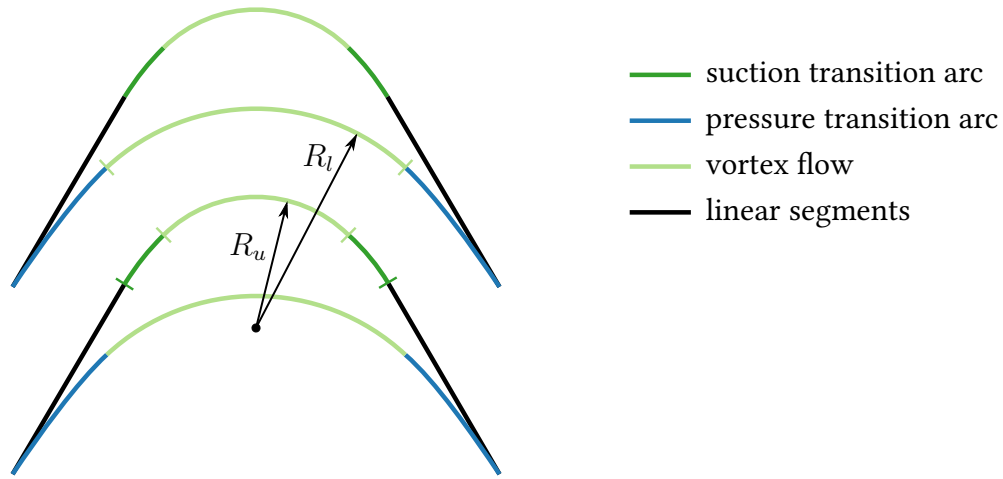


Figure 3.11.: Rotor Profile proposed by Boxer et al.^[9]

that Dejc systematically underestimates the losses induced by increased shock strength in the wake of a nozzle. If the effective area ratio in the nozzle is insufficient to generate the desired outlet Mach number, the strength of shocks emanating from the trailing edge will be increased. On the pressure side of the trailing edge, the flow will expand around the edge, and thereby be redirected towards the axial direction. To satisfy continuity, the flow at the suction side of the trailing edge will be parallel to the trailing edge. A shock must result where the two flows meet in order to make them compatible. The higher underexpansion in the nozzle, the stronger the shock will be. This shock now interacts with the boundary layer of the rotor, potentially causing a large decrease in performance. It is therefore unclear if the claimed wider operating range for underexpanded profiles can actually be realized in a turbine stage.

The situation in the rotor is more complicated still. It is known from experiments^[13,20,29] that supersonic turbines can become unstated, as was discussed in section 3.1. To estimate which values of throat area lead to an unstated rotor and should thus be avoided, one can use the design method first published by Boxer et al.^[9] as an analytical model.

This model is partly attributed to Busemann^[9], and was later modified and developed into a computer program by Goldman^[27,29-31]⁵. This method was mentioned before in the context of the Vulcain oxygen turbine (see subsection 3.1.2).

The method proposes that the flow turning in the rotor should be accomplished by a source-vortex flow. The proposed profile is designed as seen in figure 3.11. It contains four

5. Dejc and Trojanovskij^[13] also describe this as an alternative design method for rotors on their pp.124, and even reprint five figures from Boxer et al.^[9], but do not cite any source.

different kinds of segments. The suction side is formed by a straight segment, a transition curve, and a circular segment, followed by another transition curve and straight segment. The pressure side is analogous, but without transition segments. The transition segments are formed by a method-of characteristics calculation, with the objective of accepting a homogeneous supersonic flow, and transitioning it into a source-vortex flow in the inlet (i.e. a vortex flow where the velocity is inversely proportional to the radius^[84]) and vice versa in the outlet.

The main effort in a critical discussion of this method is to determine the objective of individual steps in the design method. No argument is known, for example, in any of the aforementioned works, that the source-vortex flow pattern holds any performance advantage over any other shape of flow. It is possible to conclude that the objective in selecting this solution was that it is a flow pattern for which performance parameters can be derived analytically. Considering that the known optimization studies^[38,53] reshaped the blades to depart further from source-vortex profiles than their respective baselines, it stands to reason that source-vortex flow is likely not a particularly performant choice. Elegant as the mathematics of it may be, it seems that the use of this blading method should be as a simplified model to inform parameter choice, rather than an actual solution to the blading problem.

Given this distribution of velocity, the edge case of a rotor that is just started would be one where the Mach number is unity at the circular segment of the pressure side. To achieve this, the Mach number (M'_3) at the inlet needs to be somewhat higher than unity. By inserting critical state values in the equation Boxer gives for the area^[9], a rough estimation of the required starting Mach number is made as follows⁶:

$$\left(1 - \frac{2r_{ri}}{s_r}\right) \frac{\cos(\alpha'_e)}{\cos(\alpha'_3)} = \frac{M_3^{*'}}{M_e^{*'}} \left(\frac{\kappa + 1 - (\kappa - 1)(M_3^{*'})^2}{\kappa + 1 - (\kappa - 1)(M_e^{*'})^2} \right)^{\frac{1}{\kappa-1}} \quad (3.12)$$

With

r_{ri} rotor leading edge radius

s_r rotor blade pitch

M^* critical Mach number

6. Boxer gives a normalized value for s_r in this equation. This would make the unit mismatched with the non-normalized r_{ri} , so there must be an error. Either both are meant to be normalized, or none. Whichever it is makes no difference here.

$$M^2 = \frac{2(M^*)^2}{\kappa + 1 - (\kappa - 1)(M^*)^2} \quad (3.13)$$

$$M^*(M) = \frac{M\sqrt{\kappa + 1}}{\sqrt{M^2(\kappa - 1) + 2}} \quad (3.14)$$

$$\alpha'_e = \alpha'_3 + \delta_3 + \frac{1}{2}\gamma_{ri} \quad (3.15)$$

(assuming no inlet deviation)

$$\alpha'_e = (90^\circ - \beta_3) + \frac{1}{2}\gamma_{ri} \quad (3.16)$$

With

δ_3 deviation angle

For the flow values α' and M' , there are two indices in this equation, e and 3. While 3 indicates the rotor inlet (see figure 1.1), instead of an average, the circumferential position with the lowest value of flow angle α_3 may be taken as the sample point to prevent periodic unstarts in the nozzle wakes, if the complete distribution of flow angles is known.

The location e would be the entrance of the covered channel, but behind the inlet shock and related disturbance. The location is virtual, since the effect of the inlet shock can reach far into the covered channel^[9].

The location l would be on the pressure side, where the lowest Mach number is expected, i.e. the location most at risk of unstating. For Boxer^[9], this is the end of the pressure side inlet transition arc. More generally, one could assume it is the position on the pressure side ahead of the impingement point of the first expansion waves coming from the suction side (see figure 3.8). This indicates that is advisable to turn the pressure side as little as possible between the leading edge and this location. In a first estimation, one could further assume no turning on the pressure side before this location. This yields $M'_l = M'_e$, i.e. the rotor is expected to be started if $M'_e > 1$.

If there is turning on the pressure side before the source-vortex segment, the minimum value of M'_e is estimated as follows:

$$\nu(M) = \sqrt{\frac{\kappa + 1}{\kappa - 1}} \tan^{-1} \left(\sqrt{\frac{\kappa - 1}{\kappa + 1}} (M^2 - 1) \right) - \tan^{-1} (\sqrt{M^2 - 1}) \quad (3.17)$$

$$\nu(M'_l) = \nu(M'_e) - \Delta\alpha' \quad (3.18)$$

With

- ν Prandtl-Meyer Angle
- $\Delta\alpha'$ redirection before the point p

In summary, equation 3.18 is used to estimate the required value of M'_e , if the blade shape is known. If it is not known, it may be assumed that $M'_e = M'_l = 1$. Then equation 3.16 is used to estimate α'_e , which in turn is inserted into equation 3.12 to determine the required relative inlet Mach number M'_3 .

However, there is a limitation to this method, which is that all Mach number changes are assumed to be isentropic. Isentropic compression of supersonic flow is rarely possible^[84]. Further, it is known from theory and experiment^[93] that there may be a substantial shock in the inlet of a rotor profile, depending on the leading edge geometry. The aforementioned method is therefore a guideline rather than a good determination. If the method predicts that the profile will not start, this is quite likely so, but even if the method predicts a started profile, it may become unstarted entirely or at least have a subsonic flow region on the pressure side, as can be seen intermittently on the first stage rotor of the Vulcain 2 oxygen turbine in figure 3.2.

While this concludes the discussion of unstarts because of insufficient Mach number, Boxer^[9] points out that unstarts can also happen at too high Mach numbers. To estimate this limit, the channel of the rotor can be equated to a supersonic diffuser, a convergent-divergent channel set in a supersonic external flow. If the analogous diffuser has a normal shock before the inlet and a subsonic flow throughout the channel, the turbine is predicted not to start. If the analogous diffuser has a supersonic flow until at least the throat, the rotor would be considered started.

To quantify the analogous diffuser, the variables Q and C are introduced in the following condition for a started rotor.

$$\frac{Q}{1 - C} > \frac{p'_{0e,s}}{p'_{0e}} \quad (3.20)$$

With

- Q vortex parameter^[29]
- C change in mass flow due to vortex flow velocity distribution^[9]
- $\frac{p'_{0e,s}}{p'_{0e}}$ normal shock total pressure ratio^[29] at the location e

The right side is a known function of only the (critical) Mach number^[29], generally:

$$\frac{p_{0,s}}{p_0} = f(M^*) \quad (3.21)$$

$$= (M^*)^{\frac{2\kappa}{\kappa-1}} \left[\frac{1 - \left(\frac{\kappa-1}{\kappa+1}\right)(M^*)^2}{(M^*)^2 - \frac{\kappa-1}{\kappa+1}} \right]^{\frac{1}{\kappa-1}} \quad (3.22)$$

In a source-vortex flow, the critical Mach number M^* is inversely proportional to the radius. That means, by knowing the critical Mach number and the radius of one position, the critical Mach number for any position may be determined though this reverse proportionality.

As the Mach number in location l is already determined through equations 3.12, 3.16 and 3.18, this is an easily available option. To obtain an accompanying radius, there are a number of possibilities.

If the parameter system proposed in section 3.4 is used, one of the parameters is the opening size at the rotor inlet, t_{ri} . The inlet opening can be used as an analogue for the vortex-flow channel. The curvature on the suction side is a dependent variable, which can be determined by applying the method for minimal weight conics by Frey and Field^[23]. Knowing the curvature k_{P3} on the suction side (see figure 3.9), a radius for the pressure side could be determined as follows:

$$R_l = \frac{1}{k_{P3}} + t_{ri} \quad (3.23)$$

With

t_{ri} the distance between rotors at the inlet

Another method to estimate the value would be to assume the entire pressure side is a single circular segment. The radius could then be determined from common blade parameters:

$$R_l = \frac{b_{zr}}{\cos(\beta_3) + \cos(\beta_4)} \quad (3.24)$$

With

b_{zr} the axial chord of the rotor $z_4 - z_3$

Together with the Mach number M'_l this determines the Mach number at any point between l and the adjacent point u on the suction side. Importantly, the Mach number on the

suction side can be calculated, if a distance t_{ul} from pressure side to suction side is given. As above, the opening size t_{ri} could be used, if the positions u and l are not yet determined.

$$\frac{M^{*'}}{R} = \frac{M_l^{*'}}{R_l} \quad (3.25)$$

$$M^{*'}(R) = R \frac{M_l^{*'}}{R_l} \quad (3.26)$$

$$M_u^{*'} \approx \frac{M_l^{*'}}{R - t_{ri}} \quad (3.27)$$

Using the equations from Goldman^[29], the aforementioned parameters Q and C can now be determined as follows:

1. Determine the parameter K_{\max}^* by finding the root of the integral in his equation 25
2. Determine C by as a function of K_{\max}^* , $M_u^{*'}$ and $M_l^{*'}$ using his equation 34b⁷
3. Determine Q from as a function of $M_u^{*'}$ and $M_l^{*'}$ from his equation 34a

This determines of the maximum Mach number for started operation, and together with the previously determined minimum Mach number, it determines the operational envelope for a particular rotor profile given the numerous approximations described before and assuming that the flow does not detach on the suction side.

Performance degradation and flow detachment are the last topic to be covered in this subsection. It was previously discussed how low Mach numbers on the suction side or small flow channels can lead to unstarts of a rotor. This may leave an attentive reader with the impression that the flow channel should be made as large as possible, and that the flow should never be decelerated on the pressure side.

As stated before, the critical Mach number in the rotor channel will increase towards the suction side. This is true for any rotor, but assuming source-vortex flow, the relationship between distance to a center of flow rotation and critical Mach number is inversely proportional. This means that the Mach number on the suction side is a function of the throat size t_r and the presumed vortex-flow radius on the pressure side, with a larger throat indicating a higher overspeed on the suction side.

Boxer^[9] assumes that all of this overspeed needs to be decelerated in the rotor outlet. While this is not necessarily the case, if non-uniformity in the outlet is permissible, there needs to be some amount of deceleration to equalize the pressure at both sides of the trailing

7. Goldman only covers rotors, so while relative Mach numbers are marked with a prime (') here, Goldman does not do this.

edge. Since a deceleration causes an adverse pressure gradient^[84], this leads to a thickening and potential detachment of the boundary layer^[29].

One way to reduce the overspeed would be to constrict the flow path from the pressure side, in order to lower the pressure side Mach number, if the inlet Mach number is high enough to allow this. In this case, the constriction of the pressure side would again cause an adverse pressure gradient, now at the pressure side inlet.

Goldman^[29] gives two relations to predict the occurrence of flow detachment. The first, his equation 39, relates the minimum allowable critical Mach number on the pressure side M_l^{*f} to the inlet critical Mach number. The second, his equation 40, relates the outlet critical Mach number to the maximum allowable suction side critical Mach number M_u^{*f} . Goldman bases this method on data gained from incompressible flow^[29], and experimental results^[20] indicate that the estimation is much too optimistic, but no better method is known.

While this discussion of Boxer's method and Goldman's additions^[9,29] did not yield simple rules for selecting parameters, it did offer insights into the flow implications of parameter choices for supersonic rotors. As a way to design rotor blades, the source-vortex model is flawed in many regards, like the assumption of isentropy in the inlet, or the reliance on a particular analytically predictable pattern of flow in the channel. As a method to understand the trade-offs within a rotor blade design, it is nevertheless useful.

A overlarge channel causes either a subsonic pressure side flow, or large overspeed on the suction side, depending on inlet design. Building a smaller channel, for example by lowering the pitch, may solve this issue but can cause the rotor to become unstated at higher Mach numbers, in addition to the increased relative size of boundary layers known from subsonic turbines^[22].

Especially for cases where the inlet flow is not uniform, such as a partial admission turbine, or turbines where the nozzles have thick trailing edges, different Mach numbers occur not only at different operating points, but also at different relative positions of nozzle and rotor blades. This makes it necessary to create rotor blades with as wide an operating envelope as possible.

3.5.3. Fair Curves

The last method in this section to determine parameters, and thereby reduce the optimization effort, primarily concerns the internal parameters of several curve types (see table 3.1).

Without any specific knowledge of the flow around a blade, it is still apparent that some curves are more likely to produce an efficient redirection of flow than others with the same boundary conditions. Colloquially speaking those curves appear "smooth" or "aero-

dynamic”. Mathematically, the such curves are called “fair”, although there is not one single measure of fairness, but several^[67,80]. Commonly, those measures assign worse fairness to curves that have features such as turns with high curvature, many local extrema of curvature, or in some cases sudden changes of curvature.

The importance of curvature continuity has long been known in blade design^[11,58]. A commonly used method to obtain a blade profiles with none of the aforementioned defects is giving a particular distribution of curvature as input^[1,58]. Using a generic method to determine the curve fairness has the potential to offer the same benefits while requiring less user input.

The measure that has shown the most promise in blade segment design is here called the derivative bending energy, defined below as

$$E_2 = \int_0^{s_c} \left(\frac{dk(s)}{ds} \right)^2 ds \quad (3.28)$$

With

- E_2 derivative bending energy
- k local curvature
- s distance along the curve
- s_c total cure length

In words, the square of the derivative of the curvature is integrated over the length of the Bézier curve. Lower values mean better fairness.

In a blade design, a segment curve may now be designed with a number of open variables. An optimization algorithm is then used to find the combination of variables with the lowest derivative bending energy. A common challenge with this kind of optimization is that algorithms used to numerically perform the definite integral in equation 3.28 tend to underestimate the value of this integral. Therefore, it can occur that the optimization finds not the lowest actual value, but the parameters where the numerical integration most underestimates the function.

Hagen and Bonneau^[40] have found that neither rectangle rule nor Simpson rule are adequate numerical methods here, but have had better success using trapezoid rule. For Paluszny and non-rational quartic curves, it was found that it is important to limit the parameter range, since the problems tended to occur at very low or very high parameter values. The most consistent results were obtained when possible curves were first investigated by interactively manipulating the parameters, and the fairness optimization was only used to find a local minimum in a tightly controlled parameter space. It is hoped that with

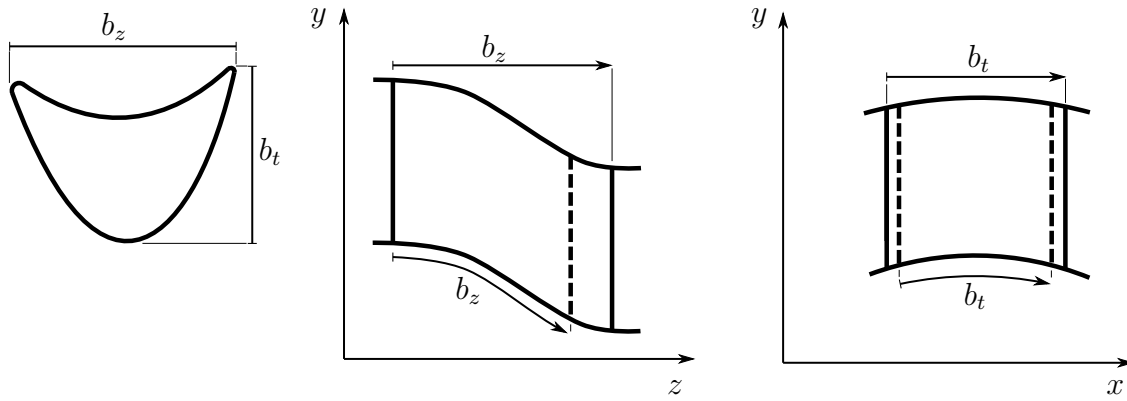


Figure 3.12.: Effect of length measures on prismatic blade geometry

some work, additional conditions, such as the number of local minima of curvature, can be added to automate the process further.

3.6. 3D Blade and Channel Shape Generation

Once a set of two-dimensional section curves is settled, the remaining task is to generate a three-dimensional blade from this. There are some ways to proceed, which will be discussed below, but before this is even started, a decision needs to be made on how to interpret the coordinate system of the 2D blade. As pictured in figure 3.12, the horizontal direction may be interpreted as the axial distance from the leading edge, or the distance from the leading edge along an assumed meridional flow path. Perhaps even more importantly, the vertical axis can be interpreted as either the height one would see when looking straight at the blade tip, or the distance along the tangential direction. Taking the horizontal chord (b_z) to mean the meridional length along the side wall ensures that the channel length remains as designed, but inlet and outlet angles are influenced by this choice, and may need to be adjusted. While the length differences are exaggerated in figure 3.12, even a minuscule change in flow angle (0.2°) can have significant effects on performance (see subsection 3.7.1).

Once a decision on the length measures is made, blade generation can proceed in several ways, which are described in the following.

3.6.1. Documented 3D Blade Generation Techniques

The simplest way to generate a blade is to extrude the two-dimensional shape along one axis. A blade center is chosen, for example the geometric center of area of the shape, and the whole curve is extruded along a straight line from this point radially inward toward the

rotor axis and outward toward the shroud. The disadvantage of this is that the resulting blade shape must be a prism; there is no control over the shape other than the 2D profile curve.

Techniques for blade shaping come into play where more control over the shape is needed. There are many techniques and not all will be covered here. Generally though, the process consists of two main steps, and for both steps there are different methods that can be used. The steps and methods will be discussed in order as listed below.

1. Generating 3D space curves from sections

- Placement of flat curves

- Placement and skewing of flat curves

- Projection onto canvases

2. Generating a 3D surface

- Point cloud interpolation

- Lofting

One way to obtain some basic control over the three-dimensional shape of the blade is to define a number of different 2D sections to be used at different radial positions between the hub and the shroud. The sections could then be placed in space as flat curves, and interpolated in the radial direction to give a three-dimensional blade. This method has some disadvantages, in that the lowest section must be at or below the lowest point of the hub and the highest section must be above the highest point of the tip. The ends of the profile that overlap with the hub or extend farther than the tip must then be cropped to generate the final profile. If the flow path is curved, as shown in figure 3.12, much of the blade design will be removed this way, and thus a sizable part of the parameter space may have no influence on the shape of the blade. For example, if the channel was shaped as in figure 3.12, the inlet angle of the lowest section and the outlet angle of the highest section may be completely irrelevant. This method is best suited for rows with many blades and straight or slightly inclined flow paths.

In cases where there is moderate inclination of the flow path, and the blade number is high enough that hub and shroud are only lightly curved, it is possible to skew the section profiles in the y-direction without changing the geometry in the xz-plane. As each dimension of a three-dimensional Bézier or NURBS curve is a separate polynomial, this operation is easily possible with these curves.

In order to obtain even better control over the blade shape, especially in the important regions of hub and shroud, an intermediate step can be taken. Herein, the 2D sections are transformed to non-flat curves in space before being used to generate a blade surface. While Dejc in 1973 specifically decries the lack of availability of such methods^[13], they appear to have since become the standard for current profiling techniques^[1,49,57].

Characteristically, they require an intermediate step in the definition of a set of surfaces, here called “canvases” to which the section curves are first fitted. A number of surfaces equal to the number of section curves is chosen with the assumption that no significant flow occurs through these surfaces, because the flow is mostly parallel to them. This can be done by defining a set of assumed meridional flow paths through the stage, and then creating surfaces of revolution by turning the meridional flow path around the turbine axial direction. In the simplest example, this is a cylinder mantle with the diameter between the smallest hub diameter (d_{4h} for the rotor in figure 1.1) and the largest shroud diameter (d_{4s}). In more complex examples, it could be a cone mantle segment, the surface of revolution of a freely defined Bézier curve, or even a general Bézier surface, if for example, end-wall shaping is desired^[79].

Several mathematical methods exist for generating a three dimensional curve from a two dimensional curve and a three-dimensional canvas surface. One could take the coordinates of a large number of points in each section curve and find corresponding points on the canvases. For example if a point on the section curve is $P_n = (1\text{ mm}, 3\text{ mm})$, a point on the surface can be located that is likewise 1 mm in one direction and 3 mm in an orthogonal direction distant from an origin. The measure of distance must be defined beforehand, as was explained in the opening of this section. The height-component of the point would then result from placing the point on the canvas.

While this would result in a projection of the section, it does carry some disadvantages. As with world maps, the projection can either be angle-preserving (conformal) or distance preserving (equidistant), but not both at the same time. Furthermore, this method only yields individual points on a 3D-curve. In order to generate a complete curve with infinite points, whoever receives it (e.g. for documentation, or manufacturing) must follow the same method to create a smooth curve. This may not be possible, for example because the method is imprecisely described, or the receiving side does not have software to perform the required computation. In such a case, either a large number of points can be generated, or a NURBS curve can be made, which interpolates the points.

Finding an interpolating NURBS curve for the point set solves the communication issue, but raises others. Such a curve is generally not precisely on the canvas. Therefore, the resulting hub section curve, for example, has a non-zero distance from the actual hub in

most places. Surfaces that do not perfectly match one another in this way are called “not watertight”, and may cause problems when forming a solid blade shape by combining hub, top and blade mantle surfaces. One solution would be to extend the hub section curve slightly into the hub, but this sacrifices some amount of control over the blade shape in order to solve a technical issue.

Furthermore, as with every interpolation, there are risks of losing curve features, such as kinks, from the original curve or gaining features that were not present in the original curve, such as waviness, by over-fitting. Methods that try to prevent such behavior exist^[73], but may not function in all cases. This would be an additional source of errors when automatically optimizing a profile without an operator checking every single candidate for defects.

The last step is to generate a blade mantle surface from the projected curves. If, in the previous step, a set of NURBS curves was generated, the mantle surface can be made by a process called “lofting”^[73]. There are several methods to generate a lofted surface^[103] and they share the property that all the section curves lie precisely on the surface, i.e. for every curve point $\vec{P}(w)$, there is a combination of surface parameters (u_P, v_P) , so that $\vec{P}(w) = \vec{S}_m(u_P, v_P)$, with \vec{P} , the projected section curve function and \vec{S}_m , the blade mantle surface function. Positions along the span of the blade, outside of the pre-defined projected section curves, are interpolations between the specified section curves. As such they can contain unwanted features, but since the number of section curves is usually low (three to seven have proven adequate), the problem is much less severe than for interpolating along the section curve.

3.6.2. Segment-Wise Context-Aware Projection Technique

Many methods have been proposed in the past to geometrically generate three dimensionally shaped profiles, and a non-exhaustive summary of common elements between some of these known methods was given in the previous segment. Along the way, several common problems were raised, and while there may be other ways to solve them, this subsection gives the solution that was developed specifically so it would fit the needs of supersonic blade shapes.

The first problem to be addressed here is that simple projection techniques cannot be at the same time angle- and distance-preserving. To circumvent this, a segmented parametric blade design, like the ones described in section 3.4, is first broken down into the individual segments. The two-dimensional segment curves are then individually transferred into three-dimensional segment curves by the algorithmic method summarized below.

While the number and type of constraints differ based on the type of segment curve, each type of segment contains a function `projectCurve`($\vec{L}(t, z), \vec{D}(u, v, \vec{D}_{t,z})$). This function is called by a canvas object and asks that the two-dimensional segment curve represents itself as a curve in the (u, v) -space of the canvas' tensor surface. For this purpose the canvas hands the segment two functions of its own: $\vec{L}(t, z) = (u, v)$ and $\vec{D}(u, v, \vec{D}_{t,z}) = \vec{D}_{u,v}$, where t is the distance along the surface from an origin, and perpendicular to the axial direction z . On a cone mantle, this is the tangential direction. Both these functions solve the inverse problem of finding a value tuple in the parameter space (u, v) that would translate to a specific tuple in the (t, z) -space⁸. The first ($\vec{L}(t, z)$; “ L ” is for “location”) reverses the tensor surface function^[73] $\vec{S}(u, v) = (x, y, z)$, and the function to translate (x, y, z) coordinates to (t, z) -coordinates on a canvas.

The second function does something similar for directions. Given a specific location in (u, v) -space, and a direction vector in (t, z) -coordinates, it looks up what direction a vector in (u, v) -space would have to point so that it will be translated to a specified direction in (t, z) -space, i.e. it calculates the partial derivatives $\frac{\partial t}{\partial v}$ and $\frac{\partial z}{\partial u}$ at the location (t, z) and applies them to a direction vector.

Using these two lookup functions, the function `projectCurve`, which is different for each type of segment, finds a way to represent itself in the (u, v) -space so that it will be translated by the surface function $\vec{S}(u, v) = (x, y, z)$ to a space curve that represents the designer's intent in defining the segment.

In a simple example, a conic segment (i.e. a rational Bézier curve of degree 2) could be transferred from (t, z) coordinates to (u, v) coordinates in the following steps:

1. Look up the positions of the control points P_0 and P_2 in the (u, v) space
2. Look up the curve directions at both ends D_0 and D_2 in the (u, v) space
3. Find the middle control point P_1 by finding the intersection of the two lines from the points with their respective directions
4. Apply the same weight to the middle control point as was applied in the 2D profile curve

This would preserve the axial and tangential length distance of the end points, and the end tangent directions. The end curvatures would not be exactly preserved, but in practical

8. Searching for a specified point in a different length measure is likewise possible (see figure 3.12). In this case, the functions would be of the coordinates in that system instead of (t, z) .

use the change in end curvature through this transfer method and the other ones described in appendix B was insignificant.

The result of this process is a curve in (u, v) -coordinates. When the surface function is applied to each point on this curve ($\vec{S}(\vec{P}(w))$)⁹, it renders a space curve in (x, y, z) Euclidean coordinates. The resulting curve is not a projection in the strictest sense, but rather a transfer. Neither the length nor the angles are precisely preserved for internal curve points, but both are preserved in the end points. This allows the generation of three-dimensional curves that exactly match the defined parameters of the parameter system, including features like the precise angle change in a kink.

The final step before lofting the curve is to generate a Bézier curve $\vec{P}'(w) = (x, y, z)$ in Cartesian coordinates from the Bézier curve in (u, v) -coordinates and the surface. Space curves that are defined in this way are called “trim curves”, because of their usage in boundary representation (B-Rep) solids, which is a common way to represent solids in CAD systems. These trim curves can be shown to have a precise representation as ordinary 3D Bézier curves in (x, y, z) -coordinates^[59]. The degree of these curves is $p \cdot (m + n)$ where p is the degree of the curve in (u, v) coordinates and m and n are the degrees of the canvas surface in u and v -directions, respectively.

Finding the three-dimensional control points of this curve and their weights is achieved using a blossoming version of the DeCasteljau algorithm, as was described by Lasser and Bonneau^[59]. The result is a set of control points that define an ordinary three-dimensional Bézier curve. It can then be used in one of the previously described lofting methods to generate a segment of the blade mantle surface. Using a knot vector^[73] these segments can then be assembled into a single mantle surface of the whole blade (as pictured in figure 3.13). The resulting NURBS surface may be written without loss of information in many common CAD data exchange formats (e.g. iges, step), and read by a wide variety of simulation or manufacturing software.

3.6.3. Possible Applications of Three-Dimensional Blade Shape Generation

The preceding subsection described a method to generate arbitrary three-dimensional blade shapes but gave no information on how this may be used to generate blades that are superior to prismatic blades.

Subsonic turbines are often designed with blades that are formed so that the flow can

9. The curve parameter is called w instead of the canonical u to distinguish it from the surface parameter of the same name.

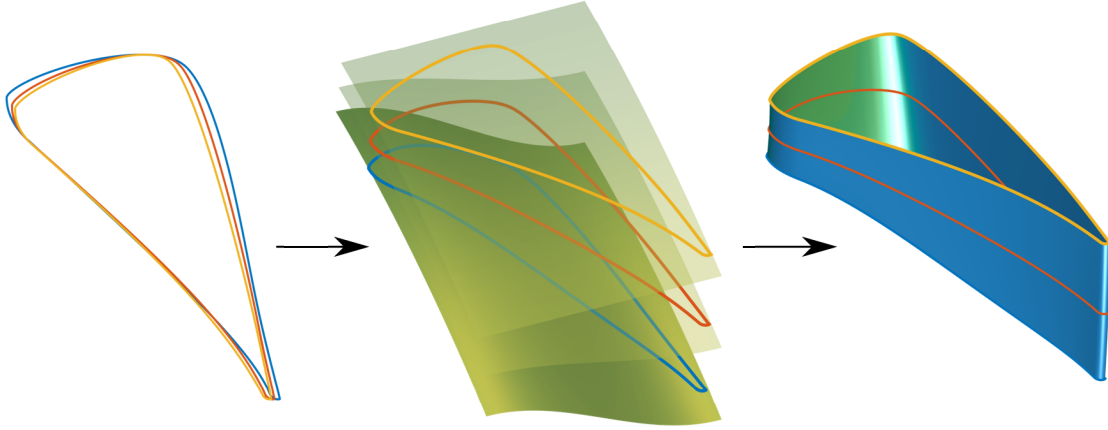


Figure 3.13.: Three profiles are getting transferred onto canvases and a mantle surface is created by lofting

leave one blade channel and still maintain a radial equilibrium of forces in the space between blade rows^[104]. At least in the idealized model, an individual flow particle can be moved towards the hub or the shroud within a blade channel due to changes in radial pressure distribution, but it passes from one row to the next without moving radially, unless the hub and shroud walls themselves are inclined in the meridional plane.

This concept has been studied extensively by various researchers^[5,88,98,104] and has at one point been widely applied in developing power plant turbines^[88] as a method to increase efficiency by giving blades a non-prismatic shape. It has also been applied to sub- and trans-sonic turbine stages in rocket engines^[38,82]. When optimizations for supersonic turbines are conducted, however, the focus appear to be less on the radial equilibrium, and more on the improvement of shock-boundary interactions^[39] and stator-rotor interactions^[71]. The shocks that are central to these considerations may make radial equilibrium calculations challenging, because they violate common assumptions^[15] such as time-steadiness or smallness of circumferential variations in flow properties (see section 2.6).

In general, documented applications of three-dimensional shaping in supersonic turbine blades for rocket engines seem to be rare, which may be due to the fact that blade heights are usually small, as described in section 2.5. Another reason may be publication bias. If specific three-dimensional shaping techniques are seen as advanced, the developers may choose not to publish them for competitive reasons.

One documented three-dimensional shaping developed by Griffin et al.^[38] used parametric optimization techniques to improve turbine performance on both blade rows of a supersonic first stage of a turbine. They optimized the profile individually in three section curves, root, mean and tip.

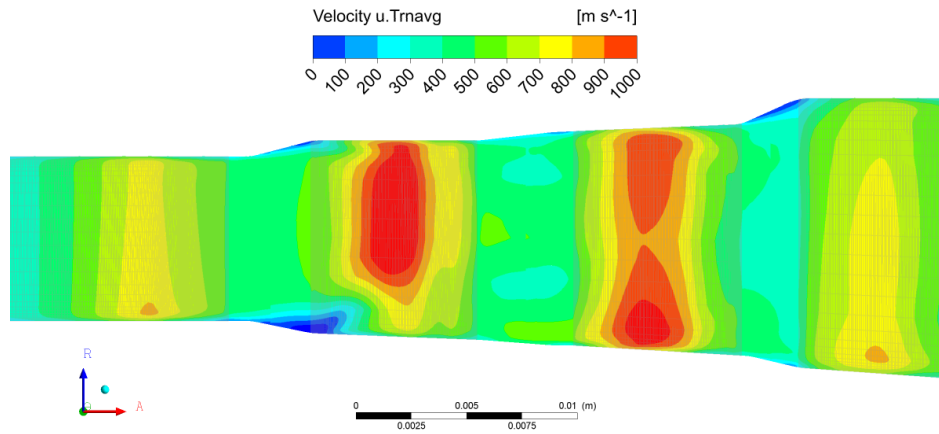


Figure 3.14.: Simulation of time-averaged, area-averaged axial velocity in a meridional cut of the M1 engine fuel turbine

The most notable results were a decrease in stagger angle towards the tip, and a smaller profile at the root, leading to a flow channel that has a similar area at hub and tip. However, this causes the profile to be heavier at the tip than at the hub, which may negatively influence durability, as centrifugal forces will be concentrated at the root.

The profile was successfully tested in a sub-scale configuration^[16,38], however it is not explicitly stated whether the rotor profiles were manufactured with the three-dimensional geometry intact or simplified to prismatic profiles.

One more three-dimensional flow phenomenon that often affects supersonic turbines is a particular pattern of flow detachment at the hub between the nozzle and first rotor row. Versions of this were seen in the development the Vulcain engine^[20] and the GGGT development program^[37]. It is also a known issue with the M1 turbine, that can be reproduced in simulations (see figure 3.14). In supersonic turbines, the tangential velocity leaving the nozzle is typically very large for the reasons described in chapter 2. This causes a large radial gradient in static pressure^[104] which can cause detachment, even without any Mach number effects^[72].

Cornelius and Lucius suggest a model of supersonic Coandă jet detachment^[12] that may produce usable analytical predictions of the detachment behavior in between nozzle and rotor rows. Evaluating this possibility is a topic for further research.

Griffin et al.^[38] changed the nozzle vane stacking and end wall distribution to address this problem. Similar solution strategies may be possible in future design projects. An optimization looking for profiles of optimal efficiency, if successful, is likely to eliminate detached regions as a by-product.

Another possible method by which this problem may be solved through modification of

the nozzle is to shorten the meridional distance between the throat and the trailing edge. Given the large nozzle outlet flow angle α_2 , this strongly reduces the distance that the flow has to travel at supersonic velocities along a curved flow channel.

3.6.4. Flow Path Shaping

The designers of Vulcain chose a different strategy by changing the nozzle flow channel from a curved design to a straight slot-design (see figure 3.1). This allows the flow to exit the nozzle without experiencing centrifugal forces.

There are geometric limits to this method. As seen in figure 3.1 and discussed in section 3.1, slotted nozzles do not fit the turbine annulus precisely. At the hub and shroud there are regions of the rotor that intermittently do not receive flow, which may disturb the flow in the rotor. In case the outlet shape is rectangular (figure 3.1 2a), the trailing edge is much thicker at the shroud than at the hub. The trailing edge thickness is a known and very significant contributor to losses^[5], although a satisfactory model of its effects on supersonic nozzle flow is not yet known. Trapezoid (figure 3.1 2b) outlets may alleviate this problem, but may need more involved manufacturing methods.

The issues of these straight-flow nozzle types, including the axisymmetric type (figure 3.1 1), increase with decreasing egress angle β_2 . For one thing, the aforementioned areas not available for flow will become larger as the area of uncovered turning becomes more elongated. Furthermore, these nozzles require that the inlet is at a larger distance from the rotational axis d_{1h} than the rotor, which requires build space outwards of the rotor that, depending on engine design, may not be available.

Mixed-Flow Nozzles

A compromise would be to shape the nozzles using profiling techniques as described in section 3.4, but to shape the hub and shroud contour in order to influence the radial component of the outlet flow. Figure 3.15 represents preliminary simulations for a study of how this may influence the radial pressure gradient behind the nozzle. The boundary condition at the simulation outlet condition (average static pressure with 5% pressure profile blend) evens out pressure differences to some degree, so the normalization of pressure in this region is not physical.

Figure 3.15 a) serves as the baseline here. It is the M1 nozzle optimization result discussed in section 3.7 and exhibits a strong radial pressure gradient. Figure 3.15 b) shows that inclining the flow path leads to a strong reduction in this gradient.

The simulation shown in figure 3.15 c) was set up to mimic the flow path in the previously

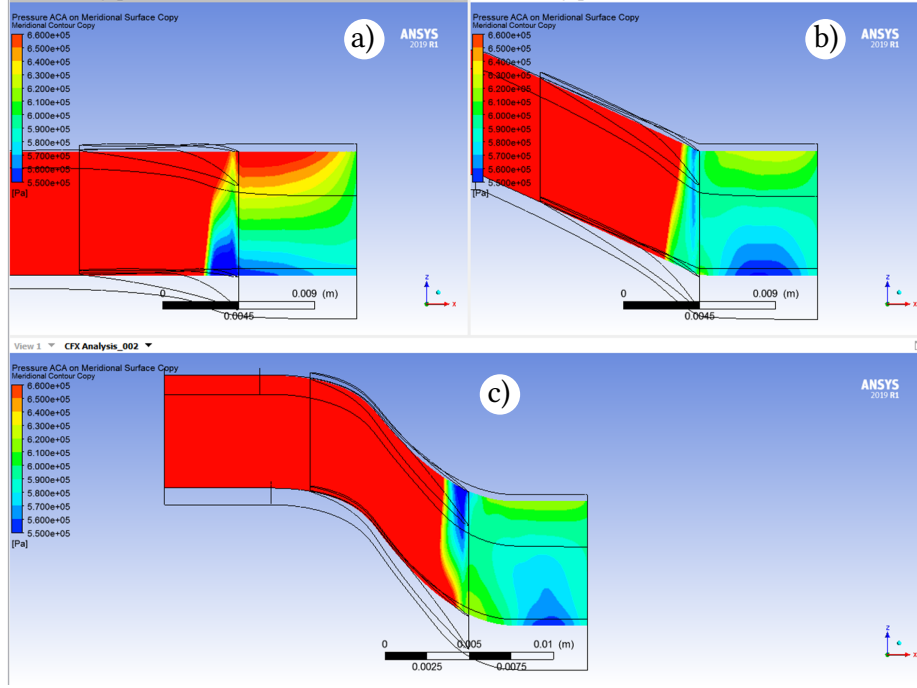


Figure 3.15.: Static pressure distribution in simulations of different flow path shapes

mentioned straight nozzles. To generate this geometry, a straight 3D line was drawn on the x - z plane from the axial position of the rotor (position z_3 in figure 1.1), with an angle between the line and the x -axis of 15.5° matching the outlet angle of the nozzle. The longer this line is drawn, the further it will depart from the initial diameter, giving the meridional diameter as a function of the distance from the rotor in the x -direction. In order to create an axial inlet and to limit the outer radius, the hub and shroud curves start bending back at an arbitrarily chosen distance of $z_3 - 8\text{mm}$. Curvature continuity of the end walls was maintained at this point.

This is only a pilot simulation to evaluate the feasibility of such an approach. Hub and shroud contours were not corrected to maintain any particular flow area. The profile was not optimized for this usage, and variables, such as the point of return to axial direction, were chosen mostly arbitrarily. The goal was to evaluate if it was possible to further reduce the radial pressure gradient using such a configuration, and indeed, the simulation indicates that a strong further reduction in radial pressure gradient is possible.

Practical use may be limited by the additional development and manufacturing effort of such a nozzle, which may have to be made by expensive techniques, such as EDM, ALM (additive layer manufacturing), or axial milling. But especially for the use case of a small high work turbine it may be worthwhile to pursue due to the strong curvature of the hub combined with large tangential velocities leading to a large radial pressure gradient^[104]. If

manufacturing allows for this, the technique could even be extended to also shape the hub and shroud walls of the rotor.

3.7. Optimization

CFD Simulation has become the bread and butter of anyone working with turbines, as it is a cost-effective method to obtain information about the internal flow. Analytical flow prediction methods, such as potential flow schemes^[11], heavily rely on assumptions which may not be accurate for any given flow simulation. For the simulation of supersonic turbines, the occurrence of shocks prevents the use of potential flow simulation, since shocks lead to an increase in entropy. Earlier investigations^[93] have used the method of characteristics (MoC) calculations to evaluate flow in a turbine. While this may lead to a better understanding of vital aspects of blade design (see subsection 3.5.2), the analysis needs to be supplemented with analytical models for the boundary layer^[31] and the position of shocks^[66]. Even then, such models do not show the influence of important transient phenomena between nozzle and rotor^[25].

The most advanced optimization methods simulate an entire turbine stage and manipulate the geometry to improve its performance, as conducted by Griffin et al.^[38] and Kawatsu et al.^[53] and discussed in section 3.4.3 and other places in this thesis.

The method used by Kawatsu^[53] is somewhat less complicated than others in that a profile and mesh was only generated once, and then deformed for the calculation. This limits the number of steps, and possibly allows the reduction of computing time, if a previous solution can be used as initial values for subsequent ones. The drawback is that the ways in which the profile can be modified are limited.

For a less constrained optimization, such as the one conducted by Griffin^[38], every evaluation involves the following steps:

1. selection of input parameters for the evaluation
2. generation of 2D profiles
3. generation of 3D blades
4. mesh generation
5. simulation
6. evaluation of output parameters

A host of problems can occur at every one of these steps. In order for such an optimization

to be feasible, each of these steps need to be conducted in a highly repeatable fashion. This section gives an overview of lessons learned for some of these steps.

For the sake of brevity, the selection of input parameters will not be discussed in this thesis. This is done by the chosen optimization method. Beside the aforementioned publications^[38,53], Spiegel^[92] has also covered this topic. Generally speaking, the choice of optimization needs to be made considering the number of input and output parameters, the projected number of necessary evaluations and the required resilience of the optimization with regards to holes in the parameter space (see section 3.3) among other considerations^[26]. Generation of profiles and blades was covered in depth earlier in this chapter.

Mesh generation in supersonic problems is an issue that deserves some consideration here, as this is complicated by the appearance of shocks. In an actual flow, shocks have almost no thickness. The gradient of speed and pressure is so high that the entire change happens within a small number of free path lengths^[75], a distance on the order of one micrometer.

In order to achieve mesh convergence of all variables, the mesh would have to have elements of similar size. A cubic centimeter with $1\text{ }\mu\text{m}$ cube elements would contain 10^{12} such elements, which would require far more computing resources than can reasonably be expected to be available. This problem can be alleviated by adaptive mesh refinement generating fine elements only in places with very large pressure gradients^[95], however, such methods are not yet state-of-the-art for transient simulations.

Conducting a mesh convergence study is still reasonable, but depending on the variable which is being optimized, a reasonable trade-off between computing resource requirements and convergence quality needs to be made. Experimental results indicate that even without mesh refinement, the effects of a shock on the overall flow are generally well represented by the averaging mechanisms built into Ansys CFX (a computational fluid simulation software) for the problem of nozzle outlet flow^[95].

For the simulation it is important that convergence is achieved reliably. Time should be allocated to perform a number of random computations of the type that are used for optimizations in order to identify possible convergence problems and to select the best variables for determining whether a simulation has converged. To achieve reliable convergence, the time steps (a relaxation parameter in CFX) had to be chosen much lower than the official manual recommended for turbines. A good measure seemed to be $1/5$ of the travel time between two adjacent trailing edges at the expected nozzle outlet tangential velocity c_{2u} .

In the post processing it must be ascertained that the chosen output variables actually represent the desired quantity. In one known instance an optimization for reduced shock strength led to a result where the strongest shock intersects with an expansion fan in the

plane where the target variable was evaluated. Thereby, the target variable was locally strongly reduced in that plane, but not globally. As a solution, the target variable was evaluated in two parallel planes and the results added together.

3.7.1. Nozzle Optimization by Uniformity

In an unpublished informal pilot study, also mentioned in the end of chapter 2, ten high turning nozzle profiles with convergent channels and zero uncovered turning angle were evaluated at 15 operating points each in order to evaluate what sources of loss are dominant and which flow patterns are stereotypical. Total pressure losses were evaluated in three planes: Between inlet and the throat, in the area of uncovered turning and between the exit of that area and a plane 0.77 of an axial cord length (one blade height) behind the rotor.

One result was that, while the last area of losses was the biggest contributor in most cases, it was especially dominant at supersonic Mach numbers. By selecting a distance to the trailing edges, almost any value for efficiency could be generated (see figure 2.4). This makes previously documented efficiency measurements for nozzle rows, such as those presented by Dejc and Trojanovskij^[13], hard to verify without precise knowledge of the position of the measuring apparatus.

Furthermore, differences in the axial gradient of pressure loss for different profiles hinted that there may be an important variable in these flows that is not revealed by measuring efficiency. A hypothesis was formed that the strength of shocks leaving the nozzle was this missing variable. Figure 2.2 shows an example of the simulation results.

Another hypotheses was put forth, that a variable characterizing the uniformity in the nozzle exit flow could characterize the additional strength of rotor-stator interactions sufficiently well so that by optimizing for this variable a good nozzle profile could be developed without the computational effort of transient simulations. Previously, Joly et al.^[49] had independently developed a similar optimization strategy and used it to considerable success, using a parametrization of limited geometrical flexibility.

Sudhof and Shimagaki^[94] presented the results of a new optimization of the M1 geometry^[42] using the parametrization presented in subsection 3.4.1, and NLPQL (Non-Linear Programming by Quadratic Lagrangian) as an optimization method. In a first step, the profile was optimized for efficiency, because it was unclear what efficiency could be expected.

The result of the efficiency optimization was then used as the initial values for the uniformity optimization. The target of this second optimization was the minimization of S_3 , the normalized span of relative total pressure in the rotor-relative frame. Although the rotor was not simulated, the circumferential speed U , was taken from the M1 engine fuel turbine.

The relative total pressure was chosen because in a blade-to-blade plot of relative total pressure, both the changes in flow direction from shocks as well as the loss of velocity in the wake are well represented. If the optimization target was a variable that only represented one or the other influence, then the optimization may find profiles that eliminate one non-uniformity at the cost of worsening another. Further, the relative total pressure relates to the stagnation pressure that the leading edge of a rotor would receive, which in turn is part of the cyclic load.

The normalization variable of S_3 is the total pressure in the exit.

$$S_3 = \frac{\max(p_{02,rel}) - \min(p_{02,rel})}{p_{exit}} \quad (3.29)$$

With

S_3 uniformity variable

This optimization was initially restricted in that the efficiency could only be reduced by 0.1% from the previous efficiency optimization, but this and other things led to problems, where the optimization had to be restarted from results that were inadequate for the following reasons:

- The initial efficiency goal was too ambitious. A reduction of 0.3% needed to be allowed.
- The outlet flow angle was not controlled strictly enough, which led to a small reduction in total usable power.
- The curvature at the throat was given too strict limits, and the optimization focused on generating curves that quickly increased the curvature immediately before and after the throat. This limit was relaxed.
- As mentioned above, the optimization had found a profile that generated a case where the uniformity was particularly good in only one position - where it was evaluated. The variable was subsequently evaluated in two parallel planes in the outlet.

A comparison between of the optimization result to the original M1 geometry can be seen in figure 3.16. A transient simulation of both stages of the M1 turbine was carried out with both the original geometry and the final optimized geometry as the first stage nozzle.

Results were positive throughout, with a 1.3% increase in efficiency of both stages combined and a 13.8% reduction of tangential load amplitude on individual first stage rotor

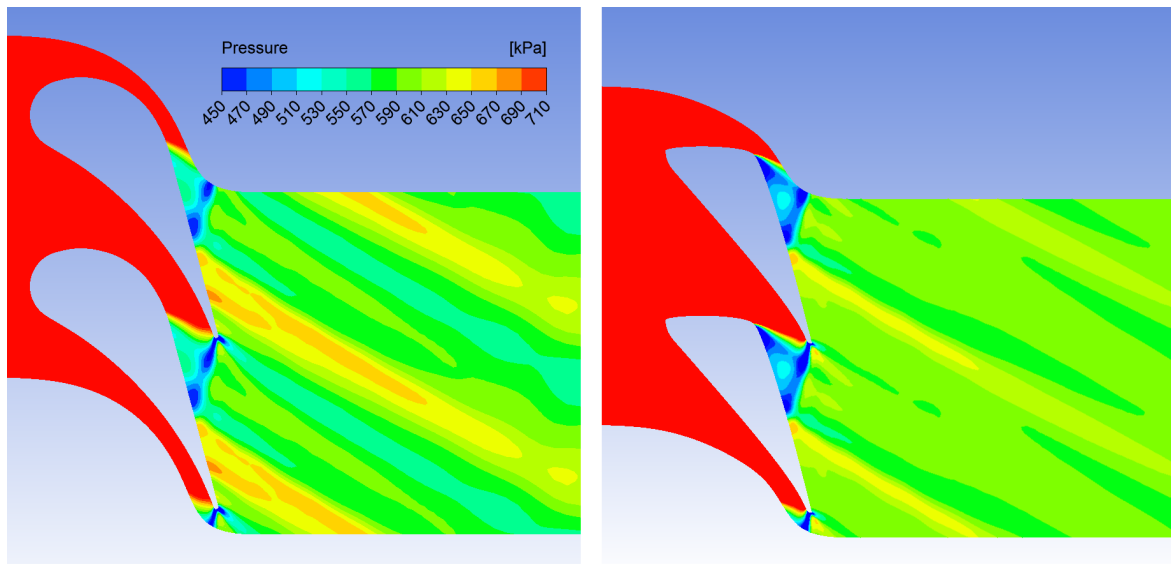


Figure 3.16.: Pressure contours of the M1 nozzle (left) and of the result of the optimization for flow uniformity(right) at design point conditions^[42]

blades, which is a valuable additional benefit due to the common problem of high cycle fatigue in first stage rotor blades^[24].

While this is an encouraging result, some caution is warranted. For example, the new profile is somewhat shorter than the M1 Nozzle profile. This alone could positively influence the rotor flow due to the hub detachment described in subsection 3.6.4. It must also be said that the kink of the nozzle at the inlet is unintentional, and a result of unintended flexibility on the suction side. It may be advisable to constrain optimization more tightly in this location in order to create a more traditional round leading edge, or to add the kink angle as a parameter and choose a suction side segment type with fewer degrees of freedom.

3.7.2. Comparison to Dejc's Throat Area Guideline

Raw data from the optimization was also studied as a potential source of data for checking and adapting correlations, but there is a caveat to this. One way to generate correlation data from a parameter study would be to identify the solutions that are Pareto-optimal, and then base a correlation only on these solutions. In the case of a gradient optimization, most solutions appear to be Pareto-optimal, because the algorithm tries to travel along a Pareto-front towards better values of a target function. However, the path that the optimization takes may only represent a local optimum, and a true Pareto-front may lie elsewhere.

A front can clearly be seen in the simulations of figure 3.17, but these points are very distant from the area ratios that would result from a pure nozzle flow calculation. Dejc

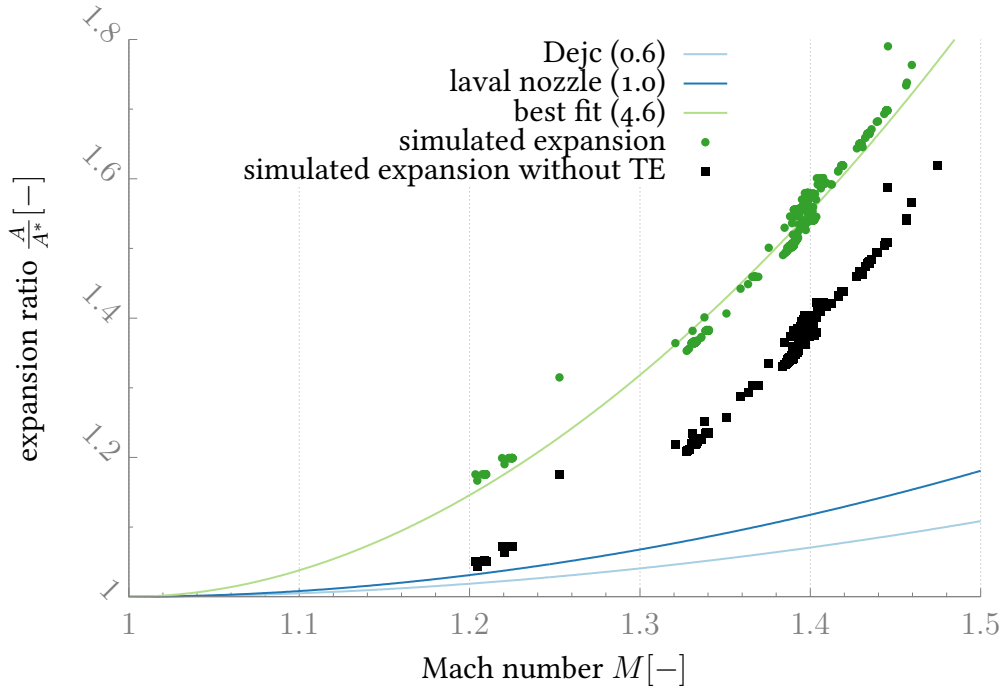


Figure 3.17.: Expansion ratio in 789 simulations of the optimization for efficiency compared to the analytical model of equation 3.11

(see equation 3.11) proposed lower expansion ratios, which are even further from this data. The best fit to the apparent Pareto-front was found by using 4.6 as the variable, where Dejc proposes 0.3 to 0.6. The legend shows the respective values for this variable in parentheses.

In an attempt to explain the discrepancy, the thickness of the trailing edge (TE) was subtracted from the outlet area of the area ratio, and this result is also presented. However, the values were still far from the analytical predictions.

Dejc states that larger values give better peak efficiency at the cost of worse off-design efficiency, so a follow-up study could be conducted to investigate whether this holds true.

3.8. Possible Inferences for Shock Management in Nozzles

As informative as Goldman's work on supersonic nozzles^[28,31] is, it contains little information on how to accommodate nozzles and rotor profiles that are mechanically sound. There seems to be an implicit assumption that the optimal usable profile is a profile that is mathematically designed without any concern for such practical considerations and then modified to accommodate finite edges.

Conversely it is put forth here that a better overall profile is possible by designing the

supersonic flow around the physical limitations of practically usable profiles.

The result presented above, while purely a result of algorithmic optimization, contains an interesting possible design strategy for nozzle profiles, which mirrors, to some degree, similar results of Griffin et al.^[38]. While the optimization started with a concave suction side in the area of uncovered turning, this was strongly reduced in the efficiency optimization and immediately replaced with a convex shape in the uniformity optimization.

One interpretation of why this is advantageous is that the constant expansion of the gas from the suction side continuously stabilizes the boundary layer, where a concave blade would cause a local compression in the area of uncovered turning, leading to a thickening of the boundary layer. Another prominent feature of the optimized profile is the stronger concentration of the expansion into something reminiscent of a Prandtl-Meyer expansion fan. There was no constraint on the parameters preventing a further concentration, so it seems that this shape was deemed optimal. The effect is a concentration of expansion waves reaching the pressure side of the trailing edge, stabilizing the boundary layer at the trailing edge and delaying detachment. This reduces the wake size, but increases the shock strength at the point of detachment.

This somewhat stronger inward-facing trailing edge shock is compensated by a larger overexpansion in a triangular area of higher Mach numbers at the end of the covered channel. The result is that the shock creates matching conditions at suction and pressure side, eliminating the trailing edge shock from the suction side almost completely. Perhaps the reflected shock could be nullified by the addition of a kink on the suction side, as proposed by Dejc^[13].

If these preliminary results can be verified by more researchers, designing the supersonic expansion in this fashion from the start could be a viable option for moderate supersonic Mach number nozzles, because the added shock strength from the trailing edge pressure side represents an insignificant loss of total pressure. Among the many things that remain to be studied here is the matter of whether the total pressure losses from this shock outweigh potential benefits at higher Mach numbers.

4. Cascade Design for Supersonic Turbine Nozzles

This chapter describes the experimental results from a newly designed setup for cascade experiments with supersonic outlet flow and their significance to future developments. The flow experiments were performed at the JAXA Kakuda Space center's CATTs facility. Much of the text is previously published in the proceedings of the 32nd International Symposium on Space Technologies and Sciences^[95].

As seen in figure 4.1, the cascade consists of eight profiles, forming seven flow channels. The first and the last profile are only half profiles. There is a shock absorbing structure ("separator") attached to the second to last profile. Above the structure, there is a room that is open to the environment on both sides to allow for the formation of an entrainment flow. The flow outlet is likewise open to the environment, and the main flow path, as well as the entrainment flow path, is pictured with arrows.

The blades themselves are generic, and not meant for a specific purpose other than the demonstration of the test bench. As such, they are similar to those in previous investigations, in that they form a convergent channel^[32]. They are curvature continuous on the suction side, and have an inlet angle of 90° and an outlet angle of 14° to the tangential direction. The suction side in the area of uncovered turning is not curved. The blade height is 14 mm; the true chord is 34.1 mm, and the pitch is 27.8 mm.

The cascade side walls (hub and shroud of the turbine) have two configurations. For static pressure measurements, one of the walls is made from stainless steel; the other wall is made of transparent acrylic. Short pipe segments are glued into holes in the walls. The pressure sensors are connected with flexible tubing to these pipes. There are twelve pressure taps in the outlet flow field on the steel side, and two on the acrylic side. Furthermore, there is one pressure tap on each side directly upstream of the blade row.

For optical experiments, the steel side wall is replaced with a second acrylic wall. Only the three pressure taps in the first acrylic wall remain. All acrylic panes are 14 mm strong.

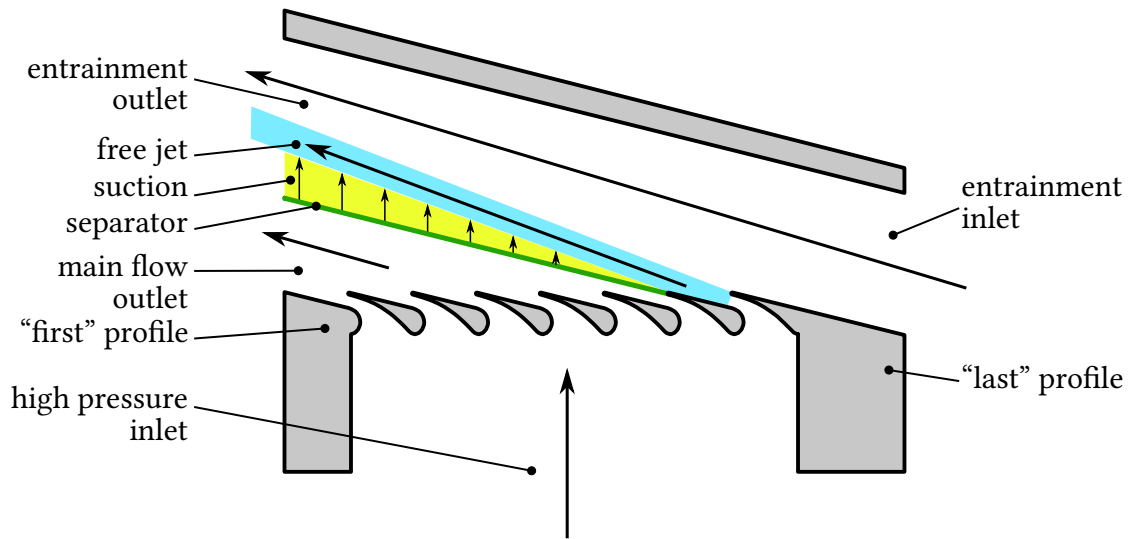


Figure 4.1.: Overview of the flow in the cascade

4.1. Shock Absorbing Structure

The shock absorbing structure is fundamentally a perforated wall, which has been documented before as a means to reduce wall influence in general supersonic wind tunnels^[68] as well as turbine cascades^[85]. However, in previous designs, there is a separate volume behind the perforated wall with very precise pressure regulation to control the amount of suction from the main flow. Too much suction disturbs the experimental flow, and too little suction fails to generate the desired effect. An analytical model to describe and predict this

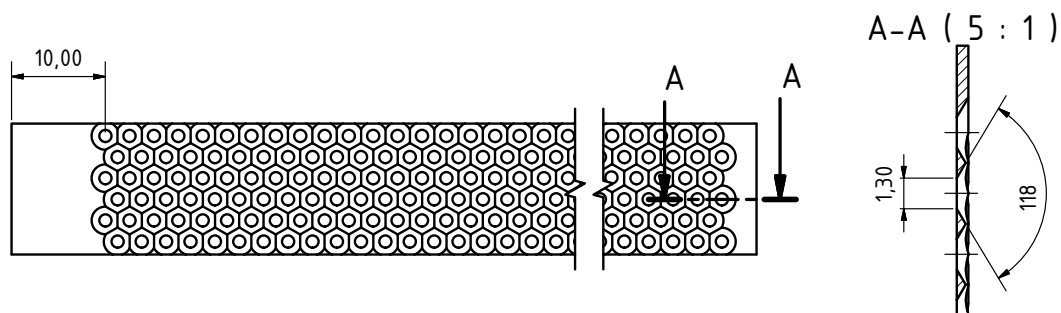


Figure 4.2.: Hole pattern of the separator

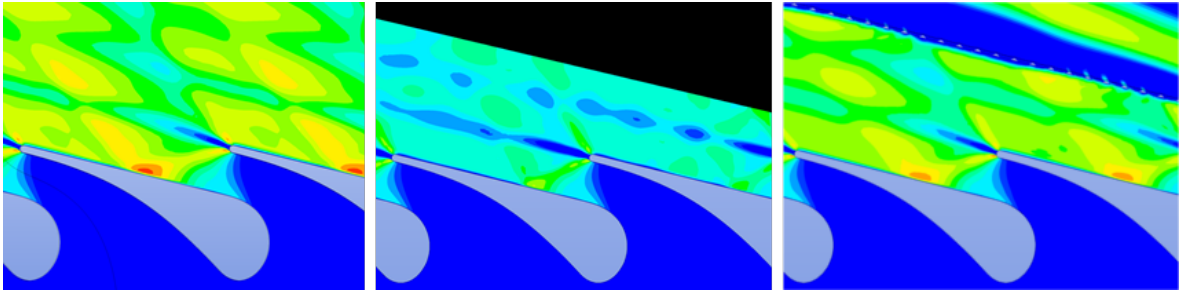


Figure 4.3.: Mach number plots of simulated configurations (range: 1.0-1.9; contour increment: 0.1)

kind of design was presented by Šimurda et al.^[86]. Rona et al. demonstrated that a perforated wall without any suction behind it does reduce shock reflections to an acceptable degree^[78].

To achieve a solution without the need for such a complicated setup, the periodic nature of the desired flow was used. One of the flow channels formed by the subject profiles is situated above the separation. The flow in this channel is able to expand freely into an open volume. This creates a self-regulating variable suction, as the outlet flow angle increases at higher inlet pressures. On both sides of the separator, the flow goes through the same redirection, and is therefore similar in speed and total pressure. The shape of the separator itself is pictured in figure 4.2. From the entrainment side, a pattern of holes is drilled into the material using a 118° opening angle drill. The drill feed is stopped when the hole on the opposite side reaches a predefined size. This is repeated to generate the pictured honeycomb pattern.

This pattern allowed the flow to pass through the separator when there is a velocity component perpendicular to the separator face. If the flow is tangential to the separator (i.e. there is no perpendicular component) the flow is not strongly influenced. The reason for the reflection of a shock at a wall is that the flow gets deflected towards the wall by the shock. Since a flow through the wall is impossible in the case of a solid wall, a reflection must result, bringing the flow back to a wall-parallel direction. With a permeable wall in place, the new boundary condition is compatible with a small component of velocity toward the wall. Thus, the reflection is not necessary^[86].

One key open variable in the design is the hole diameter seen in figure 4.2 as 1.3 mm. From simulations it appears that the larger the holes, the better the function of the separator. Figure 4.3 shows the performance with a diameter of 1.6 mm, but in order to make manufacture simpler, and the object mechanically stronger, 1.3 mm was chosen for the current iteration.

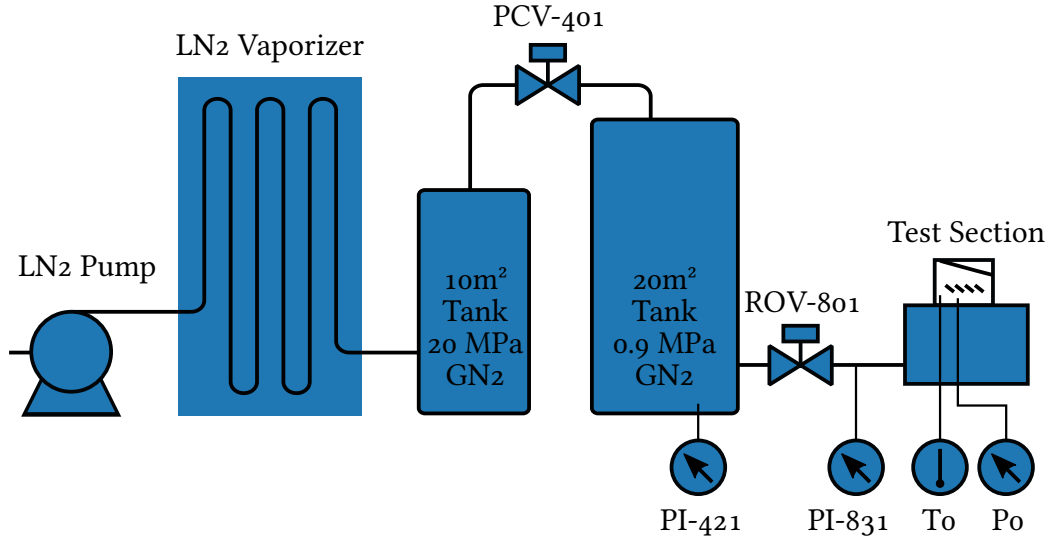


Figure 4.4.: Flow schematic of the test stand as configured

4.2. Test Facility

This section is paraphrased from a description of largely the same content that was originally written by the paper's co-author, Mitsuru Shimagaki^[95].

The experiment was conducted at the CATTs facility of the JAXA Kakuda Space Center. A wind tunnel (shown in figure 4.1) was set up using the existing nitrogen supply from a previous experiment on cavitation in a cryogenic inducer^[54].

Figure 4.4 shows a system diagram of the supersonic turbine cascade facility. It draws nitrogen gas from the 20 m³ run tank through the pictured piping.

In the test part, a chamber part is installed at the outlet of the stainless-steel pipe, and the acrylic plates incorporating the test turbine nozzle cascade are installed at the top. A pressure sensor for measuring the stagnation pressure and the PCV-401 control valve for setting the stagnation pressure are situated upstream of the test section.

Test cascade inlet conditions are generated by opening the supply valve PCV-401 part way and monitoring the run tank supply pressure PI₄₁₂ and the supply line mid-way pressure PI-831 well as the stagnation pressure Po.

4.3. Test Procedure

In the test, the stagnation pressure Po was gradually raised by opening the valve PCV-401 to reach pre-defined inlet pressure targets. Inlet pressures were held constant for several

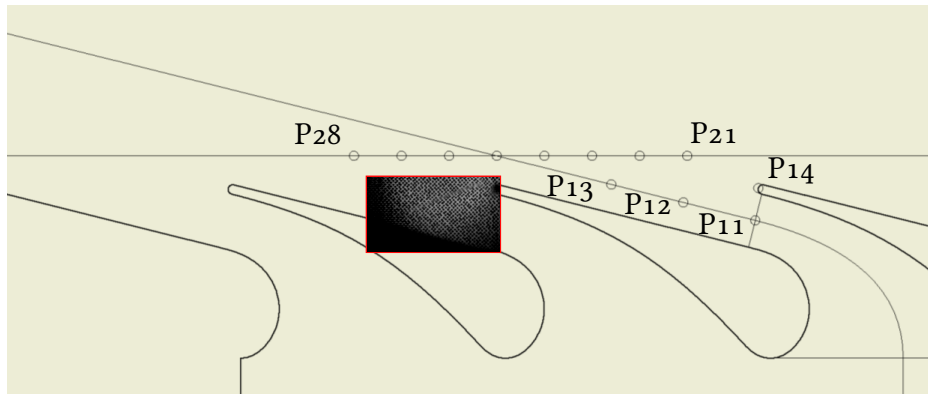


Figure 4.5.: Locations of the pressure taps and the fame of high speed camera footage

seconds before raising them to the next target. The cascade outlet pressure was not configurable, as the cascade is open to atmospheric pressure. The outlet temperature of the fluid was approximately 173 K.

Pressure data from a preliminary series of test was compared to predictions of the same values gained in CFD. It was found that towards higher inlet-pressures, the raise in the outlet pressure taps was less than predicted. One explanation put forth to explain the discrepancy was that the acrylic side walls of the cascade are insufficiently stiff. Therefore, at higher pressures, the walls slightly bulge, which causes an additional expansion and flow below and over the turbine blades. Based on this hypothesis, a c-clamp was manually attached to the outside of the test stand. To distribute clamping force, a nitrile rubber block was put between the cascade and the clamp.

Repeating the experiment with the clamp, and immediately afterwards without the clamp, showed that the test results were indeed closer to the predictions when the clamp was attached. Unfortunately, the clamping force was not controllable in this setup, which adds an unknown variable to the experiment. It would therefore be advisable to design cascades to be adequately stiff in the future.

As the clamp would have blocked part of the view, it was not attached during optical experiments.

4.4. Pressure Tap Experiments

The test facility was configured for pressure tap experiments for two test days. Pressure data from the first test day showed a marked departure from the predicted pressure values. As described above, the overall outlet pressure was lower than predicted, which was addressed with the installation of an external clamp.

Furthermore, some pressure taps showed drift in values, even with a constant inlet pressure. The flexible tubing lines of pressure taps which showed inconsistent results were replaced. The separator was raised slightly to be as exactly parallel to the outlet angle as possible, but at high inlet pressures the separator was slightly displaced, indicating that a stiffer supporting structure would be better.

The second test day started with a rerun of previous pressure settings to evaluate the changes to the test stand. In the second run, the clamp was removed to evaluate this effect alone. For the final and definitive run, the clamp was re-attached. The cycle of attachment-removal-attachment of the clamp showed that attaching the clamp had a pronounced effect on the measured pressure values.

Results of the final run are presented in figure 4.6 and figure 4.7. The abscissas represent the inlet pressure P_o and the ordinates represent the respective pressure tap values. The pressure tap locations are shown in figure 4.5.

The measurements were taken with 100 Hz sampling rate, but blocks of 100 measurements were averaged to generate one data point, represented by a circle. Since the inlet pressure was changed only slowly, there was for most data points no large variance in the data within one second intervals. Error bars are not shown, since in almost all data points they would merely obscure the measurements with many additional lines.

While the pressure was held as constant as possible for several seconds at pre-defined pressure points, the pressure data from the whole run is included, not just from the intervals with constant inlet pressure.

The measurement data in figures 4.6 and 4.7 is superimposed with simulation results. Some of the simulation data points were computed before the test and others were computed afterwards using the same settings and mesh as the other points. The post processing was slightly modified after the tests to read the pressure as an average of the pressure data over the area of the drilled hole, rather than a single pressure value in the center of the area. This caused the simulation to be slightly closer to the experiment.

Overall, the simulation matches the experimental results in most aspects. However, there are discrepancies between the results from the experiments and numerical simulation.

The following can be observed: As the inlet pressure is raised, the measured pressure rises and then abruptly falls as a shock passes the pressure tap. For some positions, this can be seen not once, but two times at different pressure levels. This gives data from these taps, such as P23, a pronounced “w”-shape. The interpretation is that there are two shocks that pass over P23, although the initial simulation only indicated one shock, which is the shock from the pressure side of the trailing edge reflected at the next blade’s suction side.

The second shock is created by shock-boundary interaction. Rather than be reflected

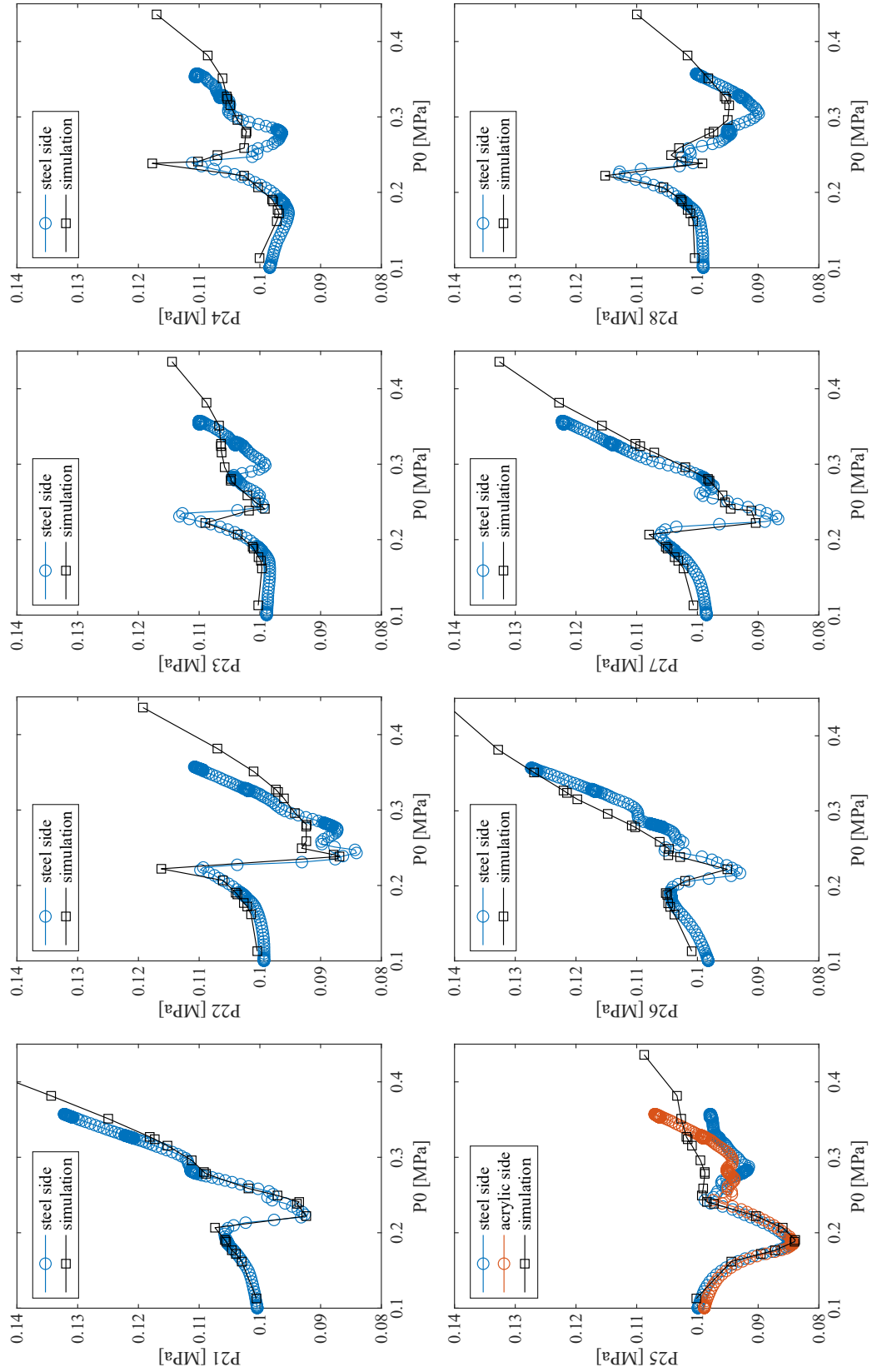


Figure 4.6.: Comparison of pressure tap data in the outlet to numerical simulations

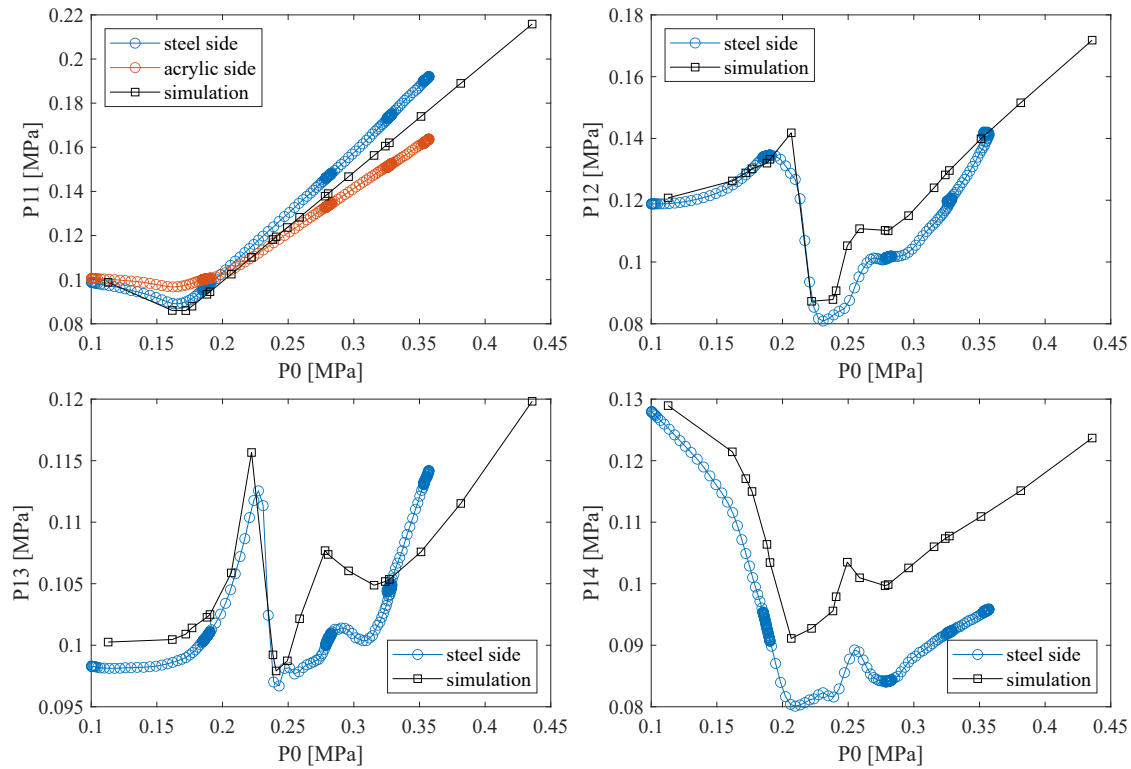


Figure 4.7.: Other pressure tap data compared to simulations

cleanly, two shocks emerge from at the suction side, in a strong boundary interaction^[34]. This was also observed by Graham^[32] in a similar experiment. The phenomenon can be seen clearly in the optical experiments.

In some locations there were pressure taps on both the acrylic and the steel side of the cascade. Differences between the pressure readings of P11 and P25 on the two sides indicate that flexibility of the acrylic panel played a role in the measurements, even with the clamp in place.

4.5. Optical Experiments

The text of this section was written in large part by Stefan General^[95] and is included for coherence.

Static images were analyzed using BoS (Background-Oriented Schlieren). This is a flow visualization technique based on the computational analysis of image variations caused by gradients in the refractive index of the propagation medium. Compared to the classical schlieren technique^[96] it has the advantage of a simpler experimental setup. The BoS setup used here can be seen in figure 4.8. A special background with a high spatial frequency

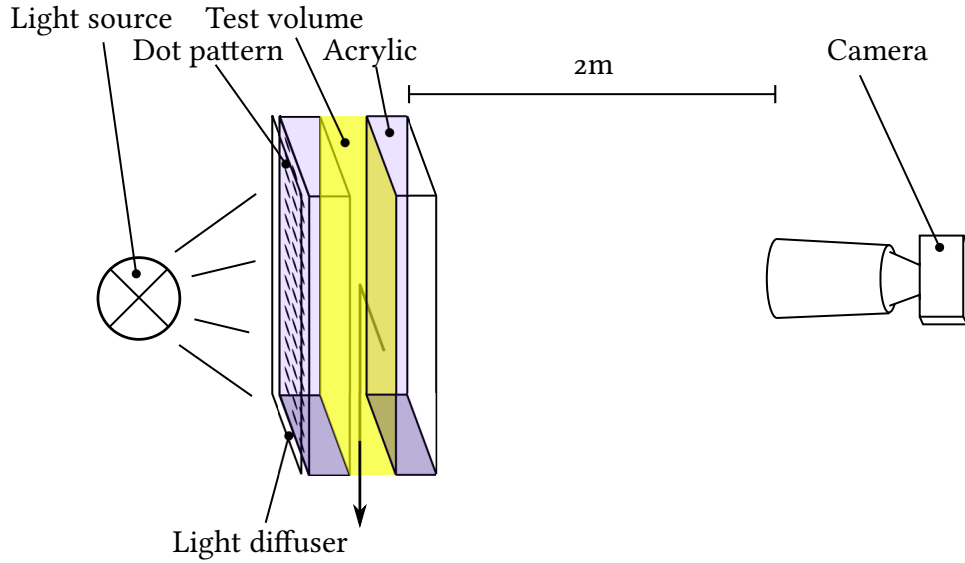


Figure 4.8.: Camera and light setup for BoS experiments

pattern is recorded by a camera. Due to refractive index gradients which are induced by the flow, light rays are deflected by a small angle. This causes a displacement of pixel in the recorded flow images compared to a reference image without flow. These displacements can then be computed by different image processing algorithms to ultimately create an image of the flow field.

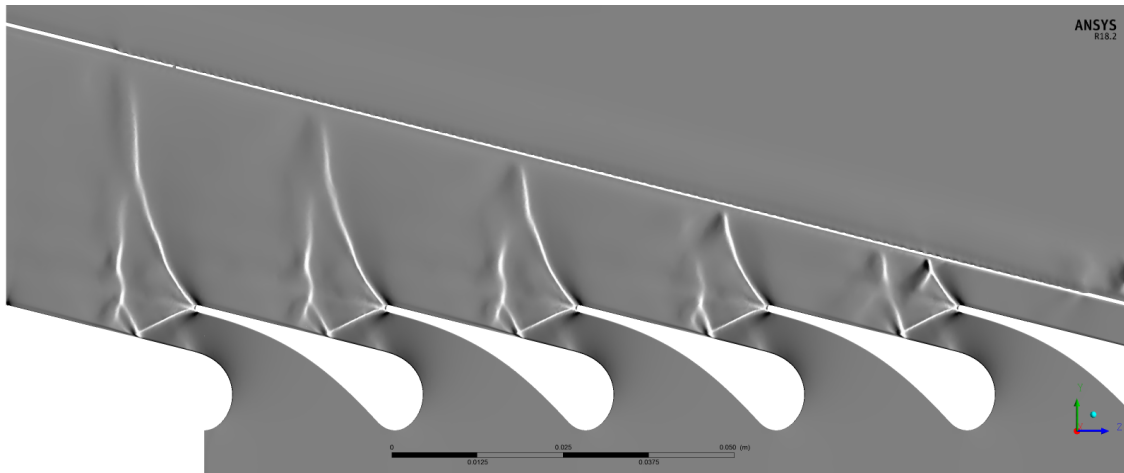
For the data presented in this article the optical flow algorithm by Horn and Schunck^[45], as implemented by Kharbat^[55], was used to calculate the flow field. Unlike cross-correlation algorithms, optical flow algorithms are able to yield one displacement vector per pixel^[43]. Thus, the calculated flow field retains the resolution of the recorded images which is especially important for low-resolution frames of high-speed video.

4.5.1. Analysis of Resulting BoS Images

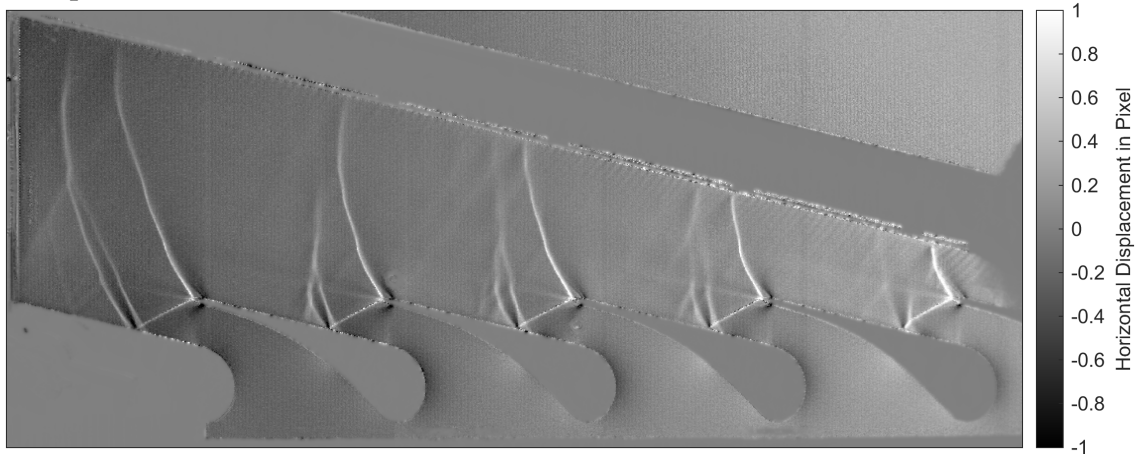
The inlet pressure was held constant at ten pressure values, long enough for a digital single-lens reflex camera to take 20 pictures per operating point. Individual pictures were taken at 1/2000 s shutter speed through a 300 mm lens with an aperture of F14 at a distance of 2 m. The sensor format was 23.6x15.8 mm.

These pictures were processed as described above, leading to one image for the horizontal and one image for the vertical displacement in each of the original pictures, a total of 400 images. To meet space restrictions, only two are reproduced here. Figure 4.9 b) is the average of horizontal displacement across all pictures with 0.24 MPa inlet pressure, while

a) simulation with adaptive mesh refinement at 0.22 MPa



b) experimental result at 0.24 MPa



c) experimental result at 0.28 MPa

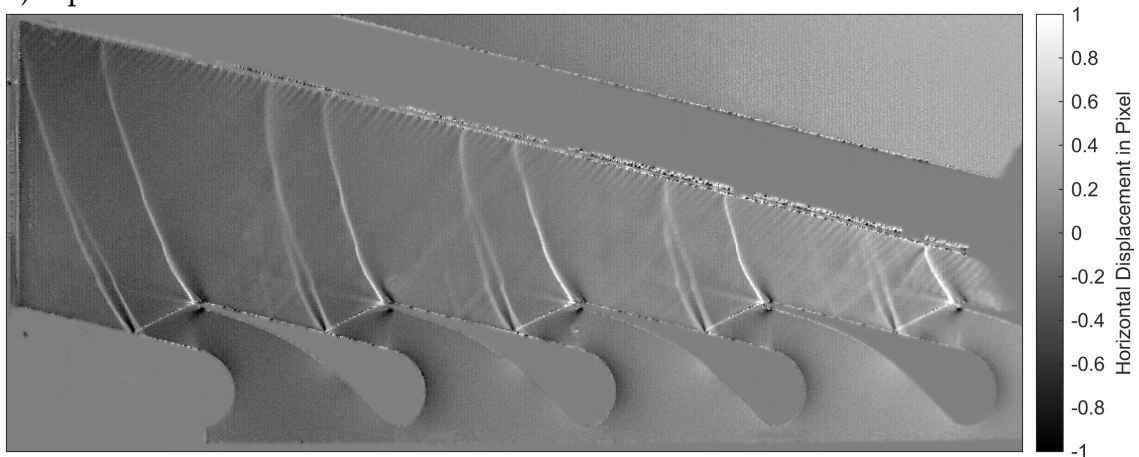


Figure 4.9.: Simulated and experimental schlieren images

figure 4.9 c) is the average of the same displacement in all pictures taken at 0.28 MPa inlet pressure.

The useful resolution of BoS images turned out to be limited not by the sensor resolution, but by the limited fidelity of the printing method used to apply the background pattern. A 4-fold increase in detail of the BoS images may be possible, given a better printing technique.

Before the experiment, a series of fixed-mesh simulations were carried out to determine the expected pressure variations. In these simulations, the shock from the trailing edge pressure side was reflected in a simple shock reflection.

Since this did not match observation, new simulations were conducted with four steps of adaptive mesh refinement to see if this would explain the difference. One result of these simulations can be seen in figure 4.9 a). The remaining pressure taps (P11 and P25) indicate that the flexibility of the side walls caused considerable differences in the resulting flow, so a precise match between the experiment and a simulation that does not account for this cannot be expected. Figure 4.9 a) is the simulation most closely matching figure 4.9 b), despite the different inlet pressure.

The simulation with mesh refinement did show the approximate pattern of shock reflection seen in the experiment, but only at moderate pressures. At higher pressures, the second reflected shock quickly abated in the simulation, while the optical experiments show the shock at persisting at higher pressures, with the pattern being largely unchanged from the one shown in figure 4.9 c). Data from the pressure tap experiments are unclear as to whether there was a significant second reflected shock at inlet pressures above 0.3 MPa in those experiments.

4.5.2. High Speed Camera Analysis

In two final test runs, the test stand was equipped with a high speed video camera instead of a still image camera. The frame only showed a small section in the outlet of the second flow channel, and back-lit with a single 400 lm white LED (example frame in figure 4.5). The frame size was effectively limited by the size of the illuminated circle. Videos were taken at six operating points with 150 000 frames per second at a resolution of 256x144. Some of the resulting footage was processed using BoS, but no additional findings resulted from this.

The data was also processed using discrete Fourier transformation. For this, 30 000 frames, representing 0.2 s in real time were isolated from each video.

Each of the 36 864 pixels of the video is represented as a numerical brightness value. This brightness was averaged for each individual pixel across all frames. The mean bright-

ness was then subtracted from each of the pixels in every frame. The result is a matrix of size $36\,864 \times 30\,000$, with each row being a brightness value that oscillates around 0. Each row was then processed using fast Fourier transformation. Of the resulting coefficients, frequencies between 100 Hz and 75 kHz were considered meaningful.

Initially, the resulting frequency amplitudes were averaged into one frequency plot. Some frequencies in this plot had much higher average amplitude than others, and a second analysis was conducted to determine where in the picture the increased amplitudes originated. To determine this, the average amplitude of ten frequencies surrounding the frequency in question was calculated for each pixel (five frequencies directly below and five directly above in the discrete Fourier transform). The amplitude of the target frequency was divided by the surrounding mean amplitude in each pixel.

This was done because plotting the amplitudes of any frequency over the whole image as brightness shows areas with oscillating shocks brightly, regardless of the frequency chosen, because of the broad-spectrum noise that shocks generate.

While the results cannot conclusively show where certain pressure fluctuations originate, they do show that significant peaks in the frequency spectrum are not equally distributed in the frame. An oscillation at 130 Hz appeared on all videos, even those taken without flow, and with amplitude closely linked to the brightness, so this is likely a fluctuation of either the LED brightness or some artifact of the camera image processing. Another strong unexplained amplitude peak occurred in all videos with flow at 15.3 kHz. One possible explanation is that this is a fluctuation in the light source or camera.

The most notable result of this analysis is that some amplitude peaks occur only in the direct shocks, some appear only in reflected shocks, some appear in both direct and reflected shocks, and others appear stronger in specific reflected shocks than in other reflected shocks. Examples of frequency spikes that are clearly localized appear in figure 4.10.

4.6. Conclusions from the Cascade Experiment

In summary, this experiment has confirmed the ability of the newly developed shock absorbing structure to cancel many of the ill effects that reflected shocks have in observations on supersonic cascades. It was shown that pressures in the flow channel outlet are largely as predicted by CFD calculations without mesh refinement, which is fortunate, because mesh refinement is not yet state-of-the-art for transient simulations or simulations involving multiple domains, such as periodic blade simulations. It was further shown that a small cascade can be used for BoS visualization, but several improvements to the technique are still possible. First and foremost, the stiffness of the sidewalls must be given adequate at-

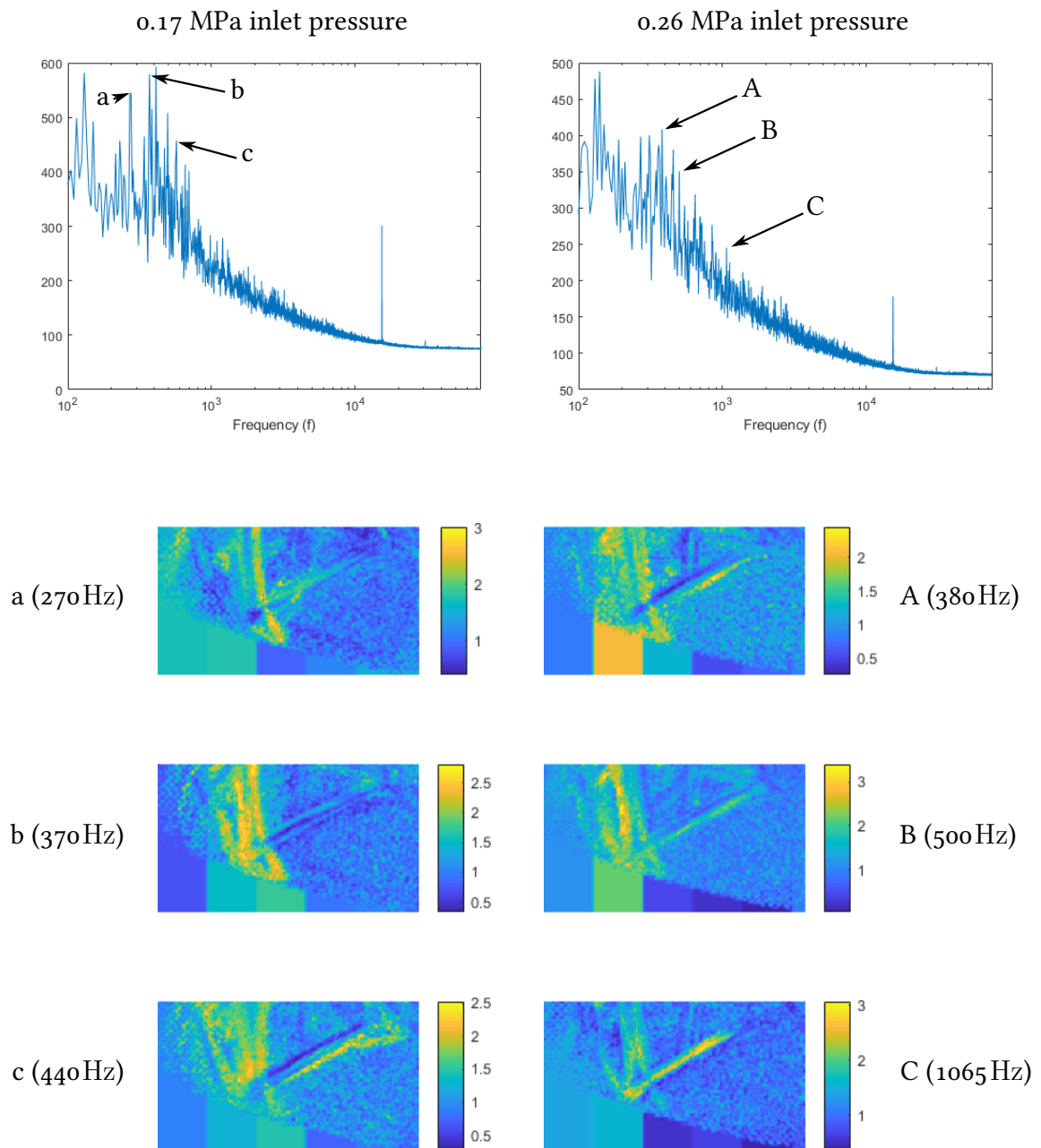


Figure 4.10.: Frequency-amplitude plots for two different pressure ratios and amplitude location plots for selected frequencies

tention. With modern high resolution cameras, it is also important to consider the limits of the printing resolution for the pattern background.

High speed video revealed that some of the image data oscillated at specific frequencies in well-defined areas (see figure 4.10). If dynamic pressure sensor data can confirm that the image oscillations correspond to pressure oscillations, this finding may prove useful in future analysis of the fluid-dynamic reasons for observed fluid behavior. It may also give specific guidance if a profile must be designed to avoid generating specific frequencies that cause resonance phenomena somewhere in a turbomachine.

5. Conclusion

The preceding chapters contain the collected experience from four years of research into the development of supersonic turbines and describes procedures for their design. Within this discussion, the state-of-the-art was pushed forward on multiple fronts.

After a brief introduction, the second chapter contains a discussion of the basic thermodynamics of turbines, from a different vantage point than most textbooks. Its objective is to be precise in the use of definitions where works on subsonic turbines are often imprecise. This enables a reader who was previously unfamiliar with supersonic turbines to understand how to apply information from such sources to their development.

In summary, the third chapter describes the development of suitable turbine blade shapes by building on this groundwork. The contributions made there are numerous and distributed over a large array of subtopics. In aggregate, they form a new method of blade shaping that facilitates a previously observed paradigm shift: In the past, profiles were first analytically studied without full consideration of practical restrictions, such as finite leading and trailing edges or shock-boundary interactions. Those aspects were considered secondarily. Modern computational capabilities allow designing blades around those restrictions from the start, opening the possibility of more efficient and durable blade geometries with a wider operational envelope.

As such bladings rely on the accuracy of the numerical models used in their development, it becomes even more important to verify that these simulations are accurate. To this end, the fourth chapter describes a new type of experimental cascade setup that can be built using an existing nitrogen gas supply at much lower expense than was previously possible.

Using this setup, the location of shocks and their influence on the overall pressure distribution was correctly predicted at all pressure ratios where the design of the test stand could reasonably be expected to yield useful data.

At the same time, it was shown that the shock system is highly dynamic, and a simulation with extreme resolution, both in element size and in time step, would be needed to represent these transient phenomena — if it is at all possible in Reynolds-averaged Navier-Stokes simulations. Where it is not possible to simulate all flow features, it becomes especially important to validate that simulations are accurate to the required degree. That is to say,

the aggregate influence of flow features that cannot be directly simulated is small enough for the principal simulation results to be valid. This emphasizes the need for cost-efficient cascade experiments.

Looking ahead and considering that engineering has recently made great progress on several problems through the use of deep learning, the proliferation of this technique may be the next paradigm shift in supersonic turbine blade design as well. If so, the parametric representations developed here may be a common language in which data from many sources can be collected and used to train the design systems of the future. A version of the newly developed experimental technique may then be used to validate the performance of those designs.

Personal Acknowledgments from the Author

As the author of this thesis it is my privilege to gratefully acknowledge these people's contributions to my research and the writing of this thesis:

First and foremost, this thesis would not have been possible without my doctoral advisor, Prof. Dr.-Ing Stefan Schlechtriem. In the past four years, his tireless work on my behalf gave me the opportunity of a lifetime — not only to study at the institute that he leads — but also to work with the renowned experts of JAXA in Japan, whose contributions are acknowledged below.

My superior at DLR Lampoldshausen, Mr. Wolfgang Kitsche, went to great lengths to be able to offer me a research position in the first place. During my research, I enjoyed an exceptional amount of freedom to pursue my interests on the thesis' topic, wherever they may lead, thanks to him. Recently he has also spent a large amount of his busy work days reading terribly rough early chapter drafts of this work in order to advise me towards a better thesis.

My sister-in-law, Dr. Carolina Malagon has greatly contributed to the quality of this thesis by scrutinizing every sentence for mistakes of grammar, spelling and logical coherence. Much like the 0.05% of germs surviving a disinfection, any mistakes of these categories that may remain are only an indication of the sheer number of them that would have been present had not been for her help. My thanks also goes to my brother, Dr.-Ing Henry Sudhof for his feedback.

During my year long-stay in Japan I was warmly welcomed and expertly advised by Dr. Mitsuru Shimagaki, who, together with Mr. Takeo Tomita, originally suggested conducting a cascade experiment. Furthermore, the experiment would not have been possible without the financing provided by Jaxa and the support of the institute's administrator,

Dr. Makoto Yoshida.

It was a great honor to work with and learn from Mr. Satoshi Hasegawa, who leads the CATTS experimental facility, at which the experiment was conducted. It is a testament to the accomplishments of his career that his name was previously known even to me through his co-authorship of foundational works of Japanese rocket tubomachinery.

Also in relation to the successful experiment, I would like to thank Mr. Keigo Shiranita, who enthusiastically led the flawless manufacturing of the test cascade and specimen profiles.

Bibliography

- [1] J. M. Anders, J. Haarmeyer, and H. Heukenkamp. “A Parametric Blade Design System (Part I+ II)”. In: *Von Karman Institute for fluid dynamics: lecture series 2002* (1999).
- [2] P. Andersson. “Turbine Design”. In: *Spacecraft Propulsion*. Ed. by F. Breugelmans. Von Karman Institute for Fluid Dynamics, 1993. Chap. 5.
- [3] S. Andersson. “A Study of Tolerance Impact on Performance of a Supersonic Turbine”. In: *43rd AIAA/ASME/SAE/ASEE Joint Propulsion Conference & Exhibit*. 2007, p. 5513.
- [4] S. Andersson, M. Lindeblad, and U. Wahlen. “Performance Test Results for the Vulcan 2 Supersonic Transonic Turbine”. In: *34th AIAA/ASME/SAE/ASEE Joint Propulsion Conference and Exhibit*. 1998, p. 3999.
- [5] R. Aungier. *Turbine Aerodynamics: Axial-flow and Radial-inflow Turbine Design and Analysis*. ASME Press, 2006. ISBN: 978-0-7918-0241-0.
- [6] R. Beer. *Aerodynamic Design and Estimated Performance of a Two-stage Curtis Turbine for the Liquid Oxygen Turbopump of the M-1 Engine*. Tech. rep. NASA-CR-54764. NASA, 1965.
- [7] W. Bohl. *Strömungsmaschinen I. Aufbau und Wirkungsweise*. Kamprath-Reihe. Vogel, 1995. ISBN: 978-3-8343-3130-4.
- [8] W. Bohl. *Strömungsmaschinen II. Berechnung und Konstruktion*. Kamprath-Reihe. Vogel, 1995. ISBN: 978-3-8023-1570-1.
- [9] E. Boxer, J. R. Sterrett, and J. Wlodarski. *Application of Supersonic Vortex-flow Theory to the Design of Supersonic Impulse Compressor or Turbine-blade Sections*. Tech. rep. NACA-RM-L52B06. NACA, 1952.
- [10] A. Carmichael. “The Aerodynamic Design of Axial-Flow and Radial-Inflow Turbines”. In: *Sawyer’s Gas Turbine Engineering*. Ed. by J. W. Sawyer. Gas Turbine Publications, 1972. Chap. 4. ISBN: 978-0937506158.
- [11] G. Cordes. *Strömungsmechanik der gasbeaufschlagten Axialturbine*. Springer, 1963. ISBN: 978-3-540-02955-7.

- [12] K. C. Cornelius and G. A. Lucius. “Physics of Coanda Jet Detachment at High-Pressure Ratio”. In: *Journal of Aircraft* 31.3 (1994), pp. 591–596.
- [13] M. Dejc and B. Trojanovskij. *Untersuchung und Berechnung axialer Turbinenstufen*. VEB Verlag Technik, 1973.
- [14] M. Dejc and G. A. Filippov. *Атлас профилей решёток осевых турбин*(*Atlas of Blade Rows for Axial-Flow Turbines*). Russian. Машиностроение, 1965.
- [15] S. Dixon. *Fluid Mechanics and Thermodynamics of Turbomachinery*. Elsevier Science, 2014. ISBN: 978-0-12-415954-9.
- [16] D. Dorney et al. “Pre-and Post-Test Predictions of the Flow in a Multi-Stage Supersonic Turbine”. In: *39th AIAA/ASME/SAE/ASEE Joint Propulsion Conference and Exhibit*. 2003, p. 5071.
- [17] H. W. Douglass et al. *Liquid Rocket Engine Turbines*. Tech. rep. SP-8110. National Aeronautics and Space Administration, Jan. 1974.
- [18] *Ellipse*. July 15, 2019. URL: <http://mathworld.wolfram.com/Ellipse.html>.
- [19] A. für Entwicklung und Forschung. *Gerätebeschreibung A4*. Tech. rep. OKH, 1945.
- [20] L. Eriksson. “Development of a Supersonic Turbine Stage for the HM60 Engine”. In: *20th Joint Propulsion Conference*. 1984.
- [21] G. E. Farin. *Curves and surfaces for CAGD: a practical guide*. Morgan Kaufmann, 2002.
- [22] L. Fielding. *Turbine Design: The Effect on Axial Flow Turbine Performance of Parameter Variation*. ASME Press, 2000. ISBN: 9780791800867.
- [23] W. H. Frey and D. A. Field. “Designing Bézier Conic Segments With Monotone Curvature”. In: *Computer Aided Geometric Design* 17.6 (2000), pp. 457–483.
- [24] Y. Fukushima and T. LMOTO. “Lessons Learned in the Development of the LE-5 and LE-7”. In: *30th Joint Propulsion Conference and Exhibit*. 1994, p. 3375.
- [25] M. B. Giles. “Stator/Rotor Interaction in a Transonic Turbine”. In: *Journal of Propulsion and Power* 6.5 (1990), pp. 621–627.
- [26] D. E. Goldberg. *Genetic Algorithms in Search, Optimization and Machine Learning*. 1st. Boston, MA, USA: Addison-Wesley Longman Publishing Co., Inc., 1989. ISBN: 0201157675.

- [27] L. J. Goldman. "Supersonic Turbine Design and Performance". In: *ASME 1972 International Gas Turbine and Fluids Engineering Conference and Products Show*. V001T01A062. American Society of Mechanical Engineers. 1972.
- [28] L. J. Goldman. "Supersonic Turbines". In: *Turbine Design and Application*. Ed. by A. J. Glassman. Vol. 2. NASA, 1994, pp. 249–278.
- [29] L. J. Goldman and V. J. Scullin. *Analytical Investigation of Supersonic Turbomachinery Blading. 1-Computer Program for Blading Design*. Tech. rep. NASA, 1968.
- [30] L. J. Goldman and V. J. Scullin. *Analytical Investigation of Supersonic Turbomachinery Blading. 2-Analysis of impulse turbine-blade sections*. Tech. rep. NASA, 1968.
- [31] L. J. Goldman and V. J. Scullin. *Computer Program for Design of Two-Dimensional Supersonic Turbine Rotor Blades With Boundary-Layer Correction*. Tech. rep. TM X-2434. NASA, 1971.
- [32] C. Graham and F. Kost. "Shock Boundary Layer Interaction on High Turning Transonic Turbine Cascades". In: *ASME 1979 International Gas Turbine Conference and Exhibit and Solar Energy Conference*. American Society of Mechanical Engineers. 1979, V01AT01A037.
- [33] J. Gräsel et al. "A Full Parametric Model for Turbomachinery Blade Design and Optimisation". In: *ASME 2004 International Design Engineering Technical Conferences and Computers and Information in Engineering Conference*. American Society of Mechanical Engineers. 2004, pp. 907–914.
- [34] J. Green. "Interactions Between Shock Waves and Turbulent Boundary Layers". In: *Progress in Aerospace Sciences* 11 (1970), pp. 235–340.
- [35] J. Green. "Reflexion of an Oblique Shock Wave by a Turbulent Boundary Layer". In: *Journal of Fluid Mechanics* 40.1 (1970), pp. 81–95.
- [36] L. W. Griffin and D. J. Dorney. "Simulations of the unsteady flow through the Fastrac supersonic turbine". In: *Journal of turbomachinery* 122.2 (2000), pp. 225–233.
- [37] L. W. Griffin and F. W. Huber. "Advancement of Turbine Aerodynamic Design Techniques". In: *ASME 1993 International Gas Turbine and Aeroengine Congress and Exposition*. American Society of Mechanical Engineers. 1993, V03CT17A031–V03CT17A031.
- [38] L. Griffin and D. Dorney. "Design and Analysis of Turbines for Space Applications". In: *33rd AIAA Fluid Dynamics Conference and Exhibit*. 2003.

- [39] L. Griffin et al. “Detailed aerodynamic design optimization of an RLV turbine”. In: *37th Joint Propulsion Conference and Exhibit*. 2001, p. 3397.
- [40] H. Hagen and G.-P. Bonneau. “Variational design of smooth rational Bézier curves”. In: *Computer Aided Geometric Design* 8.5 (1991), pp. 393–399.
- [41] R. Hahn et al. “Utilization of LOX/LCH₄ for Expander-Bleed Cycle at Upper Stage Engine Application”. In: *7th European Conference for Aeronautics and Space Science*. 2017.
- [42] R. Hashimoto et al. 液酸・液水ロケットエンジン用タービンの性能. *Performance Evaluation of LOX and LH₂ Turbopump Turbine for a 10-Ton Thrust LOX/LH₂ Rocket Engine*. Japanese. Technical Report TR-691. National Aerospace Laboratory(NAL), Dec. 1981.
- [43] K. Hayasaka et al. “Optical-Flow-based Background-Oriented Schlieren Technique for Measuring a Laser-Induced Underwater Shock Wave”. In: *Experiments in Fluids* 57.12 (2016), p. 179.
- [44] K. Holmedahl. “Analysis and Testing of the Vulcain 2 LOX Turbine Blades for Prediction of High Cycle Fatigue Life”. In: *36th AIAA/ASME/SAE/ASEE Joint Propulsion Conference and Exhibit*. 2000, p. 3680.
- [45] B. K. Horn and B. G. Schunck. “Determining optical flow”. In: *Artificial intelligence* 17.1-3 (1981), pp. 185–203.
- [46] F. W. Huber. *Turbine Aerodynamics Design Tool Development*. NASA Technical Reports Server. Presentation Slides. 20010047552. June 2001.
- [47] R. A. Huntington. “Evaluation of Polytropic Calculation Methods for Turbomachinery Performance”. In: *Journal of Engineering for Gas Turbines and Power* (1985). doi:10.1115/1.3239827.
- [48] R. Johnsson, S. Brodin, and A. Pettersson. “Development of hydrogen and oxygen pump turbines for Vinci engine”. In: *38th AIAA/ASME/SAE/ASEE Joint Propulsion Conference & Exhibit*. 2002.
- [49] M. M. Joly, T. Verstraete, and G. Paniagua. “Differential Evolution Based Soft Optimization to Attenuate Vane–Rotor Shock Interaction in High-Pressure Turbines”. In: *Applied Soft Computing* 13.4 (2013), pp. 1882–1891.
- [50] S. C. Kacker and U. Okapuu. “A mean line prediction method for axial flow turbine efficiency”. In: *Journal of Engineering for Power* 104.1 (1982), pp. 111–119.

- [51] H. Kato and K.-i. Funazaki. "POD-Driven Adaptive Sampling for Efficient Surrogate Modeling and Its Application to Supersonic Turbine Optimization". In: *ASME Turbo Expo 2014: Turbine Technical Conference and Exposition*. American Society of Mechanical Engineers. 2014, V02BT45A023.
- [52] H. Kato et al. "Robust Aerodynamic Shape Optimization of Supersonic Turbine Using Non-Intrusive Polynomial Chaos Expansion". In: *9th World Congress on Structural and Multidisciplinary Optimization, June*. 2011, pp. 13–17.
- [53] K. Kawatsu et al. "Multi Objective Optimization of a Supersonic Axial Turbine Blade Row Shape for Rocket Engine Turbopump". In: *47th AIAA/ASME/SAE/ASEE Joint Propulsion Conference & Exhibit*. 2011, p. 5784.
- [54] N. Kazuki et al. "Thermodynamic Effects on Cryogenic Cavitation Flow in Orifice". In: *Proceedings of the 7th International Symposium on Cavitation*. 2009.
- [55] M. Kharbat. *Horn-Schunk Optical Flow Method v 1.1.0.0*. Aug. 22, 2019. URL: www.mathworks.com/matlabcentral/fileexchange/22756-horn-schunck-optical-flow-method.
- [56] H. A. Klassen. *Cold-air investigation of effects of partial admission on performance of 3.75-inch mean-diameter single stage axial-flow turbine*. Tech. rep. NASA-TN-D-4700. NASA, 1968.
- [57] G. Koini, S. Sarakinos, and I. Nikolos. "A Software Tool for Parametric Design of Turbomachinery Blades". In: *Advances in Engineering Software* 40.1 (2009), pp. 41–51.
- [58] T. Korakianitis. "Prescribed-Curvature-Distribution Airfoils for the Preliminary Geometric Design of Axial-Turbomachinery Cascades". In: *ASME, Transactions, Journal of Turbomachinery* 115.2 (1993), pp. 325–333.
- [59] D. Lasser and G.-P. Bonneau. "Bézier Representation of Trim Curves". In: *Geometric modelling*. Springer, 1995, pp. 227–242.
- [60] X. Lee. *Cornu Spiral*. Aug. 2, 2019. URL: http://xahlee.info/SpecialPlaneCurves_dir/Clothoid_dir/clothoid.html.
- [61] M. Mallen and G. Saville. "Polytropic processes in the performance prediction of centrifugal compressors". In: *Scaling for performance prediction in rotodynamic machines: a conference held at the University of Stirling*. 1977, pp. 89–96.
- [62] G. Marke and P. Windstrom. "Lessons learned during the development of the Vulcan turbines". In: *31st Joint Propulsion Conference and Exhibit*. 1995, p. 2404.

- [63] D. Mee, N. Baines, and M. Oldfield. “Detailed Boundary Layer Measurements on a Transonic Turbine Cascade”. In: *Journal of Turbomachinery* 114.1 (1992), pp. 163–172.
- [64] T. Mengistu, W. Ghaly, and T. Mansour. “Global-and Local-Shape Aerodynamic Optimization of Turbine Blades”. In: *11th AIAA/ISSMO Multidisciplinary Analysis and Optimization Conference*. 2006, p. 6933.
- [65] A. Merchant and R. Haimes. “A CAD-Based Blade Geometry Model for Turbomachinery Aero Design Systems”. In: *ASME Turbo Expo 2003, collocated with the 2003 International Joint Power Generation Conference*. American Society of Mechanical Engineers. 2003, pp. 1237–1247.
- [66] W. E. Moeckel. *Approximate Method for Predicting Form and Location of Detached Shock Waves Ahead of Plane or Axially Symmetric Bodies*. Tech. rep. TN 1921. NACA, 1949.
- [67] H. P. Moreton and C. H. Séquin. *Functional optimization for fair surface design*. Vol. 26. 2. ACM, 1992.
- [68] W. J. Nelson and F. Bloetscher. *Preliminary Investigation of a Variable Mach Number Two-Dimensional Supersonic Tunnel of Fixed Geometry*. Tech. rep. RM L9D29a. NACA, 1949.
- [69] M. Paluszny, F. Tovar, and R. R. Patterson. “G2 Composite Cubic Bézier Curves”. In: *Journal of computational and applied mathematics* 102.1 (1999), pp. 49–71.
- [70] G. Paniagua et al. “Unsteady Strong Shock Interactions in a Transonic Turbine: Experimental and Numerical Analysis”. In: *Journal of propulsion and power* 24.4 (2008), pp. 722–731.
- [71] N. Papila et al. “Shape Optimization of Supersonic Turbines Using Global Approximation Methods”. In: *Journal of Propulsion and Power* 18.3 (2002), pp. 509–518.
- [72] V. Patel and F. Sotiropoulos. “Longitudinal Curvature Effects in Turbulent Boundary Layers”. In: *Progress in Aerospace Sciences* 33.1-2 (1997), pp. 1–70.
- [73] L. Piegl and W. Tiller. *The NURBS Book*. Springer Science & Business Media, 1997.
- [74] L. Pritchard. “An Eleven Parameter Axial Turbine Airfoil Geometry Model”. In: *ASME 1985 International Gas Turbine Conference and Exhibit*. American Society of Mechanical Engineers. 1985.
- [75] A. E. Puckett and H. J. Steward. “The Thickness of a Shock Wave in Air”. In: *Quarterly of Applied Mathematics* 7.4 (1950), pp. 457–463. ISSN: 0033569X, 15524485.

- [76] A. A. Rangwalla, N. K. Madavan, and P. D. Johnson. “Application of an Unsteady Navier-Stokes Solver to Transonic Turbine design”. In: *Journal of Propulsion and Power* 8.5 (1992), pp. 1079–1086.
- [77] T. W. Reynolds. *Aerodynamic Design - Model II Turbine M-1 Fuel Turbopump Assembly*. Tech. rep. National Aeronautics and Space Administration, Apr. 1966.
- [78] A. Rona et al. “Wall interference in the discharge flow in a linear cascade wind tunnel”. In: *41st Aerospace Sciences Meeting and Exhibit*. 2003, p. 455.
- [79] M. G. Rose. “Non-Axisymmetric Endwall Profiling in the HP NGV’s of an Axial Flow Gas Turbine”. In: *ASME 1994 international gas turbine and aeroengine congress and exposition*. American Society of Mechanical Engineers Digital Collection. 1994.
- [80] J. Roulier and T. Rando. “Measures of Fairness for Curves and Surfaces”. In: *Designing Fair Curves and Surfaces*. Ed. by N. S. Sapidis. Society for Industrial and Applied Mathematics, 1994, pp. 75–122.
- [81] A. Saxer and M. Giles. “Predictions of Three-Dimensional Steady and Unsteady Inviscid Transonic Stator/rotor Interaction With Inlet Radial Temperature Nonuniformity”. In: *Journal of turbomachinery* 116.3 (1994), pp. 347–357.
- [82] H. W. Schmidt et al. *Turbopump Systems for Liquid Rocket Engines*. Tech. rep. SP-8107. National Aeronautics and Space Administration, Aug. 1974.
- [83] A. Sebelev et al. “Design and Numerical Analysis of Processes in Siloxane Vapor Driven Turbine”. In: *Proceedings of the 3rd International Seminar on ORC Power Systems. Brussels, Belgium*. 2015, pp. 640–649.
- [84] A. Shapiro. *The Dynamics and Thermodynamics of Compressible Fluid Flow*. Vol. 1. Dynamics and Thermodynamics of Compressible Fluid Flow. Ronald Press Company, 1953.
- [85] T. Shibata et al. “超音速流入・流出タービンの直線翼列試験 (Linear Cascade Wind Tunnel Testing of Supersonic Inflow and Outflow Turbine Blades)”. Japanese. In: *日本機械学会論文集 B 編* 79.806 (2013), pp. 2120–2133.
- [86] D. Šimurda et al. “Measurements on supersonic turbine cascades—methodical approach”. In: *The XXII Symposium on Measuring Techniques in Turbomachinery*. 2014.
- [87] M. Smirnov et al. “Design Criteria for Novel Supersonic Nozzles With High Pitch-Chord Ratio”. In: *MATEC Web Conf.* 245 (2018), p. 09012. DOI: 10.1051/mateconf/201824509012.

- [88] L. Smith. “The Radial-Equilibrium Equation of Turbomachinery”. In: *Journal of Engineering for Power* 88.1 (1966), pp. 1–12.
- [89] S. Song and M. Martinez-Sanchez. “Rotordynamic forces due to turbine tip leakage: Part I—blade scale effects”. In: *Journal of turbomachinery* 119.4 (1997), pp. 695–703.
- [90] J. Sousa and G. Paniagua. “Entropy Minimization Design Approach of Supersonic Internal Passages”. In: *Entropy* 17.8 (2015), pp. 5593–5610.
- [91] L. Souverein et al. “On the effect of axial turbine rotor blade design on efficiency: a parametric study of the Baljé-diagram”. In: *7Th Eur Conf Aeronaut Sp Sci.* 2017.
- [92] M. S. Spiegel. *Einsatz deterministischer Optimierungsverfahren bei der Vorauslegung hochbelasteter Turbomaschinen*. Herbert Utz Verlag, 2000.
- [93] H. Starken, Z. Yongxing, and H.-A. Schreiber. “Mass Flow Limitation of Supersonic Blade Rows Due to Leading Edge Blockage”. In: *ASME 1984 International Gas Turbine Conference and Exhibit*. American Society of Mechanical Engineers. 1984, V001T01A064.
- [94] S. Sudhof and M. Shimagaki. “Gradient-Based Parametric Optimization of a Supersonic Turbine Nozzle Blade Row”. In: 第 54 回ターボ機械協会 (54th Turbomachinery Conference of the Turbomachinery Society of Japan). Turbomachinery Society of Japan, 2018.
- [95] S. Sudhof et al. “Cascade Experiments on a Supersonic Turbine Blade Row using Background-Oriented Schlieren Imaging”. In: *32nd International Symposium on Space Technology and Science*. 2019.
- [96] A. J. I. Toepler. *Beobachtungen nach einer neuen optischen Methode: Ein Beitrag zur Experimentalphysik*. Max Cohen und Sohn, 1864.
- [97] R. A. tog and A. M. Tousi. “Experimental and numerical investigation of design optimization of a partial admitted supersonic turbine”. In: *Propulsion and Power Research* 2.1 (2013), pp. 70–83.
- [98] W. Traupel. *Thermische Turbomaschinen*. Springer, 2001. ISBN: 978-3-642-62102-4.
- [99] S. Trollheden et al. “Turbopump turbines developed by Volvo”. In: *40th AIAA/ASME/SAE/ASEE Joint Propulsion Conference and Exhibit*. 2004, p. 3687.
- [100] S. Trollheden et al. “Development of the Turbines for the Vulcain 2 Turbopumps”. In: *35th Joint Propulsion Conference and Exhibit*. 1999.
- [101] J. Vance, F. Zeidan, and B. Murphy. *Machinery Vibration and Rotordynamics*. Wiley, 2010. ISBN: 978-0-470-91607-0.

- [102] U. Wåhlén. “The Aerodynamic Design of the Turbines for the Vulcain Rocket Engine”. In: *31th AIAA/ASME/SAE/ASEE Joint Propulsion Conference and Exhibit*. 10.2514/6.1995-2536. Volvo Aero Corporation. 1995.
- [103] C. D. Woodward. “Skinning Techniques for Interactive B-Spline Surface Interpolation”. In: *Computer-Aided Design* 20.8 (1988), pp. 441–451.
- [104] C.-H. Wu and L. Wolfenstein. *Application of Radial-Equilibrium Condition to Axial-Flow Compressor and Turbine Design*. Tech. rep. NACA-TR-955. NACA, 1950.
- [105] S. Yoon. “The Effect of the Degree of Reaction on the Leakage Loss in Steam Turbines”. In: *Journal of Engineering for Gas Turbines and Power* 135.2 (2013).

Appendices

A. Isentropic and Polytropic Work

This appendix discusses two ideal thermodynamic processes that are often used to calculate the denominator of a turbine efficiency. They are first discussed in general and subsequently as they relate to high specific work turbines.

First and perhaps more easily understood is isentropic work. Here, the optimal process is defined as a process with the same change in total pressure as the actual process, but with no change in entropy. If the gas is expanded from condition A to condition B , the heat released by this optimal process, called isentropic work $\Delta h_{A \rightarrow B, \text{is}}$, is calculated as follows in a perfect gas model:

$$\begin{aligned} \frac{T_{B, \text{is}}}{T_A} &= \left(\frac{p_B}{p_A} \right)^{\frac{\gamma-1}{\gamma}} \\ T_{B, \text{is}} &= T_A \left(\frac{p_B}{p_A} \right)^{\frac{\gamma-1}{\gamma}} \\ \Delta h_{A \rightarrow B, \text{is}} &= c_p (T_{B, \text{is}} - T_A) \end{aligned} \tag{A.1}$$

The efficiency is now defined as

$$\eta_{is} = \frac{\Delta h_{\text{use}}}{\Delta h_{A \rightarrow B, \text{is}}} \tag{A.2}$$

With

- Δh_{use} Useful enthalpy change ($= \Delta h_{A \rightarrow B}$)
- $\Delta h_{A \rightarrow B, \text{is}}$ Isentropic heat change between the unspecified states A and B

As an example, figure A.1 is an enthalpy-entropy plot of perfect gas (ideal gas with constant heat capacity) nitrogen¹. From the same starting point of 400 K and 10 bar, a gas is expanded. In an isentropic expansion with a total pressure ratio of 7.20, a heat of 300 kJ/kg could be extracted. If, for example, the actual process instead only extracts 100 kJ/kg from

1. $c_p = 1.098 \frac{\text{kJ}}{\text{kgK}}; \kappa = 1.37$

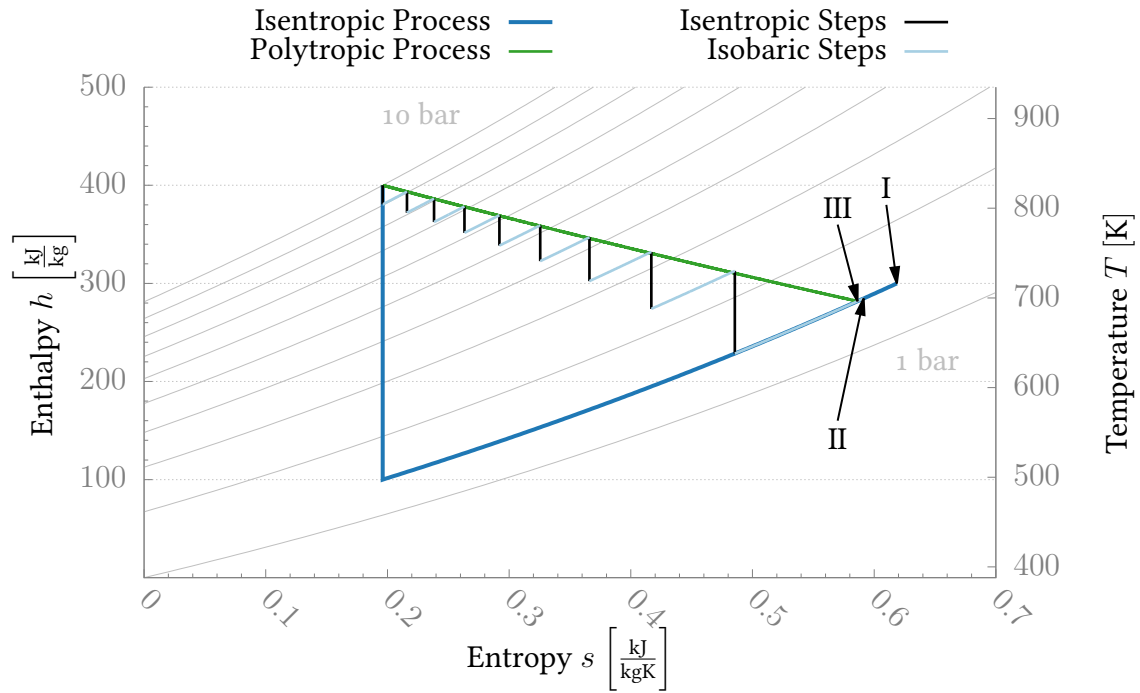


Figure A.1.: T-S Diagram for Perfect Gas Nitrogen with Isobars 10 bar to 1 bar

the same total pressure change, the process' isentropic efficiency is $1/3$. The end point of that process is marked "I" in the figure.

The imagined model process is $A \xrightarrow{\text{isentropic}} B_{\text{is}} \xrightarrow{\text{isobaric}} B$.

A complication becomes apparent when this process is split into parts. For example, if a gas is used in two sequential separate processes, each accounting for half the pressure difference, and the isentropic efficiency was $1/3$ for each step, the total extracted heat would not be 100 kJ/kg , but 107.2 kJ/kg .

This is because, even for a perfect gas, the isobars in the h - s plot are diverging towards higher entropy and the effect may be larger for ideal gases of variable heat capacity or real gasses. In practical terms, the same pressure difference has the potential to accomplish more work at a higher starting entropy level. Since the entropy is already elevated by the inefficiency of the first step, the second step is able to extract an extra 7.2 kJ/kg due to this effect, at the same isentropic efficiency.

In figure A.1 this is shown for the case of not two, but nine steps. The small vertical black bars represent isentropic pressure changes by the same pressure difference for each step. Every step is followed by a light blue line representing the isobaric heat change up to $2/3 (1 - \eta)$ of the heat extracted in the isentropic expansion. The resulting work after nine steps is the sum of the height of all nine black vertical bars, which is 115.3 kJ/kg . The imagined model process is $A \xrightarrow{\text{isentropic}} I_{1,\text{is}} \xrightarrow{\text{isobaric}} I_1 \xrightarrow{\text{isentropic}} I_{2,\text{is}} \xrightarrow{\text{isobaric}} \dots \xrightarrow{\text{isentropic}} B_{\text{is}} \xrightarrow{\text{isobaric}} B$. In

this, $I_{1...8}$ are intermediate stages. The end point is marked “II” in the figure.

With an increase in calculation steps, the extracted work increases further, but it approaches a limit. This limit is called the *polytropic efficiency*. An expansion with a polytropic efficiency of 1/3 is also pictured in figure A.1. It arrives at an enthalpy of 281.8 kJ/kg, so the extracted enthalpy is 118.2 kJ/kg, marked “III” in the figure. The model process is the same as above, but with large number of intermediate steps, instead of eight.

$$\eta_p = \frac{\Delta h_{\text{use}}}{\Delta h_{A \rightarrow B,p}} \quad (\text{A.3})$$

With

$$\begin{aligned} \Delta h_{\text{use}} & \text{ Useful enthalpy change} \\ \Delta h_{A \rightarrow B,p} & \text{ Polytropic heat change between the unspecified states A and B} \end{aligned}$$

Unfortunately, the iterative method to calculate polytropic work converges only slowly, so to achieve adequate convergence, a large number of steps may be necessary, about 20 000 in this case. Since real gas calculations can be computationally expensive, this method becomes unreasonably slow for problems where large numbers of efficiency calculations are necessary.

In order to avoid this computational cost, the polytropic process can be expressed through an algebraic curve. One way to achieve this is the polytropic exponent. The basic idea here is that the isentropic relations of ideal gases, such as equation A.1, only maintain entropy between the states A and B if the exponent variable κ matches the ratio of isobaric heat capacity c_p to isochoric heat capacity c_v . If the exponent variable is chosen as any other value but this ratio, entropy is not preserved between the states A and B . Exponents larger than 1 but smaller than c_p/c_v lead to an increase in entropy and a decrease in enthalpy, as in the polytropic process. In such a case, the letter n is used instead of κ and the variable is called the “polytropic exponent”, as shown in equation A.4.

For perfect gases, an exponent variable can be found so that the polytropic expansion exactly matches the graph of the curve^[47]. This negates the need for any iterative calculation. The exponent is determined as follows:

$$\begin{aligned} \frac{\Delta h_{A \rightarrow B}}{\Delta h_{A \rightarrow B,p}} \frac{n}{n-1} &= \frac{\kappa}{\kappa-1} \\ \frac{\kappa}{\frac{\Delta h_{A \rightarrow B}}{\Delta h_{A \rightarrow B,p}} (1-\kappa) + \kappa} &= n \end{aligned} \quad (\text{A.4})$$

With

κ the isentropic exponent

n the polytropic exponent replacing κ in equation A.1

No exact algebraic solution is possible for general gas models, however, and methods to choose a value of n that approximates the real expansion do not lead to satisfactory precision^[5]. Therefore an alternative fast solution is needed. Mallen and Saville^[61] proposed such a model, and Huntington^[47] as well as Aungier^[5] found that it matches the exact solution with high precision. Huntington gives this method in the following form:

$$\Delta h_{A \rightarrow B,p} = \Delta h_{A \rightarrow B} + (s_B - s_A) \frac{T_B - T_A}{\ln(T_B/T_A)}$$

For perfect gases, this model is also an exact solution for polytropic efficiency^[47]. The practical difference to the previous model is that it remains a good approximation for non-perfect gases^[5].

While the discussion above is not at all specific to supersonic turbines in rocket engines, the distinction between the two types of denominators is particularly important in high work turbines, because their difference becomes larger with larger pressure ratio. Two problems are specifically identified to illuminate why a polytropic efficiency should be used whenever possible.

The first is in the design of the fluid system. When one compares single-stage turbines to multiple stage turbines, or parallel to series arrangement of turbines^[82] in a rocket engine, it is vital to use the polytropic efficiency. Using isentropic efficiency, the parallel arrangement would seem to perform less efficiently, even if the overall pressure ratio and work are identical.

Another complication occurs in comparing the performance of the same turbine at different pressure ratios. Here, the peak isentropic efficiency is shifted towards higher pressure ratios, because of the growing discrepancy between the two model processes. This can negate larger losses found at higher pressure ratios, giving the impression that these would be more advantageous than they actually are.

B. Segment Curves for Blade Shaping

This appendix contains descriptions of several of the segment types for generating segmented blade profiles. The content is written to simplify the reproduction of results discussed in previous chapters. It is not thought to be necessary for understanding the overall method of profile design or blade shaping.

Unless otherwise noted, the end points and tangents of the profiles are determined by the profile generation and will not be studied as free parameters. The number of free parameters of the curve is therefore the degrees of freedom minus six. Two degrees of freedom are locked by the Cartesian coordinates of each of the end points, and one degree of freedom is locked by each of the end tangents.

In the interest of brevity it must be assumed that the reader is somewhat familiar with the geometry of rational Bézier curves. A good introduction to the topic was written by Piegl and Tiller^[73].

Throughout this appendix, the source space of transfer functions is called (t, z) and location vectors in that space are indexed \vec{P}_{tz} , indicating a tangential-axial coordinate space. This is not to limit the generality, though, and (t, z) can be freely substituted for any other parameter system, such as meridional-tangential (m, t) or depth-axial (x, z) , in which the source profile happens to be defined.

B.1. General Conic Segment

The conic segment is a rational Bézier curve of second degree. As such, it has three control points. The overall number of degrees of freedom is seven. Each control point has two degrees of freedom, and an additional degree of freedom is represented by the weight of the middle control point. The middle control point weight is the only free parameter. As with all rational Bézier curves, the weights of the end control points provide no additional degrees of freedom, and are set to unity by convention^[21]¹.

1. Differences in end point weight can have an influence on the lofting process, but it was not explored whether this could be advantageous.

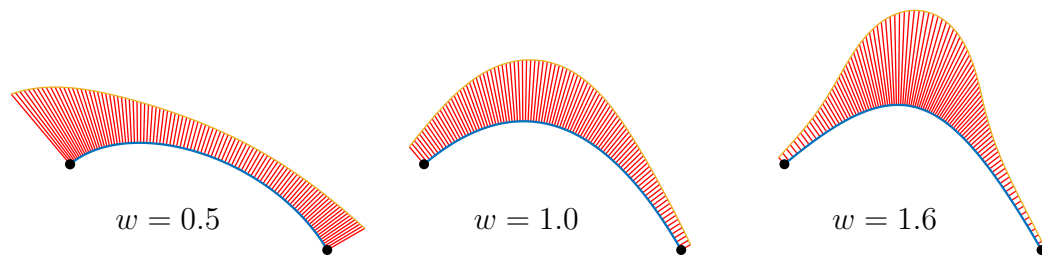


Figure B.1.: Parameter study of the mid point weight (curvature distribution shown)

Special cases of this curve include the parabola, which is generated by setting the middle control point weight to 1, and the ellipse and circle, which are handled separately.

Methods to determine the free parameter (mid point weight):

- by specifying the weight
- by specifying a point that must be interpolated
- by specifying one end curvature
- by the lowest weight that provides a monotone change of curvature^[23] (not yet implemented)

B.1.1. Parameter Study

Figure B.1 shows a parameter study with three different mid control point weights. The blue lines indicate the curve in question and the lines perpendicular to that give the relative distribution of curvature.

B.1.2. Transfer Function

The end points and their tangents are transferred to the canvas directly. The middle control point location is generated by the intersection of both end tangents. The weight of the middle control point is re-applied to the transferred control point.

Alternatively, the middle weight could be determined by a specified (x, z) -point to interpolate.

B.1.3. Considerations for Blade Shaping

Problems with lofting a number of curves can occur when the middle control point weights are very different from one section to the next. This can be avoided either by setting the same weight for each section curve or by re-approximating the curve with a higher order non-rational (polynomial) curve.

It shows that various distributions of curvature are possible. However, the end point curvature is strongly dependent on the mid point weight. Vanishing end curvatures are only possible at $w = \infty$.

B.2. Rational Cubic Curve (Paluszny Curve)

Rational cubic curves have a total of ten degrees of freedom; with the default end conditions, four degrees of freedom remain. The second and third control points can be moved along the end tangent direction and each of these control points has an open weight variable.

This allows the specification of end curvatures, including zero, without causing the curve to become degenerate. However, it is mathematically not trivial to find a way to express the remaining two degrees of freedom as parameters, especially if additional conditions have to be kept.

Paluszny et al. have found a solution to this problem where all resulting curves are c-shaped^[69]. In that paper, the open parameters are not named, but only designated B_0 on the one hand and x or z on the other, depending on the case. The variable B_0 works somewhat like the mid point weight of the conic segment, and is named “pointedness” (p) here. In the paper, the other variable changes its name based on the curve’s end conditions. Its influence can loosely be described as shifting the curvature along the curve, making it “lean” more towards one end or the other. It is therefore called “left/right bias” or just “bias” b here.

All in all, Paluszny identifies three different types (“elbow”, “sloped” and “shoulder”) of curves that have the properties described above, and each one has a separate parameter space (p, b). In order to get a single parameter space, two simplifications were made. First, the “Shoulder” curves were not used after an initial experimentation showed that they often had quite sharp turns, and were unlikely to be suitable as profile segments. Second, since the parameter spaces for “elbow” and “sloped” curves are adjacent, they were combined to one kind of curve, called “Paluszny Curve” here.

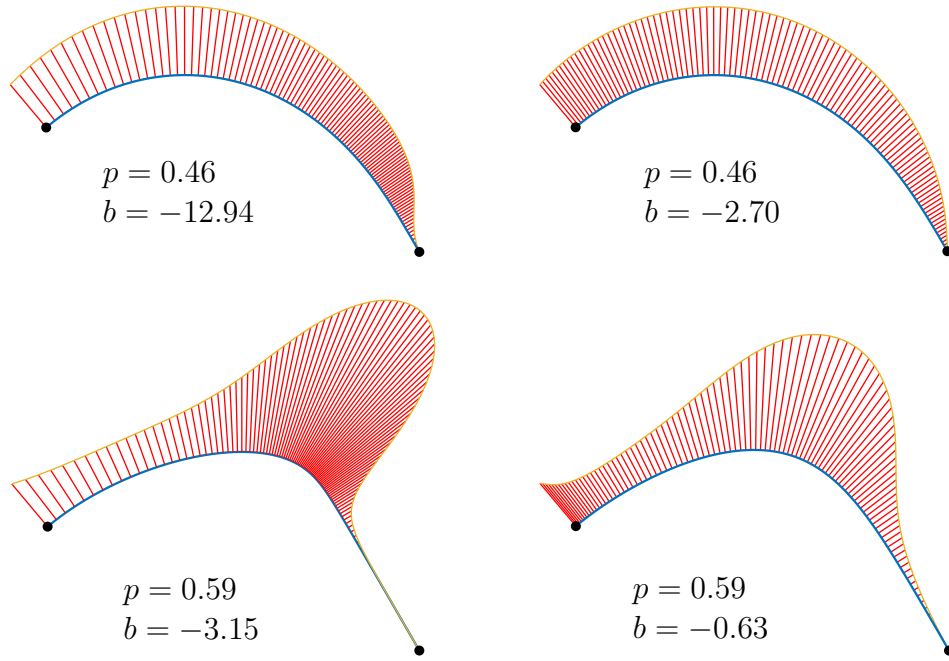


Figure B.2.: Parameter study of the Paluszny parameters with vanishing curvature at one end

B.2.1. Parameter Study

Paluszny curves offer a large amount of control over the shape of the curve. If unrestricted, the internal parameters can be used to circumvent specified end conditions, as seen in figure 3.16. Here, the Paluszny curve on the subsonic part of the pressure side appears to make a sharp turn at the leading edge. Mathematically speaking, this location is curvature continuous, in that there is no true jump in curvature. However, the curvature changes from the ellipse curvature to a very high curvature and back to a low curvature within micrometers. While this can hint at the possibility that better profiles are possible with a different parameter systems, there are cases where it should be avoided. One way to avoid this is to impose a lower limit on the p -parameter. Another way would be to limit the maximum internal curvature of the segment, for example by passing the value to the optimization program and setting a maximum value as an auxiliary condition.

B.2.2. Transfer Function

A point M is generated at the intersection of the end tangent of first and last control points (P_0 and P_3). The locations of the middle control points P_1 and P_2 are transferred to barycen-

tric coordinates in the (P_0, M, P_3) system. The points P_0 and P_3 as well as their tangents are transferred to (u, v) coordinates, and a new point M in (u, v) coordinates is generated. The points P_1 and P_2 are set in (u, v) coordinates in the same barycentric coordinates, but in the transferred (P_0, M, P_3) coordinate system. Thereupon, the curves' respective weights are re-applied.

It must be noted that the method does not exactly preserve end curvature, but in mildly curved canvases, this has never led to a significant curvature discontinuity.

B.2.3. Considerations for Blade Shaping

As in conics, changes in internal control point weights between adjacent sections can make lofting problematic, so increase of the number of section curves or re-approximation may be necessary. Because of the fine local control over curvature that these curves have, they are often hard to recreate using non-rational curves. Typically, about three quartic non-rational curves were necessary to approximate a single Paluszny blade segment to a deviation smaller than 1/100 mm.

In order to limit the parameter space, only one single parameter set (p, b) was applied to all section curves. In such a case, the parameter boundaries must be set to the broadest span that is compatible with the boundary conditions for each individual section.

B.3. Non-Rational Quartic Curve

Like rational cubic curves, non-rational quartic curves have ten degrees of freedom; two degrees of freedom in each of the five control points. That means that it is likewise possible to determine the end point curvatures and have two remaining open internal parameters.

The end tangent directions D_0 and D_4 are known, but the distance between the control points $\|\vec{P}_1 - \vec{P}_0\|$ and $\|\vec{P}_4 - \vec{P}_3\|$ are open. These represent the two open degrees of freedom that will be used to define the input variables. At first, the variables g and h are defined. They specify the distances $\|\vec{P}_1 - \vec{P}_0\|$ and $\|\vec{P}_4 - \vec{P}_3\|$.

The shorthands G and H are introduced. The distances are then normalized.

$$G = \|\vec{P}_1 - \vec{P}_0\| \quad (\text{B.1})$$

$$H = \|\vec{P}_3 - \vec{P}_4\| \quad (\text{B.2})$$

$$g = \frac{G}{\|\vec{P}_4 - \vec{P}_0\|} \quad (\text{B.3})$$

$$h = \frac{H}{\|\vec{P}_4 - \vec{P}_0\|} \quad (\text{B.4})$$

To give a more easily readable parameter set g and h are expressed through the variables p and b , analogous to the Paluszny parameters. The normalization and the definition of p and b has been iterated upon, but is still not perfect. It would be better if the geometry of the curve (e.g. if it will be c-shaped s-shaped or even self-intersecting) could be easily read from the input parameters, so that undesired curves can be more easily avoided.

$$p = g^2 + h^2 \quad (\text{B.5})$$

$$b = \frac{g^2}{g^2 + h^2} \quad (\text{B.6})$$

With all these parameters (end points, end tangents, end curvatures, p and b), the curve is completely defined, but determining the coordinates (P_{2x}, P_{2y}) of the control point P_2 is still somewhat involved.

Curvature of a parametric curve $C^{[21]}$

$$k(t) = \frac{\|\vec{C}'(t) \times \vec{C}''(t)\|}{\|\vec{C}'(t)\|^3} \quad (\text{B.7})$$

Piegl and Tiller give the first and second end derivatives of a Bézier curve^[73]

$$\vec{C}'(0) = n(\vec{P}_1 - \vec{P}_0) \quad (\text{B.8})$$

$$\vec{C}'(1) = n(\vec{P}_n - \vec{P}_{n-1}) \quad (\text{B.9})$$

$$\vec{C}''(0) = n(n-1)(\vec{P}_0 - 2\vec{P}_1 + \vec{P}_2) \quad (\text{B.10})$$

$$\vec{C}''(1) = n(n-1)(\vec{P}_n - 2\vec{P}_{n-1} + \vec{P}_{n-2}) \quad (\text{B.11})$$

With

n the degree of the curve (here $n = 4$)

Using B.8, and B.9, the denominator of expression B.7 can be simplified.

$$k(0) = \frac{\|\vec{C}'(0) \times \vec{C}''(0)\|}{n^3 G^3} \quad (\text{B.12})$$

$$k(1) = \frac{\|\vec{C}'(1) \times \vec{C}''(1)\|}{n^3 H^3} \quad (\text{B.13})$$

Expressions B.8 and B.10 are inserted into B.12. The expansion of the cross product yields a rather long expression:

$$\begin{aligned} \frac{G^3 n^2 \cdot k(0)}{n-1} = & (P_{1x} - P_{0x})(P_{0y} - 2P_{1y} + P_{2y}) \\ & - (P_{1y} - P_{0y})(P_{0x} - 2P_{1x} + P_{2x}) \end{aligned} \quad (\text{B.14})$$

Analogously for the other end of the curve:

$$\begin{aligned} \frac{H^3 n^2 \cdot k(1)}{n-1} = & (P_{4x} - P_{3x})(P_{4y} - 2P_{3y} + P_{2y}) \\ & - (P_{4y} - P_{3y})(P_{4x} - 2P_{3x} + P_{2x}) \end{aligned} \quad (\text{B.15})$$

Equations B.14 and B.15 form an equation system with two unknowns, P_{2x} and P_{2y} , which is solvable. Doing so is easier with some additional short hands:

$$\begin{aligned} P_{ax} &= P_{1x} - P_{0x} \\ P_{ay} &= P_{1y} - P_{0y} \\ P_{bx} &= P_{4x} - P_{3x} \\ P_{by} &= P_{4y} - P_{3y} \\ E_{1a} &= P_{ax}(P_{0y} - 2P_{1y}) \\ E_{2a} &= P_{ay}(P_{0x} - 2P_{1x}) \\ E_{1b} &= P_{bx}(P_{4y} - 2P_{3y}) \\ E_{2b} &= P_{by}(P_{4x} - 2P_{3x}) \\ L_a &= \frac{G^3 n \cdot k(0)}{n-1} \\ L_b &= \frac{H^3 n \cdot k(1)}{n-1} \end{aligned}$$

All these short hands are comprised of variables that are known at this point, so their numerical values can be calculated. Equations B.14 and B.15 become

$$L_a = E_{1a} + P_{ax}P_{2y} - E_{2a} - P_{ay}P_{2x} \quad (\text{B.16})$$

$$L_b = E_{1b} + P_{bx}P_{2y} - E_{2b} - P_{by}P_{2x} \quad (\text{B.17})$$

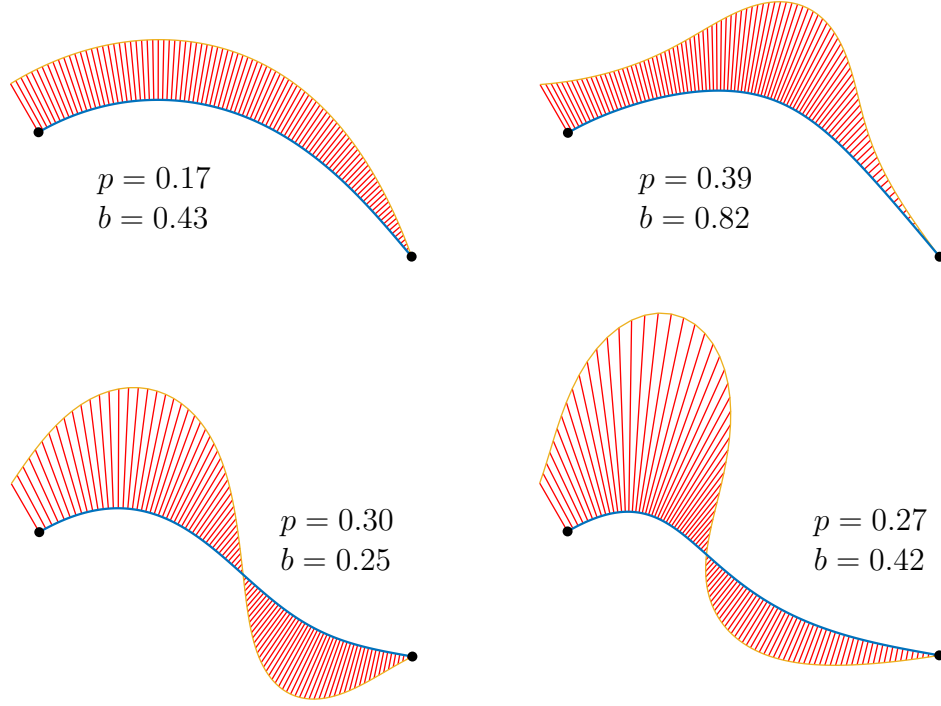


Figure B.3.: Parameter study of the Quartic parameters with vanishing curvature at one end, showing two c-shaped (top) and two s-shaped curves (bottom)

And finally

$$P_{2x} = \frac{P_{bx}(L_a - E_{1a} + E_{2a}) - P_{ax}(L_b - E_{1b} + E_{2b})}{P_{ax}P_{by} - P_{ay}P_{bx}} \quad (\text{B.18})$$

$$P_{2y} = \frac{L_b - E_{1b} + E_{2b} + P_{by}P_{2x}}{P_{bx}} \quad (\text{B.19})$$

With $\vec{P}_2 = (P_{2x}, P_{2y})$ calculated, all degrees of freedom are well defined.

B.3.1. Parameter Study

The parameters of Non-Rational Quartic curve as described above are harder to choose than the Paluszny parameters, since the latter method rules out several kinds of curve defects by the way the curve is generated^[69]. For example, no method was implemented to determine the parameter values at which an additional inflection point may appear or even the parameter values at which the curve may self-intersect. Such methods seem likely possible given the convex hull and variation diminishing properties of Bézier curves^[73]. Currently b can be chosen from $]0, 1[$, and p can be chosen from $]0, \infty[$, although it is unlikely that $p > 1$

would yield a usable curve, because the distance between the first and second as well as between the second to last and last control point would be too large for most applications.

While in many cases, functionally identical curves are possible in both methods, in all cases that appeared so far, it was possible to find fairer (see subsection 3.5.3) Paluszny curves than quartic curves, especially in cases where the minimum possible derivative bending energy was large for both curves. The advantage of quartic non-rational curves lies in the ability to form s-shapes and in the reduced complexity of finding an adequate lofted mantle surface.

B.3.2. Transfer Function

For transferring the curve onto a canvas, the curve parameters (p, b) are used again. The reference length $\|\vec{P}_4 - \vec{P}_0\|$ is calculated in (u, v) -coordinates and control points \vec{P}_1 and \vec{P}_3 are created using these variables. The middle control point \vec{P}_2 should best be specified using a technique that preserves the relative relationship between this point and the end points.

One way would be to express the distance vector $\vec{P}_2 - \vec{P}_0$ in terms of the end derivatives and the normalization distance $\|\vec{P}_4 - \vec{P}_0\|$, for example like this:

$$N_{tz} = \|\vec{P}_{4,tz} - \vec{P}_{0,tz}\| \quad (\text{B.20})$$

$$\vec{P}_{2,tz} - \vec{P}_{0,tz} = aN_{tz}\vec{D}_{0,tz} + bN_{tz}\vec{D}_{4,tz} \quad (\text{B.21})$$

$$N_{uv} = \|\vec{P}_{4,uv} - \vec{P}_{0,uv}\| \quad (\text{B.22})$$

$$\vec{P}_{2,uv} - \vec{P}_{0,uv} = aN_{uv}\vec{D}_{0,uv} + bN_{uv}\vec{D}_{4,uv} \quad (\text{B.23})$$

Here, the coefficients a and b are defined by the linear combination in equation B.21.

Unfortunately this fails if the end tangents D_0 and D_4 are exactly or nearly parallel, which can happen in s-shaped cases. Therefore, this solution was not implemented.

Instead, the point P_2 is being transferred as-is using the lookup function $P_{uv} = \vec{L}(P_{tz})$, as a working, but imperfect placeholder solution. It may lead to a significant discrepancy in the end curvatures between the input profile curve and the output section curve.

A different method would be to calculate P_2 from specified end point curvatures in (u, v) -space, for example by taking the curvature of both adjacent curves. Unfortunately, these curvatures are not currently available as input to the transfer function.

B.3.3. Considerations for Blade Shaping

Since the curve is non-rational, the risk of unforeseen lofting behavior is lower than for rational curves. Unsatisfactory results are possible if parameter values from one section curve to the next vary too much to form a reasonable lofting surface between them. If a curve is optimized for a fairness variable, it is therefore prudent to choose the same parameters (p, b) for all section curves and minimize either sum of all the segment's fairness values or the sum of their squares.

B.4. Other Curves

The curves discussed in detail above have been studied in the most depth, but a number of other curves were also implemented, they will be discussed briefly in the final section of this appendix.

Ellipse and Circular Segments

These are used for leading and trailing edges. As they are special conic segments, they are implemented as a daughter class of those, which means that all methods available for conic segments are also available for ellipse and circular segments. In addition, they can be initialized using the ellipse parameters of eccentricity and inclination^[18], with the eccentricity of a circle being 0.

Specifically for the circle, there also exists the option to initialize the curve using the same boundary conditions as Pritchard used for the uncovered turning. Pritchard's iterative method of finding a matching circle was replaced by a closed-form solution of the problem, which was derived from tangent circle relations.

Non-Rational Cubic Curves

No specialized parameter system for non-rational cubic curves was implemented, and no attempt was made here to define them based on end curvature, although methods for this are described by Farin^[21].

Instead, this curve type was used to adapt a curve to approximate an arbitrary number of points, by minimizing the least squares of distances, while maintaining end points and tangents. The points need to be chosen such that they are compatible with the end tangents, and for best results, there should be some distance between the end points and the first approximation point.

Straight Lines or Nearly Straight Curves

If a straight line is required, both end points must lie on the same end tangent, so the default set of parameters cannot be chosen. This curve type is most useful in catching the degenerate case of a circle with infinite radius, in a Pritchard profile with zero uncovered redirection. As a straight line is right at the transition point between a c-shaped and an s-shaped curve in terms of end tangents, it is possible that a nearly straight curve is c-shaped in the (t, z) space in which the profile is defined, but s-shaped in the (u, v) canvas parameter space.

To address such cases, a class of non-rational cubic curves was implemented with a special routine that approximates a straight line in the (t, z) parameter space by generating a set of points on the line in (t, z) space and determining the middle control point locations in (u, v) -space by finding the locations that lead to the curve with the lowest sum of squares between the curve and the pre-calculated points.

Lebenslauf

Name: Samuel Louis Sudhof
Wohnsitz: Simon-Elsässer Straße 14
74219 Möckmühl
Telefon: 0176/24969958
E-Mail: Samuel.Sudhof@gmail.com
Geburtsdatum: 28.12.1987
Familienstand: Ledig



Studium

2007-2009 Technische Universität Berlin

Studiengang: Verkehrswesen
Studienrichtung: Luft- und Raumfahrttechnik

2009-2011 Technische Universität Berlin

Studiengang: Maschinenbau
Abschluss: Bachelor of Science (2,7)

Abschlussarbeit: „Development of an Electromechanic Release System for an Engineering-Modell of a Small Sattelite Separation System“ in Zusammenarbeit mit Dr.-Ing Harry Adirim und Norbert Pilz von Aerospace Innovation GmbH, betreut durch Prof. Dr.-Ing Klaus Brieß. Note: 1,0

2011-2014 Technische Universität München

Studiengang: Luft- und Raumfahrttechnik
Spezialisierung: Raumfahrttechnik und Luftfahrtantriebe
Abschluss: Master of Science (2,3)

Abschlussarbeit: „Engineering Fundamentals of Expander Cycle Engine Oxygen Turbopumps and their Application“ betreut durch Prof. Dr.-Ing Oskar Haidn. Note: 1,3

Berufliche Erfahrung

2015 Technische Universität München

Position: Wissenschaftlicher Mitarbeiter
Projekt: Vorbetrachtungen für die Einrichtung eines Lagerprüfstands

2015-2019 Deutsches Zentrum für Luft- und Raumfahrttechnik in Lampoldshausen

Position: Wissenschaftlicher Mitarbeiter / Doktorand
Projekt: Konzipierung, Auslegung und Test von Überschallturbinenschaufeln